Cortical function and structure of human colour perception

Rebecca Lowndes

PhD by Publication

University of York

Psychology

May 2024

Abstract

Chromatic and achromatic signals in the brain have historically been studied independently. This thesis examines the combinations of chromatic and achromatic signals using both functional Magnetic Resonance Imaging (fMRI), structural MRI, and behavioural measurements to understand how these essential facets of human vision interact. Chapter one utilises random luminance masking to examine functional cortical responses to colour stimuli, and whether they can be used to predict behavioural threshold measurements. First, I examine the potential independence and interdependence of chromatic and achromatic signals in primary visual cortex. I found evidence of interdependence in a manner consistent with a normalising effect of achromatic contrast on chromatic signals, which can accurately predict behavioural thresholds. Then I used the same methods to examine the differing responses to L-M and S cone signals at two spatial frequencies, between which the behavioural sensitivity difference is greater for S cone than L-M stimuli. I found responses in early visual cortex which aligned well with behavioural sensitivity. In both projects described in chapter one, I have shown that chromatic responses do not reduce dramatically up the visual hierarchy, while achromatic responses do. In chapter two, I present research collected from a cohort of rare participants with congenital achromatopsia, who have no functional cone-mediated vision from birth, leading to a total loss of chromatic and central vision. This cohort, known as rod achromats, represents a unique opportunity to investigate the effects of chromatic deprivation on the brain. Using structural MRI, I found widespread reduction in cortical surface area in the achromat group compared to healthy controls, suggesting that the loss of chromatic vision or the loss of high acuity foveal vision significantly affects cortical morphology. I conclude with some areas for future research which would further expand the understanding of the links between chromatic perception and the structure and function of the human brain.

Contents

List of figures

List of tables

Declarations

I, Rebecca Helen Lowndes, declare that this thesis is a presentation of original work, carried out under the supervision of Professor Antony Morland and Professor Alex Wade, and I am the sole author. This work has not previously been presented for a degree or other qualification at this University or elsewhere. All sources are acknowledged as references. All the studies contained in this thesis were conducted in accordance with the ethical standards of the Department of Psychology at the University of York and the York Neuroimaging Centre. Data in Chapter 2 was collected in collaboration with Dr Barbara Molz.

The work presented in Chapter 1 has been published in the form of the following articles:

Lowndes, R., Aveyard, R., Welbourne, L. E., Wade, A., & Morland, A. B. (2024). In primary visual cortex fMRI responses to chromatic and achromatic stimuli are interdependent and predict contrast detection thresholds. *Vision Research*, *218*, 108398.

Rebecca Lowndes: Writing – review & editing, Writing – original draft, Software, Methodology, Investigation, Formal analysis, Data curation, Conceptualization. Richard Aveyard: Software. Lauren E. Welbourne: Investigation. Alex Wade: Supervision, Software. Antony B. Morland: Writing – review & editing, Supervision, Software, Methodology, Investigation, Formal analysis, Conceptualization.

Lowndes, R., Welbourne, L., Williams, M., Gouws, A., Wade, A., & Morland, A. (2023). Increasing spatial frequency of S-cone defined gratings reduces their visibility and brain response more than for gratings defined by LM cone contrast. *Vision Research*, *207*, 108209.

Rebecca Lowndes: Conceptualization, Methodology, Software, Investigation, Formal analysis, Data curation, Writing – original draft, Writing – review & editing. Lauren Welbourne: Formal analysis, Visualization. Molly Williams: Investigation. Andre Gouws: Software. Alex Wade: Supervision, Software, Writing – review & editing. Antony Morland: Conceptualization, Writing – review & editing, Methodology, Software, Investigation, Formal analysis, Supervision.

The work presented in Chapter 2 has been published in the form of the following article:

Lowndes, R., Molz, B., Warriner, L., Herbik, A., De Best, P. B., Raz, N., ... & Baseler, H. A. (2021). Structural differences across multiple visual cortical regions in the absence of cone function in congenital achromatopsia. *Frontiers in Neuroscience*, *15*, 718958.

HB, NL, MH, AM, and BM conceived and designed the experiments. BM, PB, AH, RL, NL, NR, AG, KA, RM, IG, SK, LC, JM, MK, BK-K, IW, and EB data acquisition. BM, AH, and PB performed the experiments. RL, LW, and BM analysed the data. RL and LW wrote the paper. HB, RL, LW, BM, AM, MH, PB, AH, NL, NR, AG, KA, RM, IG, SK, LC, JM, MK, BK-K, IW, and EB revised the manuscript. All authors contributed to the article and approved the submitted version.

Antony B Morland, PhD
13/09/2024

Rebecca H Lowndes
13/09/2024

Acknowledgements

When a PhD takes *slightly* longer than usual, there will naturally be many people who have contributed significantly to its completion, both in direct research support and personal support along the way. I would like to start by thanking all those who have participated in my research over the years. This literally would not be possible without you.

Tony – my supervisor and mentor in life as well as science for many years – this thesis would be a lot longer were I to thank you properly for your guidance, support, and friendship. Instead, I will just say: thank you for everything, and that I have and continue to enjoy working with you a great deal.

I would like to thank all my co-authors sincerely for their contributions. There are many of you who have all helped in big and small ways in the journey from inception to publication of the papers herein, and I cannot name you all. However, special thanks go to Alex Wade and Heidi Baseler. Alex - my second supervisor - you provided invaluable insight on all aspects of my work throughout this PhD. Heidi, thank you for working with me during strange and difficult times. I am pretty sure that project kept me sane!

None of this would have been possible without my wonderful colleagues and friends at YNiC, both past and present. All of you have helped me in your own ways and I cannot thank you enough. Special thanks to Jackie, my 'work Mum' who sat with me through countless reception days, always providing a laugh and a chat when (very often) needed.

Thank you to all the members of the various labs that have allowed me to call them home for the last six years: Morland/Baseler lab, Baker/Wade lab and Jefferies lab. Thank you to Katya for being so welcoming and introducing me to a different aspect of neuroscience and so many lovely people.

So many thanks to Lauren Welbourne, who arrived early in my PhD journey and helped my research in immeasurable ways.

For starting all of this, I must thank Barbara Molz, who welcomed a lowly undergraduate and gave me the time and faith that I could be genuinely helpful during her own PhD journey. I hope I was slightly more helpful than time consuming.

Holly – your friendship means the world to me. Thank you for everything. Social bubbles really are for life.

To Susan Lowndes, David Lowndes, and David Blackwood. Thank you. There is a great deal of peace in knowing you always have people in your corner.

Phil - I could not have done any of this without you. Thank you forever.

Introduction

Chromatic vision can be difficult to research above threshold due to the nature of defining 'pure' colour stimuli, which is affected by factors within the eye. For this reason, colour vision research in fMRI, which by its nature requires large stimuli presented at many multiples of threshold, may be unduly affected by luminance artefacts. The papers bound in this thesis (Lowndes et al., 2024; Lowndes et al., 2021; Lowndes et al., 2023) attempt to overcome these issues at York Neuroimaging Centre using two main methods. I developed a random luminance modulating background, first designed by Birch et al (1992), for use in the neuroimaging centre using new state-of-the-art projector equipment. In using this method I sought to remove luminance artefacts by overstimulating the luminance sensitive mechanisms in visual cortex to access 'pure' chromatic responses. In chapter two, I was involved with a project investigating a population who are born without functioning cones. This condition presents a unique opportunity to probe the effects of an absence of chromatic vision from birth on cortical structure. Paradoxically, looking at the structure of the brain after the complete deprivation of chromatic information can teach us about the processing of colour in the normal population. Another way of describing this thesis is that chapter one reports two papers that use a luminance mask to attenuate the signal we can measure from the cone additive pathway (achromatic), while in chapter two I have investigated a population in which both chromatic pathways are naturally attenuated.

These methods allow this thesis to answer three questions:

- How do chromatic and achromatic signals combine in the brain, and can models of this combination be used to predict detection thresholds?
- How do the different behavioural effects of spatial frequency in different chromatic directions relate to brain responses?
- How does a complete loss of chromatic (as well as central) vision affect the structure of visual cortex?

This introduction will provide the context that is essential for answering these questions.

Cells in the retina and beyond

Two types of photoreceptors mediate human vision: rods and cones. Rods are responsible for vision in scotopic, or very low, illumination conditions, while cones are responsible for vision at photopic, or high light levels. Light levels that produce signals in both rods and cones are termed mesopic (Forbes,

1928). Rods and cones contain the photopigment rhodopsin and iodopsin respectively (Brown & Wald, 1964; Wald et al., 1955). There are around 92 million rods in each eye, compared to around 5 million cones (Curcio et al., 1990). Despite the densely packed rod mosaic, rod-initiated vision has poor visual acuity. The signals from many rods map onto single retinal neurons leading to high sensitivity to light at the cost spatial resolution. Conversely, many retinal neurons receive input from very small numbers of cone photoreceptors, leading to high spatial resolution, particularly in the cone-only foveola, at the cost of absolute light sensitivity. Cones are tightly packed together in the fovea, decreasing in spatial density with increasing eccentricity. Gaps in the parafoveal cone photoreceptor mosaic are filled with the smaller outer segments of rods (Curcio et al., 1990).

There are three classes of cone photoreceptors, known as short (S), medium (M) and long (L) wavelength (Hurvich & Jameson, 1957; Jameson & Hurvich, 1968) which are named for their differing absorption properties. L and M cones maximally absorb the longer (557nm) and medium (530nm) wavelengths respectively. S cones maximally absorb the shortest wavelength of the three, at 426nm (Merbs & Nathans, 1992). Though the photopigments in each type of cone preferentially absorb certain wavelengths, they also absorb light at other wavelengths, and each photoreceptor can only make a single univariate response to light (Rushton & Baker, 1964). Thus, combinations of opponent cone responses are necessary to discriminate between light spectra (De Valois, Smith, Karoly, & Kitai, 1958; De Valois, Smith, Kitai, & Karoly, 1958).

Retinal ganglion cells combine cone photoreceptors into one cone-additive and two cone-opponent pathways that project to different layers of the lateral geniculate nucleus (LGN). These layers are defined by the structural characteristics of the cells that make up each layer. Magnocellular (M) cells are found in the lowest two layers of LGN and receive inputs from ganglion cells forming the L+M+S (achromatic) pathway. Parvocellular (P) cells form the next four LGN layers and receive input from ganglion cells forming the L-M (red-green) pathway. Koniocellular (K) cells form layers in between the main six LGN layers and receive inputs from the S-(L+M) pathway (blue-yellow). From the LGN, all three pathways project to primary visual cortex (referred to as V1 from here on). Chromatic and achromatic pathways terminate in separate layers of V1, leading researchers to believe that their signals remain initially segregated (Livingstone & Hubel, 1988). Bound in my first chapter is a paper suggesting that these signals are not as separate and independent as the historical work would suggest and that V1 must therefore integrate signals arising from the canonical pathways (Lowndes et al., 2024).

Cortical visual areas

From V1 information is passed to V2 (Federer et al., 2009). V1 and V2 pass information to V3, V3a and V4 (see figure 1). V4, on the ventral surface, has been shown to be very sensitive to chromatic stimuli (Goddard et al., 2011; McKeefry & Zeki, 1997; Mullen, 2019; Mullen et al., 2015; Wade et al., 2002; Zeki et al., 1991). Continuing along the ventral visual stream, VO1 and VO2 are also associated with chromatic vision (Arcaro et al., 2009; Brewer et al., 2005; Jiang et al., 2007). Conversely, dorsal V3a is associated with motion selectivity (Klaver et al., 2008; Mikellidou et al., 2018; Tootell et al., 1997) and previous work has shown no chromatic stimuli activation in V3a (Wade et al., 2008) and a strong preference for achromatic stimuli (Mullen et al., 2007). However, other work has shown V3a involvement in colour processing (Castaldi et al., 2013; D'Souza et al., 2011; Liu & Wandell, 2005; Mullen et al., 2010). Bound in my first chapter is my paper which has also found evidence of chromatic processing in V3a (Lowndes et al., 2023). Continuing along the dorsal visual stream, TO1 and TO2, the retinotopic analogue of human MT+, are considered colour invariant and associated with motion processing (Amano et al., 2009; Zeki et al., 1991).

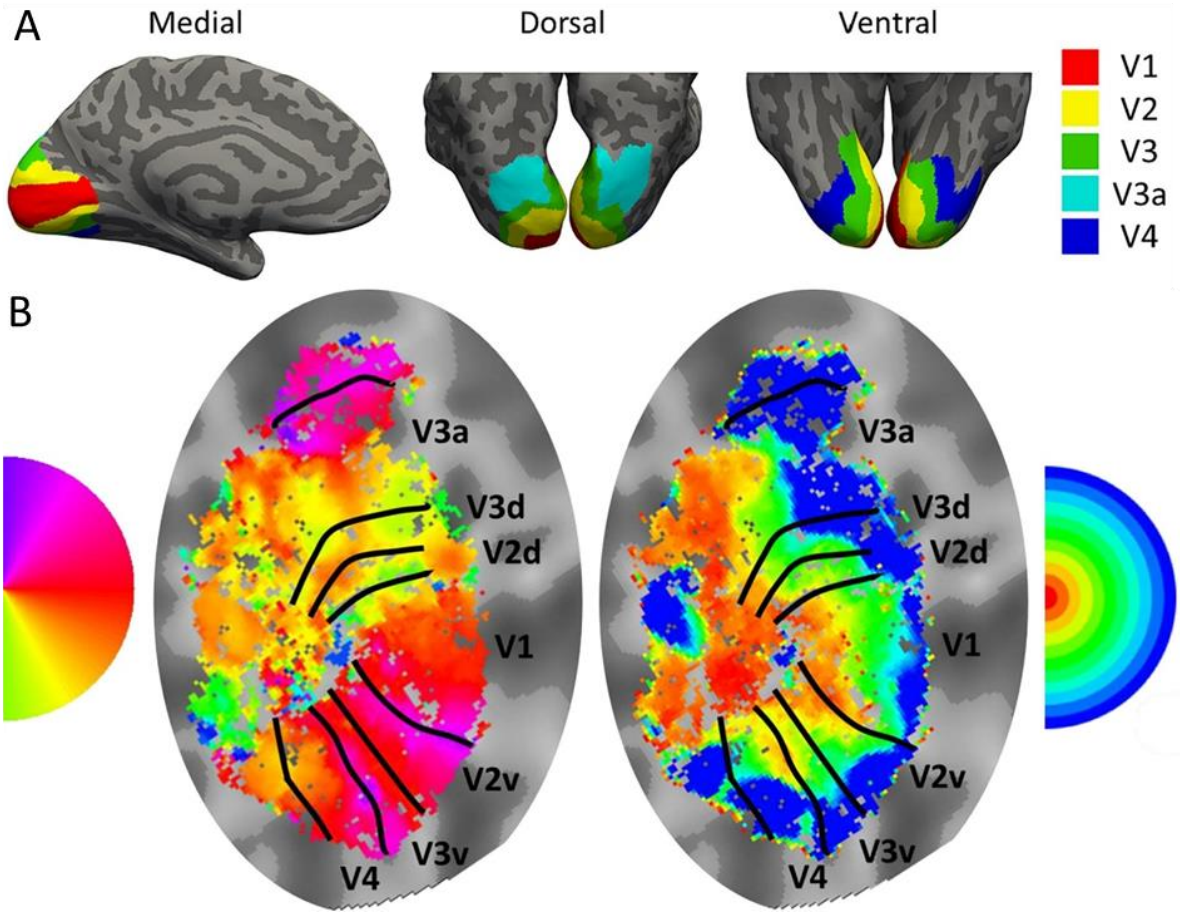

Figure 1: A) Adapted from Lowndes et al (2024). The medial, dorsal and ventral views of an inflated brain surface for one participant. B) Adapted from Lowndes et al (2023). The flattened representation of the left hemisphere of the same participant showing phase map (left) and eccentricity map (right). Visual area boundaries are displayed on the maps. Lowercase "v" and "d" indicate ventral and dorsal areas respectively.

An area of the brain can be considered retinotopically organised if the inputs that drive neurons in that area are arranged in a specific reflection of retinal geometry. That is, each area of visual space is represented cortically near to its neighbour in retinal space. This is adhered to across visual cortex, but the map of visual space is unevenly represented due to cortical magnification of the central visual field (Tootell et al., 1998). Because visual cortex represents the visual field in a series of contiguous maps, fMRI can reveal those mappings by acquiring responses during the presentation of a visual stimulus that moves systematically through the visual field as a function of time. The timing of the brain response therefore codes the position of the visual stimulus to which a location in the brain is sensitive. Visual field map boundaries occur at representations of the vertical and horizontal meridians. As a result, flattened representations of timing (phase) of the BOLD responses allow boundaries of visual areas to be drawn at reversals of map of phases as shown in Figure 1 B.

The work in chapter one used retinotopic mapping techniques outlined in detail by Welbourne et al (2018) to define visual areas V1, V2, V3, V3a, and V4. Defining the maps and drawing ROIs for each participant individually is time-consuming, but worthwhile for the accurate specification of individual areas. Individual ROI definition is particularly advantageous in the studies I have reported, with low numbers of participants being scanned numerous times. The study described in chapter two mapped visual areas of the cortex using the Benson atlas (Benson et al., 2014; Benson & Winawer, 2018). This allowed me to investigate more anterior visual areas than could feasibly be drawn using retinotopic mapping: V1, V2, V3, V3a, V3b, TO1, TO2, V4, VO1, VO2, LO1, and LO2. While an atlas-based approach is not as robust as a retinotopic approach, the necessity to scan many rare participants over numerous scanning sites outweighed the potential problems with this method.

Current understanding of chromatic vision

Psychophysical research is instrumental to our understanding of chromatic vision. The work in this thesis primarily relies on contrast detection threshold measurements, using staircase procedures. An important example for my first chapter is work by Mullen (1985), who showed that contrast sensitivity reduced as spatial frequency increases in L-M and S-(L+M) colour directions. I have also drawn from studies that used other psychophysical methods. For example, the same paper (Lowndes et al., 2023)

utilises the findings of Poirson and Wandell (1993), who used an above threshold colour matching task to show that S cone has poorer sensitivity to high spatial frequencies than L-M stimuli.

Another behavioural study central to the first chapter of this thesis is that by Barbur et al (1994). They used a background with randomly modulated achromatic luminance checks between certain contrasts to mask the effects of luminance artefacts in a detection threshold study and reported that the chromatic target and achromatic background components of the stimuli were independent of each other, suggesting that signals elicited by chromatic and achromatic stimuli are entirely separable over the range of conditions tested. However, Chen et al (2000a) found that chromatic and achromatic detection thresholds were actually interdependent in a manner that could be effectively modelled by a divisive contrast normalisation mechanism (Chen et al., 2000b). Divisive contrast normalisation is thought of as canonical of human neural computation (Carandini & Heeger, 2012) and all chromatic cortical neurons show evidence of divisive contrast normalisation in the primary visual cortex of macaques (Solomon & Lennie, 2005). To arbitrate between the apparent independence shown by Barbur (1994) and the interdependence found by Chen (2000a), my first chapter describes a psychophysical and fMRI study on the combinations of responses to achromatic and chromatic stimuli (Lowndes et al., 2024).

Functional neuroimaging has also attempted to understand colour perception in humans. One particular study that influenced my research was Engel, Zhang and Wandell (1997) who demonstrated that cortical responses in V1 and V2 to colour stimuli strongly resembled their psychophysical measurements in both the S-(L+M) and L-M chromatic planes. This finding led me to ensure that each of the functional neuroimaging studies I have reported included an analogous psychophysical detection threshold experiment. When results from neural and behavioural modalities can agree about an effect, there is more convincing evidence for that effect.

In the same vein, fully understanding colour vision requires more than just understanding the function and behaviour of colour perception in the normally sighted. I was fortunate enough to have been involved in a consortium project which scanned a cohort of congenital achromats, who had no cone function from birth, discussed in chapter two of this thesis (Lowndes et al., 2021; Molz et al., 2023; Molz et al., 2022) . Visual deficits like this can act as a lesion model for the type of vision that is deficient allowing researchers to non-invasively investigate the relationship between visual deficits and cortical architecture. Extensive research has shown grey matter abnormalities in the visual cortex of people with congenital visual loss caused by congenital cataracts (Guerreiro et al., 2015), albinism (Neveu et al., 2008; von dem Hagen et al., 2008), amblyopia (Chan et al., 2004; Li et al., 2013; Xiao et al., 2007), as well as in later visual loss, caused by macular degeneration (Boucard et al., 2009; Hernowo et al.,

2014), retinitis pigmentosa (Kitajima et al., 1997) and glaucoma (Boucard et al., 2009; Chen et al., 2013; Li et al., 2012). Similarly, functional MRI has shown a large body of evidence for cortical reorganisation related to visual loss (Bridge & Watkins, 2019; Cheung & Legge, 2005; Eysel et al., 1999; Merabet & Pascual-Leone, 2010; Sanda et al., 2018), though this remains controversial (Makin & Krakauer, 2023). For review of structural abnormalities related to visual deficits see Brown and colleagues (2016).

Chapter 1: A novel method to investigate chromatic vision reveals cortical responses can predict behavioural thresholds

Bound thesis paper 1: Lowndes, R., Aveyard, R., Welbourne, L., Wade, A., & Morland, A. (2024). In primary visual cortex fMRI responses to chromatic and achromatic stimuli are interdependent and predict contrast detection thresholds

Bound thesis paper 2: Lowndes, R., Welbourne, L., Williams, M., Gouws, A., Wade, A., & Morland, A. (2023). Increasing spatial frequency of S-cone defined gratings reduces their visibility and brain response more than for gratings defined by L-M cone contrast. *Vision Research*, *207*, 108209.

The first method I employed to investigate chromatic vision in the brain was to look at functional MRI responses to colour stimuli in visual cortex. York NeuroImaging Centre was well-placed at the time to examine this, having acquired a state-of-the-art projection system alongside MRI facilities. As a technician, part of my role was to provide users of the centre with new methods to push forward with their science. Historically, work on colour has needed to use relatively low contrast and small stimuli to ensure correct cone contrast, but in fMRI this would lead to a poor signal-to-noise ratio. Due to the need for high contrast stimuli that subtended much of the visual field for use in fMRI, many researchers expressed that they never felt completely sure that their results were not due to aberrations or poor specification of cone contrast, particularly in the periphery. I wanted to develop and provide proof-of-concept for a method of investigating colour vision in normally sighted people that allowed for large, higher contrast stimuli, without having to specify cone contrast for each individual. Barbur (1993; 1994) had reported independence of the random luminance modulation (RLM) background he developed and chromatic overlays in his study, so I developed this further for use in fMRI.

Random luminance modulation background development

Barbur et al developed a random luminance modulating stimuli that they claimed effectively masked the luminance signals present in chromatic target stimuli (1993; 1994; 1992). The original design consisted of an array of checks subtending 4 degrees of visual angle. Each check was 12 arcmin (or 0.2 degrees of visual angle) squared. Each check chose a randomly selected value between given contrast

values every 0.05 seconds. Overlayed on the checks were colour target stimuli, which were either solid squares of colour, or vertical bars of colour over every other column of checks. The task was to determine the presence or absence of vertical bars. The study reported chromatic contrast detection thresholds that were independent of the background luminance contrast, which the authors suggest shows that chromatic and achromatic signals are processed separately. Following this work, another group of researchers used this method to investigate colour responses in visual cortex using fMRI (Wade et al., 2008). I used these works together to inform my stimulus definition as shown in table 1.

	Barbur et al., 1994	Wade et al., 2008	Lowndes et al., 2024	Lowndes et al., 2023
Check size (°)	0.2	1	0.2	0.2-0.4
Check update rate	20Hz	1Hz	20Hz	20Hz
RLM contrasts	0-35%	<24%	3.125-50%	50%
Target size (°)	4	12	20	10
Target type	Vertical bars or squares	Random	Gratings	Gratings
Target SF	1.25cpd (vertical bars)	NA	1.25cpd	1.25 and 2.5cpd

Table 1. A table showing the different parameters used for stimuli set up of two previous experiments which used random luminance modulating backgrounds (Barbur et al., 1994; Wade et al., 2008) alongside the papers bound in this thesis (Lowndes et al., 2024; Lowndes et al., 2023). My work matched the work by Barbur as closely as possible, but with larger stimuli sizes for use in fMRI.

The Random Luminance Modulation (RLM) stimuli I developed from Barbur et al (1992) consists of two components: an achromatic background and a chromatic or achromatic target grating. The background consists of checks which were specified to be as similar as possible to the original work, consisting of 0.2° (or 12arcmin) checks which randomly select a luminance level between 3.125 and

50% contrast and update every 0.05 seconds. The target gratings were superimposed onto this background at differing chromatic directions and spatial frequencies. The rationale behind the stimuli was that it is very difficult or impossible to display chromatic stimuli for every individual and across the large eccentricities of the retina without some amount of luminance artefacts affecting the response. The higher the chromatic contrast, and the larger the area of vision covered by chromatic stimuli, the more luminance artefacts we would expect. The RLM background I employed ensured that there was a high baseline response to achromatic stimulus, so responses to achromatic luminance artefacts from mechanisms that respond to achromatic stimulation would be undetectable. This is particularly helpful in fMRI studies, in which we need to display stimuli at relatively high cone contrasts and sizes in order to increase the signal and be able to detect responses from the brain.

I attempted to conform to as many of the stimulus parameters outlined in Barbur et al (1992) as possible, given the nature of the fMRI studies I wanted to conduct. However, the original stimuli only subtended 4°, and I wanted to use larger stimuli to ensure the signal was as high as possible for use in fMRI, to ensure I could access stimulus responses from the brain. For that reason, my grid extended 20 degrees of visual angle with the chromatic element consisting of the entire extent of the background for one study (Lowndes et al., 2024) and 10 degrees for the other (Lowndes et al., 2023).

Combinations of chromatic and achromatic signals

Before we can use the RLM background to answer questions about chromatic vision in the brain, we must first determine how separable signals arising from the RLM background and chromatic targets are. Barbur, Harlow and Plant (1994) suggested that responses to the RLM background and target are completely independent, demonstrating no change in threshold for chromatic targets dependent on achromatic background contrast in normal participants. However, close inspection of the results from this study shows some increases in threshold may be present at the highest RLM contrast modulation (35%). I was interested in whether I could show the independence that Barbur suggested in threshold data, and whether the neural signals I could detect in fMRI followed any independence or interdependence.

To uncover the nature of combinations of achromatic and chromatic signals in the brain I applied the RLM method both behaviourally and in fMRI (Lowndes et al., 2024). In both parts of my study, I used five different contrast levels of the achromatic background with chromatic targets superimposed. In the behavioural study, I used a standard staircase procedure to estimate detection threshold of the target grating in on achromatic (L+M+S) and two chromatic (L-M and S-cone) directions. The results showed that achromatic contrast detection thresholds increased linearly with background contrast,

which follows the results found previously (Barbur et al., 1993; Barbur et al., 1994). For L-M targets, thresholds remained consistent up to 12.5% background contrast, then showed clear increases at 25 and 50% background contrast. S- cone signals showed a similar pattern. This is not consistent with the conclusions made by Barbur and colleagues (1994) who suggested that the background and target were independent of each other up to 35% RLM background contrast in all chromatic directions.

To investigate the nature of independence or potential interdependence of chromatic and achromatic signals in the cortex, I also performed an event-related fMRI experiment. I recruited 7 participants with normal or corrected-to-normal vision with refractive correction no more than five dioptres. This used similar stimuli as before, now presenting the achromatic background and chromatic target concurrently in two second trials. I then averaged the percent signal change found in V1 for each participant for each of 25 compound conditions. The results of this analysis are shown in figure 2, which show an increase in response with increasing achromatic contrast, and a smaller increase in response as chromatic contrast increases in both directions (L-M and S). The range of chromatic responses reduces with increasing achromatic contrast, suggestive of some interdependence of the chromatic and achromatic signals, as was the case in the behavioural experiment. I also noted that L-M and S-cone responses were remarkably similar, despite the L-M contrasts used being many more multiples of threshold than S – cone. Past research has shown that BOLD response to S cone stimuli correlates better with contrast than threshold (Mullen et al., 2007).

I initially used three models to investigate the potential mechanisms behind these results, shown in the left columns of figure 2 A, B and C. The independent model assumes no dependence of achromatic contrast on chromatic responses and vice-versa. The selective chromatic contrast normalisation model is drawn from Chen et al (2000b) and assumes that there is a normalising effect of achromatic contrast on chromatic responses, but not vice-versa. The mutual chromatic-achromatic contrast normalisation model assumes that there is mutual normalisation between chromatic and achromatic contrast and responses. Of these three models, the selective model best described the fMRI results in V1, closely followed by the mutual model.

Engel, Zhang and Wandell (1997) previously showed that signals in the brain elicited by chromatic stimuli can reflect behavioural thresholds, so my next step was to investigate whether the models that fit the brain data well could also predict behavioural thresholds. I achieved this by calculating the response to chromatic and achromatic contrast separately for each model. I then calculated the gradient of these responses with respect to chromatic contrast at every achromatic response level. That result was then multiplied by a free parameter (see Lowndes et al,. 2024 section 2.6 for details). The results of this model fit are show in the left three graphs of figure 3. It is clear from the figure and

the AIC and R^2 values shown that the selective model provides the best fit for the behavioural data, as well as the fMRI data, suggesting that achromatic contrast has a normalising effect on chromatic responses, but not vice-versa.

I also extracted the ROIs for other visual areas up the visual hierarchy: V2, V3, V3a and V4. The results of this analysis showed that responses to achromatic responses were increasingly compressive further up the visual hierarchy, while chromatic responses largely retained their dynamic range. Maintaining a large dynamic range for encoding colour, while reducing the response to achromatic contrast, could allow the visual system to optimise processing to more salient aspects of an image, for example colourful objects in a scene. Responses to L-M and S cone stimuli were again similar to each other, despite the large difference in multiples of threshold.

Alternative models

A fourth model that accounted for potential non-linearities in the fMRI responses in V1 was also considered. The alternative model assumed a linear combination of chromatic and achromatic neural responses, the result of which was then passed through a further compressive non-linearity (Naka-Rushton), which would occur if the neural to hemodynamic response function was not linear. This model fit my fMRI data in V1 very well (Figure 2 A right column), with a lower AIC value (-113.44) than the previous best model, selective chromatic contrast normalisation (-98.42). A nonlinearity between neural and BOLD responses (which will henceforth be denoted with a * symbol) is possible but evidence has shown that the neural to hemodynamic response can be modelled as linear in V1 (Boynton et al., 1996). As outlined in Lowndes et al (2024), the independent* model would not be able to account for the changes we found in chromatic detection thresholds with increasing achromatic background contrast, due to there being no dependence of chromatic response on achromatic contrast so I chose not to take this model further into the analysis.

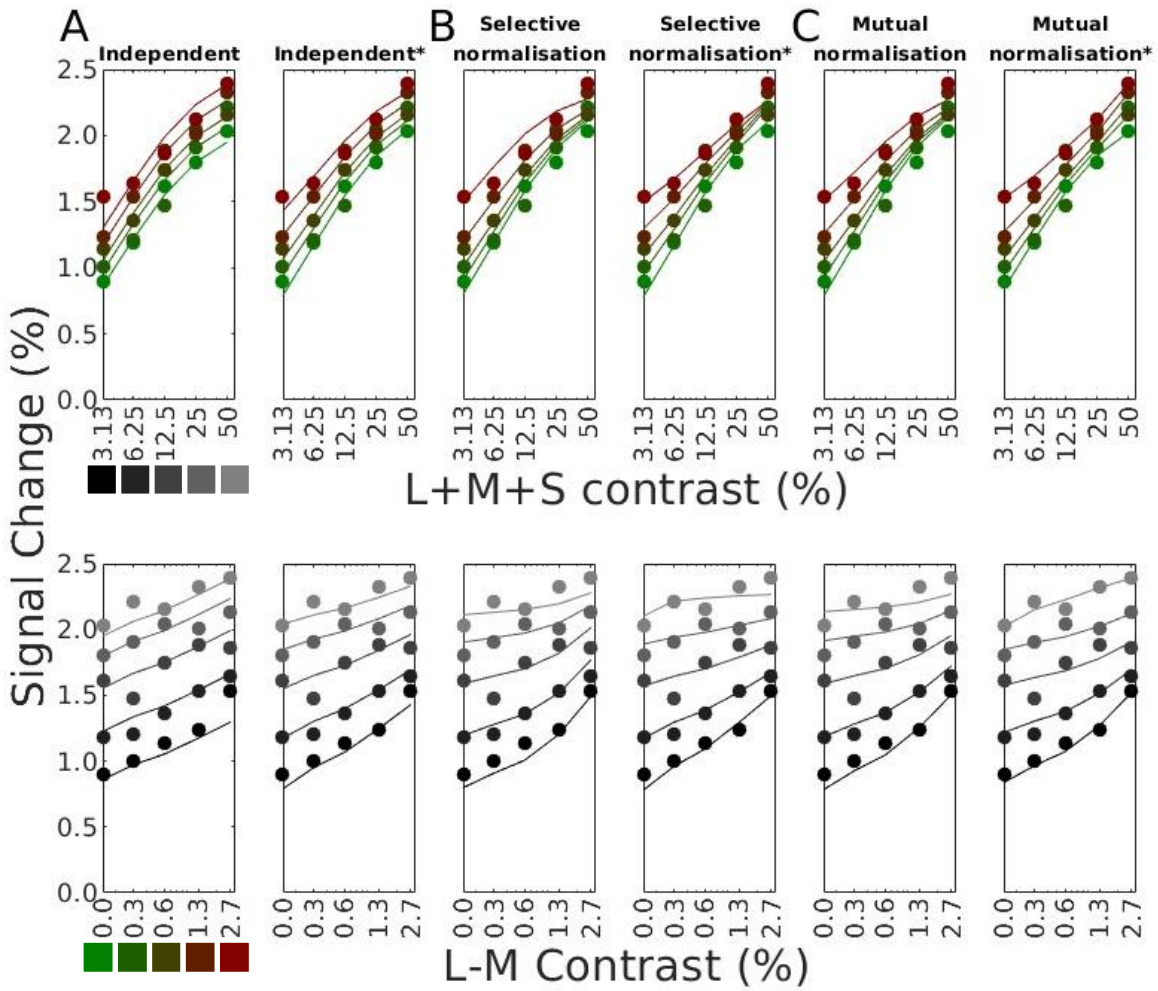

Figure 2: Adapted from Lowndes et al (2024). A figure showing the percentage signal change averaged across all participants and both runs for all 25 stimulus conditions in the fMRI sessions, with the L-M condition used as an example. Top panels are responses to L-M plotted along the achromatic contrast axis, with the chromatic contrast increasing from green to red. Bottom graphs show the same data, this time plotted against the L-M contrast axis with the achromatic contrast increasing as the dots move from black to grey. A: The graphs in the first column show the independent model fits, the second show the independent model fits with an additional compressive model of the BOLD response. B: The graphs in the first column show the selective chromatic contrast normalisation model fits, the second show this model with an additional compressive model of the BOLD response. C: The graphs in the first column show the mutual chromatic achromatic contrast normalisation model fits, the second show this model with an additional compressive model of the BOLD response.

There are some models of hemodynamic non-linearities that could theoretically predict changes in detection thresholds. For completeness, I extend the published work here by taking each of the other candidate models (from the paper) and passed the resultant sum through a further Naka-Rushton

equation (Figure 2 B and C) and found that each model was improved by the addition of post-neural compressive non-linearity (selective*: -98.86, mutual*: -114.74) indicating that these models are more likely to explain the data in V1 than the models outlined in the paper. I then used the parameters found for V1 for each of these models to predict behavioural thresholds as before (Figure 3). The independent* model fits the data better than the original independent model, owing to an improved ability to predict the achromatic detection thresholds but, as in the original independent model, chromatic threshold predictions are flat. Interestingly, the models that would in theory be able to predict chromatic detection threshold changes perform even worse, often predicting a reduction in chromatic detection threshold with increasing achromatic contrast. The AIC and adjusted R^2 values are poor when compared to the original candidate models. The inconsistency between brain models and behaviour further supports our conclusion that this data is capturing the interdependencies of neural populations and not the non-linearity of BOLD response.

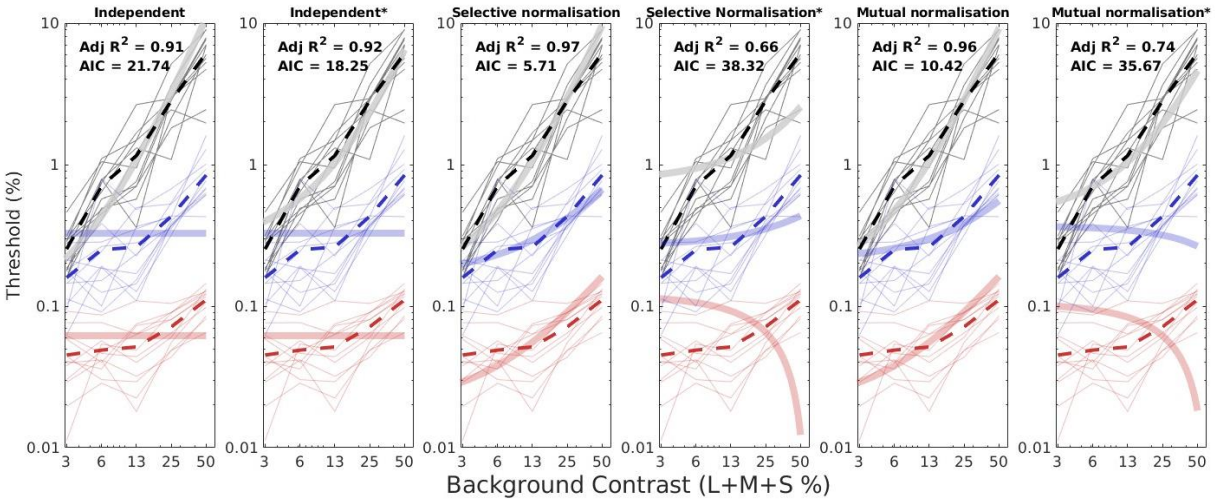

Figure 3. Adapted from Lowndes et al (2024). A figure showing the behavioural thresholds obtained by individuals (thin light grey, blue and red lines) and the mean (dashed lines) for L+M+S, L-M and S colour directions against the different achromatic background contrast levels (3.125-50%). Each graph displays the same data. The thick transparent lines show the model fit for each model as predicted by the models of V1 results for the independent, selective chromatic contrast normalisation, and mutual chromatic-achromatic contrast normalisation models, alongside their compressive BOLD model counterparts. The AIC value at the top of each graph is the sum of the individual AIC values for each colour direction.

In conclusion, this work added to understanding about how chromatic and achromatic signals combine in the brain. Chromatic and achromatic signals are interdependent in a way that can be modelled with divisive contrast normalisation. Although the signals are not independent from each other, we can still

detect strong chromatic responses using the RLM background even at high background contrasts. This chromatic response is also well preserved up the visual hierarchy, while the response to achromatic background contrast is not.

Chromatic responses to different spatial frequencies

Having shown that chromatic responses can be detected using the RLM background at 50% achromatic contrast, I will now describe another study I conducted using this same background. This time, I aimed to uncover whether the RLM background could be used to demonstrate longstanding psychophysical effects, and how that is reflected in cortical responses. I chose to look at spatial frequency since visibility of chromatic stimuli reduced as spatial frequency increased, due to the low-pass nature of chromatic vision (Mullen, 1985, 2002; Poirson & Wandell, 1996; Welbourne et al., 2018). Furthermore, the effect of increasing spatial frequency on sensitivity is greater for S cone than for L-M stimuli (Poirson & Wandell, 1993). I first aimed to assess whether this effect could be replicated using the RLM background, then I investigated whether the effect was reflected in the cortical response using fMRI. The spatial frequencies chosen were based on previous work on colour-matching of suprathreshold stimuli (Poirson & Wandell, 1993). They showed differences in sensitivity to S cone and L-M stimuli which starts to emerge between ~1.25 and ~2.5cpd (figure 4).

I used a standard two interval forced choice procedure to calculate ~80% detection thresholds at 1.25cpd and 2.5cpd for both L-M and S cone stimuli (figure 4). The L-M stimuli had greater sensitivity (lower threshold) than S cone stimuli at both spatial frequencies in every participant tested. A 2x2 ANOVA showed a significant interaction between colour direction and spatial frequency. Though there is some reduction in L-M sensitivity at higher spatial frequencies, the interaction was driven by the greater reduction in sensitivity (increase in threshold) for S cone stimuli. This is in line with the previous work by Poirson and Wandell (1993).

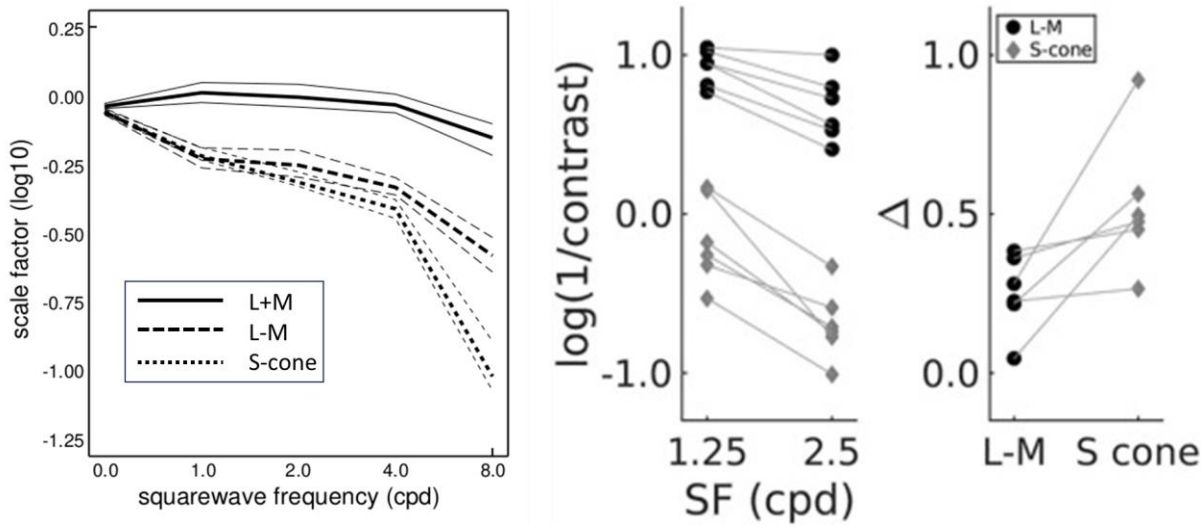

Figure 4. Left plot is adapted from Poirson and Wandell (1993) showing results of an above threshold colour-matching task in two participants. The y-axis 'scale factor' is analogous to sensitivity, and the x-axis is spatial frequency in cycles per degree. The middle and right figures are taken from Lowndes et al (2023). The middle plot shows the inverse log of the cone contrast thresholds (analogous to sensitivity) for L-M and S-cone conditions at the test spatial frequencies of 1.25 and 2.5 cpd. The dots and diamonds represent each participant's individual threshold and lines are drawn between each participant's threshold at each spatial frequency. The right plot shows the difference (Δ) between sensitivities shown in the left panel at 1.25 cpd and 2.5 cpd for L-M and S-cone conditions. Dots represent the difference for each participant and lines are drawn between their L-M and S-cone Δ values.

My next aim was to assess if this behavioural effect was reflected in the brain data. I used a block design to scan participants in L-M and S cone directions, using the highest contrast (2.7% and 10.5% respectively) used in the previous paper (Lowndes et al., 2024) at both 1.25 and 2.5 cpd. ROIs were defined retinotopically using a separate scan as shown in figure 1 B in the introduction (V1, V2, V3, V3a, V4). Additionally, TO1/2 was defined using the Benson atlas (Benson & Winawer, 2018). TO1/TO2 combined serve as an analogue to MT+ which shows preferences for motion stimuli and low responses to chromatic stimuli (Mullen et al., 2007; Wandell et al., 1999). The responses from each brain area to both chromatic conditions and spatial frequencies are shown in figure 5 and reveal a robust response to colour in all ROIs tested excluding TO1/2, which showed minimal responses in all conditions. There is a reduction in response for both L-M and S cone gratings at the higher spatial frequency (2.5cpd) which appears to be consistent across visual areas. A 3-way ANOVA revealed a significant interaction between visual area, colour direction and spatial frequency. There was also a significant interaction between spatial frequency and colour direction, which seems to be driven by the low response to

higher spatial frequency S cone stimuli present in all visual areas. To confirm this, I then ran a 2x2 ANOVA for each visual area separately, which revealed a significant interaction between spatial frequency and colour direction in V1 and V2, with V4 approaching significance (p = .053).

I also added an achromatic grating condition at 15% contrast to assess whether any achromatic luminance artefacts would affect the BOLD response in the chromatic conditions. The achromatic condition revealed very minimal responses to the relatively high contrast grating, especially when compared with the significantly higher responses found for chromatic stimuli. That I found little response to relatively high contrast achromatic stimulation reassures me that the responses I detected to chromatic stimuli will not be influenced by luminance artefacts, because any artefact would be of much lower contrast than we have tested.

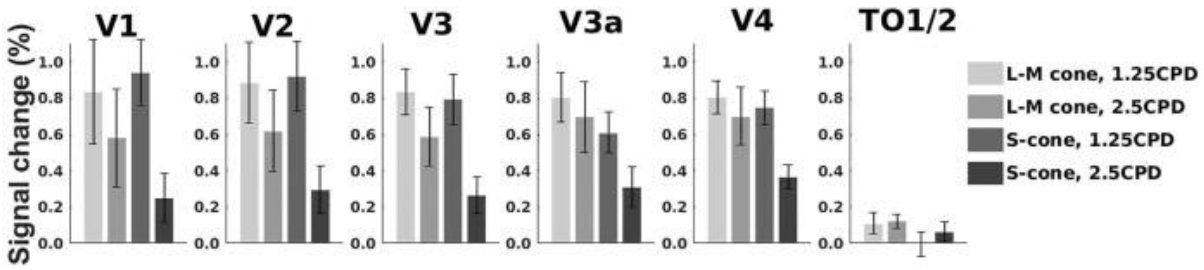

Figure 5: Taken from Lowndes et al (2023), a figure showing the fMRI responses to L-M and S cone conditions at each visual area tested (V1, V2, V3, V3a, V4 and TO1/2).

Interim discussion: chapter 1

The work bound in this chapter has demonstrated the utility of the RLM background in colour vision research. I have calculated behavioural thresholds and found that achromatic detection thresholds are dependent on achromatic background contrast, as was shown in the original Barbur work (Barbur et al., 1993; Barbur et al., 1994). Additionally, I have shown that chromatic detection thresholds increase with achromatic RLM background contrast, unlike the historical work, but aligning well with more recent research (Chen et al., 2000a). In fMRI, I have again demonstrated that responses to chromatic gratings are dependent on achromatic background contrast, but not vice versa. I have also replicated the historical work that showed an increase in detection threshold for higher spatial frequency S gratings that is more dramatic than for L-M gratings (Poirson & Wandell, 1993, 1996).

Both projects have demonstrated a link between brain responses and behaviour. In one project, I used modelling of V1 responses to accurately predict behavioural thresholds (Lowndes et al., 2024). In another project, brain responses to chromatic gratings aligned with behaviour in V1 and V2. Using

brain responses and behavioural thresholds in tandem allows us to draw stronger conclusions from our data since we have results from two different metrics. The following chapter will investigate a third modality to investigate colour vision by looking at the structure of visual cortex.

Examining the extrastriate results for both projects, we can see that in both the chromatic response does not reduce much up the visual hierarchy, while in one experiment the achromatic response became increasingly compressive. That chromatic information is preserved in more anterior visual regions while achromatic information is downweighted, may allow for more efficient visual processing. Additionally, in both projects S cone responses were surprisingly similar to L-M responses despite the latter being many more times psychophysically defined threshold. Other work has shown that cortical S cone response correlates better with contrast than detection threshold (Mullen et al., 2007). There is evidence from single-cell recordings in primates that S cone responses are processed differently, doubling in response between LGN and V1 when compared to the contribution of L and M cells (De Valois et al., 2000). My research along with others is therefore suggestive of some additional contrast normalisation of S cone stimuli, leading to amplified signals in V1 (Georgeson & Sullivan, 1975; Mullen et al., 2007). However, it is also of note that S-cone responses are slower in primary visual cortex than L/M opponent signals which could suggest that S cone signals are amplified in V1 through recurrent excitatory networks (Cottaris & De Valois, 1998). Further research is needed to determine the relative contributions of contrast normalisation and amplifications through recurrent networks.

Chapter 2: Structure of the brain in the absence of chromatic vision

Bound thesis paper 3. Lowndes, R., Molz, B., Warriner, L., Herbik, A., De Best, P. B., Raz, N., ... & Baseler, H. A. (2021). Structural differences across multiple visual cortical regions in the absence of cone function in congenital achromatopsia. *Frontiers in Neuroscience*, *15*, 718958.

Other relevant co-authored papers:
Molz, B., Herbik, A., Baseler, H. A., de Best, P. B., Vernon, R. W., Raz, N., … Lowndes, R., … & Morland, A. B. (2022). Structural changes to primary visual cortex in the congenital absence of cone input in achromatopsia. *NeuroImage: Clinical*, *33*, 102925.

Molz, B., Herbik, A., Baseler, H. A., de Best, P., Raz, N., Gouws, A., … Lowndes, R., … & Hoffmann, M. B. (2023). Achromatopsia—Visual Cortex Stability and Plasticity in the Absence of Functional Cones. *Investigative ophthalmology & visual science*, *64*(13), 23-23.

My contribution
I assisted with the data collection of ACHM participants and controls collected at York (14 total). I also helped with the preprocessing of the data and early analysis. These contributions led to me being selected as a co-author on the two papers written by Molz (2023; 2022). Subsequently, I conducted an independent analysis with my own research questions and hypotheses, supervised by Heidi Baseler and Antony Morland, which led to bound thesis paper 3.

As part of my role as a technician, I collaborated with a multi-centre consortium investigating the effects of achromatopsia (ACHM) on visual cortex. ACHM is a rare, largely stationary, congenital disorder characterised, in its complete form, by a dysfunction in all three cone photoreceptors from birth (Hirji et al., 2018; Remmer et al., 2015), leading to a total loss of colour perception. As the central fovea is solely occupied by cone photoreceptors, ACHM also leads to a loss of central vision. Though ACHM causes other symptoms, such as nystagmus and photophobia, I was most interested in the effects of colour and central vision loss. Following my work in chapter one, which showed consistencies between colour perception and neural responses, ACHM participants provided the opportunity to investigate how a total absence of colour perception can impact the anatomy of visual cortex. I can therefore use ACHM as a 'colour lesion' model to investigate the same visual areas as before and hopefully demonstrate some similar areas that play a role in perception in the normally sighted in my first chapter and are affected by a lack of colour in this chapter. Despite the wealth of evidence of structural and functional abnormalities in visual cortex in people with visual deficits (Brown et al., 2016), there was very little MRI work in ACHM at the inception of this work (Baseler et

al., 2002; Morland et al., 2001). Though my interests are primarily in chromatic vision, it will be difficult to parse whether effects we see in ACHM are caused by the loss of chromatic vision alone or the loss of central vision, but I can make estimations based on what we know about the behaviour of individual ROIs in previous research.

While ACHM provides a lesion model of colour, linking with the other chapters of this thesis, there are other important potential impacts of this work. The consequences of changes in the structure and function of visual cortex in ACHM could limit the efficacy of gene therapeutic interventions which has shown promise in other ophthalmologic diseases (Ashtari et al., 2011; DiCarlo et al., 2018). Nothing close to full restoration of colour perception in ACHM has yet been achieved (McKyton et al., 2023) and while this outcome may result from a lack of recovery at a retinal level, structural cortical changes may also affect these outcomes. In congenital cataracts the degree of visual restoration is inversely related to the extent of the abnormalities found in the visual cortex (Guerreiro et al., 2015; Guerreiro et al., 2016). However, despite some previous work showing functional cortical reorganisation in visual cortex of ACHM participants (Baseler et al., 2002), structural differences between ACHM and controls had not yet been investigated. Detailed structural reporting may provide a non-invasive confirmation of the feasibility of gene therapeutic interventions in ACHM populations, perhaps even on an individual-by-individual basis. The consortium project data we had collected therefore provided me the opportunity to investigate the structural differences in ACHM across visual cortex to answer the following hypotheses:

1. Differences in visual cortex will be present in visual areas that have large central representations. Due to the central rod scotoma, these areas have been deprived of input since birth. Early visual areas with large central representations, V1, V2 and V3 may therefore show differences.
2. Ventral visual areas such as V4, VO1 and VO2 would also be expected to show differences due to the central bias of these regions (Arcaro et al., 2009; Brewer et al., 2005; Winawer & Witthoft, 2015) and their preferential colour responses (Jiang et al., 2007; Mullen, 2019; Zeki et al., 1991).
3. I would not expect changes in the dorsal stream due to the peripheral bias of these areas (Tootell et al., 1997; Wandell et al., 2007) and their invariance to chromatic stimulation (Wade et al., 2008).

Cohort data collection approach

In total, we recruited 17 ACHM participants and 42 normal vision controls. We genetically confirmed the most common ACHM gene mutations, CNGA3 and CNGB3 in all participants, and electroretinographically confirmed total absence of cone function (McCulloch et al., 2015) to ensure that there would be no residual cone function affecting the results. The necessity to recruit as many as we could of this extremely rare cohort outweighed the potential negatives of scanning at three different sites (University of York, Hadassah Medical Centre and University of Magdeburg). We tried to mitigate these differences by reducing the variability in parameters we could control. Two sites used the same type of MRI scanner, and all three sites used Siemens 3T MRI scanners to take a single, T1-weighted anatomical scan for each participant, with the parameters matched as closely as possible across sites. All data was transferred for analysis in York and underwent identical analysis pipelines.

In brief, the analysis pipeline consisted of the following: anatomical scans were first segmented into grey and white matter using Freesurfer (Dale et al., 1999; Fischl et al., 1999). An anatomically defined retinotopic atlas (Benson & Winawer, 2018) was used to delineate 12 ROIs (V1, V2, V3, V3a, V3b, TO1, TO2, V4, VO1, VO2, LO1, LO2, see Figure 6). I extracted the entire cortical field representation of each hemisphere, rather than restricting by eccentricity, because chromatic deficits are not specific to central vision; also, eccentricity is less accurately quantified in higher visual areas (but see Molz et al (2022) for eccentricity analysis). I then computed cortical volume, thickness and surface area using Freesurfer (Dale et al., 1999; Fischl et al., 1999).

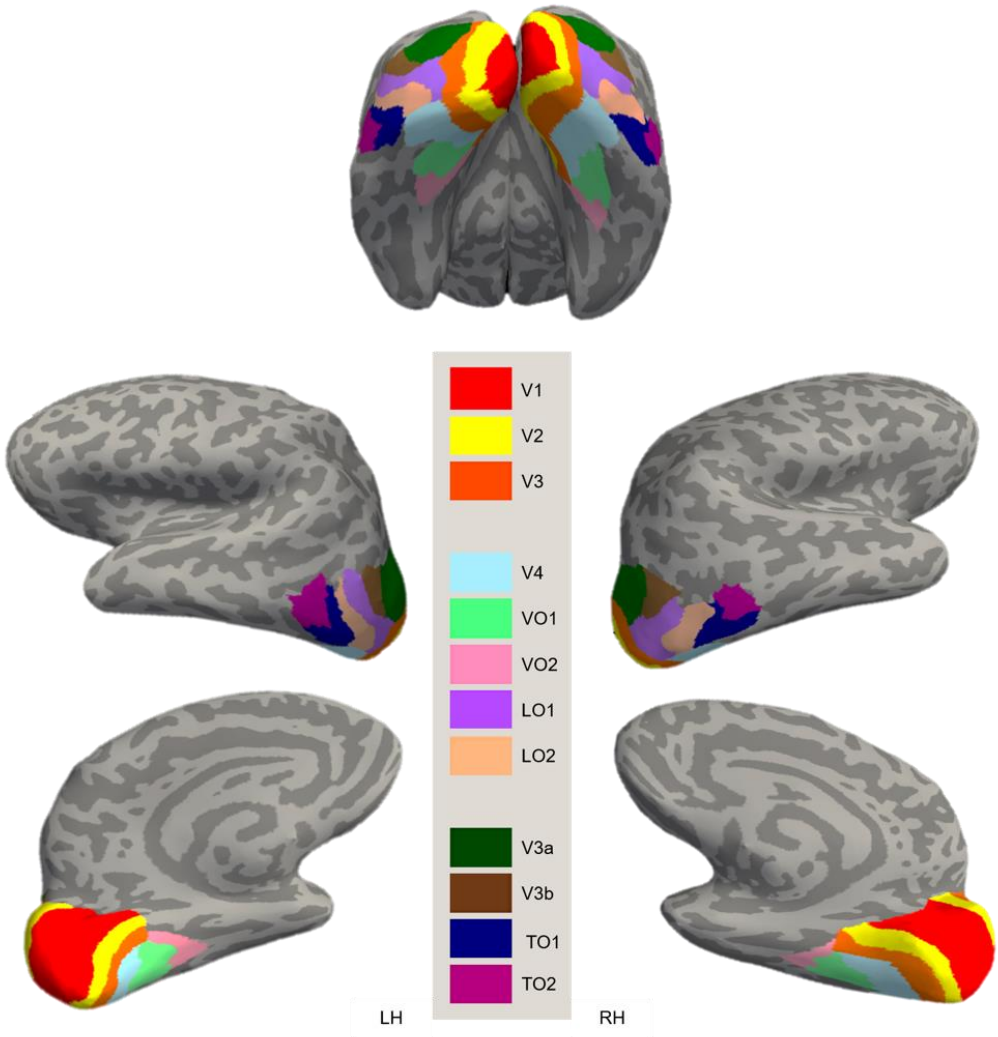

Figure 6: Adapted from Lowndes et al (2021). A figure showing an example of the ROIs used for analysis in one participant. All ROIs were taken from the anatomical retinotopic Benson atlas (Benson et al., 2014; Benson & Winawer, 2018).

Structural Changes across Visual Cortex

This led to a large amount of data to manage and interpret. To reduce the degrees of freedom, it would be beneficial to average values across hemispheres. For this reason, I first conducted a 2x2x12 mixed-measures ANOVA (subject group x hemisphere x ROI) which showed no significant interactions with hemisphere for any metric tested (grey matter volume, cortical thickness and cortical surface area). This allowed me to simplify the data to be analysed by combining across hemispheres. I have summarised the combined cortical thickness, cortical surface area and grey matter volume data into violin plots (see figure 7). As shown, grey matter volume and surface area generally decrease with more anterior regions up to V3b, while cortical thickness increases. ACHM generally show smaller

values than controls in grey matter volume and surface area, but the picture is less clear for cortical thickness. Some ROIs could be argued to show higher thickness values in ACHM, particularly V3b and LO1.

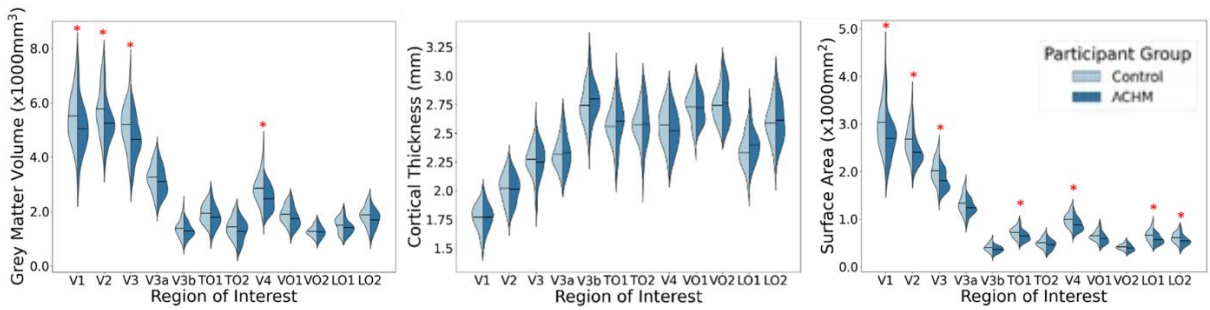

Figure 7: Adapted from Lowndes et al (Lowndes et al., 2021). A figure showing a violin plot for each metric of grey matter volume (left), cortical thickness (middle) and surface area (right) for ACHM and controls. Red stars indicate significant differences between groups for that ROI in post-hoc comparisons.

Subsequently, I performed three Analyses of Covariance (ANCOVAs), separately for each metric, which considered many potential explanatory variables. The categorical variables were participant group (ACHM and control), ROI, gender and scanner site while the potential covariates were age and the global sum (or average when considering thickness) of that metric. The important interaction was the ROI x participant group interaction, as a significant interaction here would mean that there is a difference in the way ACHM affects some ROIs and not others in the metric being tested. Participant group by ROI interaction was significant for both surface area and grey matter volume but not for cortical thickness. The decrease in volume we found is thus likely to be driven by the decrease in surface area.

I then conducted post-hoc tests for each ROI individually for both cortical volume and surface area (Figure 7). There were significant reductions in cortical surface area in ACHM participants in numerous visual areas: V1, V2, V3, TO1, V4 and LO1. Grey matter volume was reduced in ACHM in a smaller subset of ROIs: V1, V2, V3 and V4. This is consistent with hypothesis one, which suggests early visual areas V1, V2 and V3 with large central field representations would show differences in ACHM. I have also shown differences in ventral visual area V4, consistent with our second hypothesis, but no differences in higher ventral visual areas VO1 and VO2. These areas have both been associated with chromatic vision (Arcaro et al., 2009; Brewer et al., 2005; Jiang et al., 2007), so we were surprised by this result. These areas are very small, and may be more susceptible to type two errors, which may explain our lack of significant effect in these areas. That I found our most profound differences in V1,

V2, V3 and V4, is consistent with the work outlined in chapter one, which showed that functional responses in V1, V2 and V4 align well with behavioural measures of colour perception.

I found no significant changes in dorsal visual areas V3a and V3b, despite their sharing hierarchical position with V4, aligning well with hypothesis three. Dorsal visual areas have been shown to be invariant to chromatic stimuli in certain circumstances (Wade et al., 2008) but see Lowndes et al (2023). Dorsal regions also show a more peripheral field bias (Tootell et al., 1997; Wandell et al., 2007) so we would not necessarily expect these areas to be affected by ACHM. I also found a lack of consistency of response to colour stimuli and behavioural colour responses in V3a in chapter one.

The decreases we saw in ACHM participants were in the metrics of surface area and grey matter volume, but we did not show any increases in cortical thickness, unlike previous work which has shown increases in cortical thickness (Aguirre et al., 2016; Molz et al., 2022; Park et al., 2009). We have used the entire cortical representation of each visual area, and our measurements may not be sensitive to any localised increase in thickness. This led to our further study, examining different eccentricity representations of V1.

Eccentricity analysis increases sensitivity to cortical thickening

Since my analysis took the entire eccentricity representation of each ROI tested, it is impossible to say whether any null results we found were from a lack of sensitivity to differences in specific eccentricities. For example, we might have expected increases in thickness in ACHM in cortical areas representing the visual loss. For that reason, a follow-up study investigating V1 at different eccentricities, fovea (0°-2°), parafovea (2°-4°), and paracentral (4°-8°), was conducted and reported here for context (Molz et al., 2022). This time we found a significant increase in cortical thickness in ACHM compared to controls which was restricted to the fovea. This thickening may seem counter-intuitive, as there should be little to no input to this region due to the central rod scotoma. However, previous research on the congenitally blind has shown increased cortical thickness in primary visual cortex (Aguirre et al., 2016; Park et al., 2009). Increased cortical thickness may be explained by an aberrant synaptic pruning process (Aguirre et al., 2017; Bourgeois et al., 1989; Guerreiro et al., 2015). Synaptic pruning is an essential facet of early neural development, whereby strong connections are reinforced, and weak connections are abolished. Normal pruning may be abolished in areas of congenital visual loss, due to lack of sensory input. That we did not find thickening in V1 in the first paper, is not surprising as we took the entire eccentricity representation of V1 for analysis, which in theory extends to 90° (Benson et al., 2014), so my previous measurements may not have been sensitive enough to pick up this difference. It should be noted that cortical thickness measurements

can be influenced by the amount of myelination (Glasser & Van Essen, 2011). Therefore, the apparent measurement of increased cortical thickness could be an effect of a reduction in myelination (Aguirre et al., 2016; Park et al., 2009).

We also examined surface area and grey matter volume in these new ROIs and we found that surface area was significantly reduced in every ROI tested, showing that surface area is affected even by areas not representing the central rod scotoma. Visual deficits in ACHM are not confined to the central fovea, as cone photoreceptors are spread across the retina, so visual deficits are present across the visual field, which appear to lead to a lack of maturation or degeneration in terms of surface area in V1 in our study. While I found significant reductions in grey matter volume in the previous study, in this work reductions in overall grey matter volume were more subtle, did not survive multiple comparisons, and was only found in the areas not representing the fovea. Grey matter volume is essentially a combination of cortical thickness and surface area, which showed opposing differences. Assessing cortical volume alone would thus not be sufficient to uncover the potential effects of sensory deprivation on visual cortex maturation and degeneration. That we found significant decreases in grey matter volume in V1 in the previous study but not this one, may show that surface area is decreasing across the eccentricity representation, or that the areas tested in this study were too small to show significant changes.

No corresponding functional changes

Following the structural research, further work has investigated the effects of ACHM on the function of the visual cortex (Molz et al., 2023). Changes related to function imply functional reorganisation and may provide further evidence supporting the functional work I have outlined in the first chapter of this thesis. Additionally, functional reorganisation may have further implications for gene therapeutic interventions for ACHM; if the cortex is sufficiently reorganised, the mature cortex may not be sufficiently plastic to process the new cone signals after treatment. Previous work had shown that ACHM participants exhibited rod-initiated responses in areas dedicated to cone responses in normal controls, indicating some plasticity and reallocation of the otherwise unused cortical space (Baseler et al., 2002). The consortium aimed to build on the earlier case study work with a larger more representative cohort of ACHM participants. Each participant completed up to standard pRF mapping and eccentricity mapping scans both in photopic (daylight) and in scotopic (dark adapted) conditions. This study found no evidence of functional reorganisation in ACHM participants, in contrast to the previous case study work (Baseler et al., 2002) suggesting that functional reorganisation may occur in individuals, but is not a general feature of ACHM.

Interim discussion: chapter 2

Molz (2023) suggested that the structural differences we found in both structural papers were due to a lack of maturation. Since synaptic pruning is required for mature cortex to develop, the absence of synaptic pruning may be an indicator of a poorly developed cortex. Two out of the three ACHM participants who have shown reorganisation in primary visual cortex previously in Baseler et al (2002) had some residual cone function which may have given some early input to central areas of V1, leading to maturation of the cortical region. This may have given the more normally functioning area the ability to reorganise to be able to represent more peripheral areas. Our work may in the future offer a non-invasive method of testing if ACHM participants would benefit from gene therapeutic intervention ahead of time to inform patient choices, and perhaps eventually give individualised estimates of outcomes.

Taken together, these studies show significant structural differences, but little evidence of functional differences between ACHM and controls. We cannot conclude that functional differences do not exist between these populations however, as the functional experiments can by their nature only be performed on stimuli that the participants can see. Restoring the function of cones in ACHM is still in its infancy, but early research suggests some restoration of ability to perceive the colour red (McKyton et al., 2023). Further work should investigate any structural and functional reorganisation that may occur in these cone-restored participants over time.

Discussion

The aim of this thesis was to understand the cortical function and structure underpinning colour perception in humans. The studies that address this aim have been presented in this thesis in two parts: the normal behaviour and cortical signals associated with chromatic vision, and a lesion model of how no chromatic visual information from birth is associated with brain structure. Since each chapter has been individually discussed, this section will focus on avenues for future research related to the studies described.

Although in each study I examined both dorsal and ventral visual areas, I have not conducted any explicit testing of ventral and dorsal differences in chromatic processing or structural changes. The structural work outlined in chapter two did not show any structural differences between ACHM and control participants in dorsal areas V3a and V3b, which could suggest a lack of chromatic processing in these areas. However, dorsal cortical areas are also associated with a more peripheral bias than ventral areas (Tootell et al., 1997; Wandell et al., 2007), which could also explain the lack of difference in structure compared to controls in this population, in which peripheral vision remains relatively intact. However, both studies outlined in the first chapter indicate that there is some processing of chromatic stimuli in dorsal visual area V3a (Lowndes et al., 2024; Lowndes et al., 2023), unlike previous work using the RLM background which showed no dorsal involvement in colour processing (Wade et al., 2008). In future work I would like to explicitly test dorsal chromatic processing to understand these inconsistencies. For example, Wade and colleagues (2008) used a similar RLM background but their chromatic stimuli were spatially identical to the RLM background, with checks of colour and achromatic background updating in the same way, unlike my work which has used gratings. Perhaps the lack of chromatic effect in dorsal areas in Wade's work, and the presence of an effect in mine, could be due to the preference of dorsal areas for structure in motion (Koyama et al., 2005). The chromatic grating maybe a potent stimulus for dorsal visual areas, while coloured 'noise' with no structure, and unidirectional blocks of colour would not. I would therefore hypothesise that a dorsal response to chromatic stimuli would be present for chromatic gratings, but not for structureless chromatic 'noise' or blocks of colour. The responses in primary visual cortex will be a useful gauge of whether double opponent neurons with spatial frequency tuning (Johnson et al., 2008) or the silencing or edge detectors in unstructured noise stimuli (Hubel & Wiesel, 1962, 1968) are affecting responses, or lack thereof, in dorsal visual areas.

Another surprising result in colour vision research is that of Welbourne et al (2018) who showed that there was no significant difference in pRF sizes for chromatic and achromatic stimuli. Larger pRF sizes would be expected for chromatic stimuli due to the lower spatial resolution of chromatic vision which

I have discussed in chapter one (Lowndes et al., 2023). There may be some achromatic artefacts affecting the pRF size results. Due to my success in utilising the RLM method, I would be interested to replicate this study with a noise background to determine whether the previous results were due to an artefact of the stimulus, or a genuine, yet surprising, absence of an effect.

The RLM technique used in chapter one allows for a wide range of stimulus parameters to be investigated. For example, it would be worthwhile to examine responses in V1 many more spatial frequencies in order to model BOLD derived contrast-sensitivity functions, which could be informative of the relative contributions of band-pass and low-pass mechanisms. It is worth noting however, that these studies would require many more scans hours, and a dedicated participant pool who were willing to be scanned many times.

At the time of publishing the paper bound in chapter two (Lowndes et al., 2021), research on gene therapeutic interventions in ACHM was in its infancy but had shown some improvements in reductions in photo aversion and an increased ability to see red (Fischer et al., 2020; McKyton et al., 2021). Since this work, researchers have focused on the application of the treatment to younger populations (Farahbakhsh et al., 2020; Michaelides et al., 2023), which may align with our finding of widespread cortical differences in an adult population. The next step in this research should look at the brains of children with ACHM, to map the cortical changes across childhood, and inform appropriate age of intervention. However, this intervention is generally safe and adult ACHM participants have shown some benefits (Fischer et al., 2020), so whenever in the lifespan intervention is available it should be offered. Additional future work should look at the visual cortex structure of ACHM participants who receive gene therapeutic intervention longitudinally, to understand the plasticity of the cortex and whether this is correlated with any behavioural improvements.

The paper bound in chapter two cannot sufficiently separate the effects of the loss of high acuity vision and the loss of chromatic vision. One way to overcome this may be to recruit S cone monochromat participants, who have similarly poor acuity, but some colour discrimination (Green, 1972) as well as some dichromats, with high visual acuity, but poor colour discrimination (Jägle et al., 2006). Assessing the relative differences between these participants and the normally sighted, should allow for separation of the effects of the loss of chromatic vision, and of high acuity vision.

In conclusion, this thesis has provided novel contributions to the field of colour vision in our understanding of how the early visual cortex and beyond processes colour stimuli functionally, and how chromatic deprivation affects brain structure. The differing approaches in chapter one and two have allowed for a more complete dissemination of the current understanding of colour vision in this thesis than either method alone. The future directions suggested will together build a more full picture of colour-sensitive cortical structures and how they function.

References

Aguirre, G. K., Butt, O. H., Datta, R., Roman, A. J., Sumaroka, A., Schwartz, S. B., Cideciyan, A. V., & Jacobson, S. G. (2017). Postretinal structure and function in severe congenital photoreceptor blindness caused by mutations in the GUCY2D gene. *Investigative ophthalmology & visual science*, *58*(2), 959-973.

Aguirre, G. K., Datta, R., Benson, N. C., Prasad, S., Jacobson, S. G., Cideciyan, A. V., Bridge, H., Watkins, K. E., Butt, O. H., & Dain, A. S. (2016). Patterns of individual variation in visual pathway structure and function in the sighted and blind. *PLoS One*, *11*(11), e0164677.

Amano, K., Wandell, B. A., & Dumoulin, S. O. (2009). Visual field maps, population receptive field sizes, and visual field coverage in the human MT+ complex. *Journal of neurophysiology*, *102*(5), 2704-2718.

Arcaro, M. J., McMains, S. A., Singer, B. D., & Kastner, S. (2009). Retinotopic organization of human ventral visual cortex. *Journal of Neuroscience*, *29*(34), 10638-10652.

Ashtari, M., Cyckowski, L. L., Monroe, J. F., Marshall, K. A., Chung, D. C., Auricchio, A., Simonelli, F., Leroy, B. P., Maguire, A. M., & Shindler, K. S. (2011). The human visual cortex responds to gene therapy–mediated recovery of retinal function. *The Journal of clinical investigation*, *121*(6), 2160-2168.

Barbur, J. L., Birch, J., & Harlow, A. J. (1993). Colour vision testing using spatiotemporal luminance masking. In *Colour vision deficiencies XI* (pp. 417-426). Springer.

Barbur, J. L., Harlow, J., & Plant, G. T. (1994). Insights into the different exploits of colour in the visual cortex. *Proceedings of the Royal Society of London. Series B: Biological Sciences*, *258*(1353), 327-334.

Baseler, H. A., Brewer, A. A., Sharpe, L. T., Morland, A. B., Jägle, H., & Wandell, B. A. (2002). Reorganization of human cortical maps caused by inherited photoreceptor abnormalities. *Nature neuroscience*, *5*(4), 364-370.

Benson, N. C., Butt, O. H., Brainard, D. H., & Aguirre, G. K. (2014). Correction of distortion in flattened representations of the cortical surface allows prediction of V1-V3 functional organization from anatomy. *PLoS computational biology*, *10*(3), e1003538.

Benson, N. C., & Winawer, J. (2018). Bayesian analysis of retinotopic maps. *elife*, *7*, e40224.

Birch, J., Barbur, J. L., & Harlow, A. J. (1992). New method based on random luminance masking for measuring isochromatic zones using high resolution colour displays. *Ophthalmic and Physiological Optics*, *12*(2), 133-136.

Boucard, C. C., Hernowo, A. T., Maguire, R. P., Jansonius, N. M., Roerdink, J. B. T. M., Hooymans, J. M. M., & Cornelissen, F. W. (2009). Changes in cortical grey matter density associated with long-standing retinal visual field defects. *Brain*, *132*(7), 1898-1906.

Bourgeois, J.-P., Jastreboff, P. J., & Rakic, P. (1989). Synaptogenesis in visual cortex of normal and preterm monkeys: evidence for intrinsic regulation of synaptic overproduction. *Proceedings of the National Academy of Sciences*, *86*(11), 4297-4301.

Boynton, G. M., Engel, S. A., Glover, G. H., & Heeger, D. J. (1996). Linear systems analysis of functional magnetic resonance imaging in human V1. *Journal of Neuroscience*, *16*(13), 4207-4221.

Brewer, A. A., Liu, J., Wade, A. R., & Wandell, B. A. (2005). Visual field maps and stimulus selectivity in human ventral occipital cortex. *Nature neuroscience*, *8*(8), 1102-1109.

Bridge, H., & Watkins, K. E. (2019). Structural and functional brain reorganisation due to blindness: the special case of bilateral congenital anophthalmia. *Neuroscience & Biobehavioral Reviews*, *107*, 765-774.

Brown, H. D. H., Woodall, R. L., Kitching, R. E., Baseler, H. A., & Morland, A. B. (2016). Using magnetic resonance imaging to assess visual deficits: a review. *Ophthalmic and Physiological Optics*, *36*(3), 240-265.

Brown, P. K., & Wald, G. (1964). Visual pigments in single rods and cones of the human retina. *Science*, *144*(3614), 45-52.
Carandini, M., & Heeger, D. J. (2012). Normalization as a canonical neural computation. *Nature Reviews Neuroscience*, *13*(1), 51-62.
Castaldi, E., Frijia, F., Montanaro, D., Tosetti, M., & Morrone, M. C. (2013). BOLD human responses to chromatic spatial features. *European Journal of Neuroscience*, *38*(2), 2290-2299.
Chan, S.-t., Tang, K.-w., Lam, K.-c., Chan, L.-k., Mendola, J. D., & Kwong, K. K. (2004). Neuroanatomy of adult strabismus: a voxel-based morphometric analysis of magnetic resonance structural scans. *NeuroImage*, *22*(2), 986-994.
Chen, C.-C., Foley, J. M., & Brainard, D. H. (2000a). Detection of chromoluminance patterns on chromoluminance pedestals I: threshold measurements. *Vision research*, *40*(7), 773-788.
Chen, C.-C., Foley, J. M., & Brainard, D. H. (2000b). Detection of chromoluminance patterns on chromoluminance pedestals II: model. *Vision research*, *40*(7), 789-803.
Chen, W. W., Wang, N., Cai, S., Fang, Z., Yu, M., Wu, Q., Tang, L., Guo, B., Feng, Y., & Jonas, J. B. (2013). Structural brain abnormalities in patients with primary open-angle glaucoma: a study with 3T MR imaging. *Investigative ophthalmology & visual science*, *54*(1), 545-554.
Cheung, S.-H., & Legge, G. E. (2005). Functional and cortical adaptations to central vision loss. *Visual neuroscience*, *22*(2), 187-201.
Cottaris, N. P., & De Valois, R. L. (1998). Temporal dynamics of chromatic tuning in macaque primary visual cortex. *Nature*, *395*(6705), 896-900.
Curcio, C. A., Sloan, K. R., Kalina, R. E., & Hendrickson, A. E. (1990). Human photoreceptor topography. *Journal of Comparative Neurology*, *292*(4), 497-523.
D'Souza, D. V., Auer, T., Strasburger, H., Frahm, J., & Lee, B. B. (2011). Temporal frequency and chromatic processing in humans: an fMRI study of the cortical visual areas. *Journal of Vision*, *11*(8), 8-8.
Dale, A. M., Fischl, B., & Sereno, M. I. (1999). Cortical surface-based analysis: I. Segmentation and surface reconstruction. *NeuroImage*, *9*(2), 179-194.
De Valois, R. L., Cottaris, N. P., Elfar, S. D., Mahon, L. E., & Wilson, J. A. (2000). Some transformations of color information from lateral geniculate nucleus to striate cortex. *Proceedings of the National Academy of Sciences*, *97*(9), 4997-5002.
De Valois, R. L., Smith, C. J., Karoly, A. J., & Kitai, S. T. (1958). Electrical responses of primate visual system: I. Different layers of macaque lateral geniculate nucleus. *Journal of comparative and physiological psychology*, *51*(6), 662.
De Valois, R. L., Smith, C. J., Kitai, S. T., & Karoly, A. J. (1958). Response of single cells in monkey lateral geniculate nucleus to monochromatic light. *Science*, *127*(3292), 238-239.
DiCarlo, J. E., Mahajan, V. B., & Tsang, S. H. (2018). Gene therapy and genome surgery in the retina. *The Journal of clinical investigation*, *128*(6), 2177-2188.
Engel, S., Zhang, X., & Wandell, B. (1997). Colour tuning in human visual cortex measured with functional magnetic resonance imaging. *Nature*, *388*(6637), 68-71.
Eysel, U. T., Schweigart, G., Mittmann, T., Eyding, D., Qu, Y., Vandesande, F., Orban, G., & Arckens, L. (1999). Reorganization in the visual cortex after retinal and cortical damage. *Restorative neurology and neuroscience*, *15*(2-3), 153-164.
Farahbakhsh, M., Anderson, E. J., Rider, A., Greenwood, J. A., Hirji, N., Zaman, S., Jones, P. R., Schwarzkopf, D. S., Rees, G., & Michaelides, M. (2020). A demonstration of cone function plasticity after gene therapy in achromatopsia. *medRxiv*, 2020-2012.
Federer, F., Ichida, J. M., Jeffs, J., Schiessl, I., McLoughlin, N., & Angelucci, A. (2009). Four projection streams from primate V1 to the cytochrome oxidase stripes of V2. *Journal of Neuroscience*, *29*(49), 15455-15471.
Fischer, M. D., Michalakis, S., Wilhelm, B., Zobor, D., Muehlfriedel, R., Kohl, S., Weisschuh, N., Ochakovski, G. A., Klein, R., & Schoen, C. (2020). Safety and vision outcomes of

subretinal gene therapy targeting cone photoreceptors in achromatopsia: a nonrandomized controlled trial. *JAMA ophthalmology*, *138*(6), 643-651.
Fischl, B., Sereno, M. I., & Dale, A. M. (1999). Cortical surface-based analysis: II: inflation, flattening, and a surface-based coordinate system. *NeuroImage*, *9*(2), 195-207.
Forbes, W. T. M. (1928). An interference theory of color vision. *The American Journal of Psychology*, *40*(1), 1-25.
Georgeson, M. A., & Sullivan, G. D. (1975). Contrast constancy: deblurring in human vision by spatial frequency channels. *The Journal of physiology*, *252*(3), 627-656.
Glasser, M. F., & Van Essen, D. C. (2011). Mapping human cortical areas in vivo based on myelin content as revealed by T1-and T2-weighted MRI. *Journal of Neuroscience*, *31*(32), 11597-11616.
Goddard, E., Mannion, D. J., McDonald, J. S., Solomon, S. G., & Clifford, C. W. G. (2011). Color responsiveness argues against a dorsal component of human V4. *Journal of Vision*, *11*(4), 3-3.
Green, D. G. (1972). Visual acuity in the blue cone monochromat. *The Journal of physiology*, *222*(2), 419-426.
Guerreiro, M. J. S., Erfort, M. V., Henssler, J., Putzar, L., & Röder, B. (2015). Increased visual cortical thickness in sight-recovery individuals. *Human brain mapping*, *36*(12), 5265-5274.
Guerreiro, M. J. S., Putzar, L., & Röder, B. (2016). Persisting cross-modal changes in sight-recovery individuals modulate visual perception. *Current Biology*, *26*(22), 3096-3100.
Hernowo, A. T., Prins, D., Baseler, H. A., Plank, T., Gouws, A. D., Hooymans, J. M. M., Morland, A. B., Greenlee, M. W., & Cornelissen, F. W. (2014). Morphometric analyses of the visual pathways in macular degeneration. *Cortex*, *56*, 99-110.
Hirji, N., Georgiou, M., Kalitzeos, A., Bainbridge, J. W., Kumaran, N., Aboshiha, J., Carroll, J., & Michaelides, M. (2018). Longitudinal assessment of retinal structure in achromatopsia patients with long-term follow-up. *Investigative ophthalmology & visual science*, *59*(15), 5735-5744.
Hubel, D. H., & Wiesel, T. N. (1962). Receptive fields, binocular interaction and functional architecture in the cat's visual cortex. *The Journal of physiology*, *160*(1), 106.
Hubel, D. H., & Wiesel, T. N. (1968). Receptive fields and functional architecture of monkey striate cortex. *The Journal of physiology*, *195*(1), 215-243.
Hurvich, L. M., & Jameson, D. (1957). An opponent-process theory of color vision. *Psychological review*, *64*(6p1), 384.
Jägle, H., de Luca, E., Serey, L., Bach, M., & Sharpe, L. T. (2006). Visual acuity and X-linked color blindness. *Graefe's Archive for Clinical and Experimental Ophthalmology*, *244*, 447-453.
Jameson, D., & Hurvich, L. M. (1968). Opponent-response functions related to measured cone photopigments. *JOSA*, *58*(3), 429_421-430.
Jiang, Y., Zhou, K., & He, S. (2007). Human visual cortex responds to invisible chromatic flicker. *Nature neuroscience*, *10*(5), 657-662.
Johnson, E. N., Hawken, M. J., & Shapley, R. (2008). The orientation selectivity of color-responsive neurons in macaque V1. *Journal of Neuroscience*, *28*(32), 8096-8106.
Kitajima, M., Korogi, Y., Hirai, T., Hamatake, S., Ikushima, I., Sugahara, T., Shigematsu, Y., Takahashi, M., & Mukuno, K. (1997). MR changes in the calcarine area resulting from retinal degeneration. *American journal of neuroradiology*, *18*(7), 1291-1295.
Klaver, P., Lichtensteiger, J., Bucher, K., Dietrich, T., Loenneker, T., & Martin, E. (2008). Dorsal stream development in motion and structure-from-motion perception. *NeuroImage*, *39*(4), 1815-1823.
Koyama, S., Sasaki, Y., Andersen, G. J., Tootell, R. B. H., Matsuura, M., & Watanabe, T. (2005). Separate processing of different global-motion structures in visual cortex is revealed by FMRI. *Current Biology*, *15*(22), 2027-2032.
Li, C., Cai, P., Shi, L., Lin, Y., Zhang, J., Liu, S., Xie, B., Shi, Y., Yang, H., & Li, S. (2012). Voxel-based morphometry of the visual-related cortex in primary open angle glaucoma. *Current Eye Research*, *37*(9), 794-802.

Li, Q., Jiang, Q., Guo, M., Li, Q., Cai, C., & Yin, X. (2013). Grey and white matter changes in children with monocular amblyopia: voxel-based morphometry and diffusion tensor imaging study. *British Journal of Ophthalmology*.

Liu, J., & Wandell, B. A. (2005). Specializations for chromatic and temporal signals in human visual cortex. *Journal of Neuroscience*, *25*(13), 3459-3468.

Livingstone, M., & Hubel, D. (1988). Segregation of form, color, movement, and depth: anatomy, physiology, and perception. *Science*, *240*(4853), 740-749.

Lowndes, R., Aveyard, R., Welbourne, L. E., Wade, A., & Morland, A. B. (2024). In primary visual cortex fMRI responses to chromatic and achromatic stimuli are interdependent and predict contrast detection thresholds. *Vision research*, *218*, 108398.

Lowndes, R., Molz, B., Warriner, L., Herbik, A., De Best, P. B., Raz, N., Gouws, A., Ahmadi, K., McLean, R. J., & Gottlob, I. (2021). Structural differences across multiple visual cortical regions in the absence of cone function in congenital achromatopsia. *Frontiers in Neuroscience*, *15*, 718958.

Lowndes, R., Welbourne, L., Williams, M., Gouws, A., Wade, A., & Morland, A. (2023). Increasing spatial frequency of S-cone defined gratings reduces their visibility and brain response more than for gratings defined by LM cone contrast. *Vision research*, *207*, 108209.

Makin, T. R., & Krakauer, J. W. (2023). Against cortical reorganisation. *elife*, *12*, e84716.

McCulloch, D. L., Marmor, M. F., Brigell, M. G., Hamilton, R., Holder, G. E., Tzekov, R., & Bach, M. (2015). ISCEV Standard for full-field clinical electroretinography (2015 update). *Documenta ophthalmologica*, *130*(1), 1-12.

McKeefry, D. J., & Zeki, S. (1997). The position and topography of the human colour centre as revealed by functional magnetic resonance imaging. *Brain: a journal of neurology*, *120*(12), 2229-2242.

McKyton, A., Averbukh, E., Ohana, D. M., Levin, N., & Banin, E. (2021). Cortical visual mapping following ocular gene augmentation therapy for achromatopsia. *Journal of Neuroscience*, *41*(35), 7363-7371.

McKyton, A., Marks Ohana, D., Nahmany, E., Banin, E., & Levin, N. (2023). Seeing color following gene augmentation therapy in achromatopsia. *Current Biology*, *33*(16), 3489-3494.e3482. https://doi.org/https://doi.org/10.1016/j.cub.2023.06.041

Merabet, L. B., & Pascual-Leone, A. (2010). Neural reorganization following sensory loss: the opportunity of change. *Nature Reviews Neuroscience*, *11*(1), 44-52.

Merbs, S. L., & Nathans, J. (1992). Absorption spectra of human cone pigments. *Nature*, *356*(6368), 433-435.

Michaelides, M., Hirji, N., Wong, S. C., Besirli, C. G., Zaman, S., Kumaran, N., Georgiadis, A., Smith, A. J., Ripamonti, C., & Gottlob, I. (2023). First-in-human gene therapy trial of AAV8-hCARp. hCNGB3 in adults and children with CNGB3-associated Achromatopsia. *American journal of ophthalmology*, *253*, 243-251.

Mikellidou, K., Frijia, F., Montanaro, D., Greco, V., Burr, D. C., & Morrone, M. C. (2018). Cortical BOLD responses to moderate-and high-speed motion in the human visual cortex. *Scientific reports*, *8*(1), 1-12.

Molz, B., Herbik, A., Baseler, H. A., de Best, P., Raz, N., Gouws, A., Ahmadi, K., Lowndes, R., McLean, R. J., & Gottlob, I. (2023). Achromatopsia—Visual Cortex Stability and Plasticity in the Absence of Functional Cones. *Investigative ophthalmology & visual science*, *64*(13), 23-23.

Molz, B., Herbik, A., Baseler, H. A., de Best, P. B., Vernon, R. W., Raz, N., Gouws, A. D., Ahmadi, K., Lowndes, R., & McLean, R. J. (2022). Structural changes to primary visual cortex in the congenital absence of cone input in achromatopsia. *NeuroImage: Clinical*, *33*, 102925.

Morland, A. B., Baseler, H. A., Hoffmann, M. B., Sharpe, L. T., & Wandell, B. A. (2001). Abnormal retinotopic representations in human visual cortex revealed by fMRI. *Acta psychologica*, *107*(1-3), 229-247.

Mullen, K. T. (1985). The contrast sensitivity of human colour vision to red-green and blue-yellow chromatic gratings. *The Journal of physiology*, *359*(1), 381-400.

Mullen, K. T. (2002). Differential distributions of red–green and blue–yellow cone opponency across the visual field. *Visual neuroscience*, *19*(1), 109-118.
Mullen, K. T. (2019). The response to colour in the human visual cortex: the fMRI approach. *Current Opinion in Behavioral Sciences*, *30*, 141-148.
Mullen, K. T., Chang, D. H. F., & Hess, R. F. (2015). The selectivity of responses to red-green colour and achromatic contrast in the human visual cortex: an fMRI adaptation study. *European Journal of Neuroscience*, *42*(11), 2923-2933.
Mullen, K. T., Dumoulin, S. O., McMahon, K. L., De Zubicaray, G. I., & Hess, R. F. (2007). Selectivity of human retinotopic visual cortex to S-cone-opponent, L/M-cone-opponent and achromatic stimulation. *European Journal of Neuroscience*, *25*(2), 491-502.
Mullen, K. T., Thompson, B., & Hess, R. F. (2010). Responses of the human visual cortex and LGN to achromatic and chromatic temporal modulations: an fMRI study. *Journal of Vision*, *10*(13), 13-13.
Neveu, M. M., Von Dem Hagen, E., Morland, A. B., & Jeffery, G. (2008). The fovea regulates symmetrical development of the visual cortex. *Journal of Comparative Neurology*, *506*(5), 791-800.
Park, H.-J., Lee, J. D., Kim, E. Y., Park, B., Oh, M.-K., Lee, S., & Kim, J.-J. (2009). Morphological alterations in the congenital blind based on the analysis of cortical thickness and surface area. *NeuroImage*, *47*(1), 98-106.
Poirson, A. B., & Wandell, B. A. (1993). Appearance of colored patterns: pattern–color separability. *JOSA A*, *10*(12), 2458-2470.
Poirson, A. B., & Wandell, B. A. (1996). Pattern—color separable pathways predict sensitivity to simple colored patterns. *Vision research*, *36*(4), 515-526.
Remmer, M. H., Rastogi, N., Ranka, M. P., & Ceisler, E. J. (2015). Achromatopsia: a review. *Current Opinion in Ophthalmology*, *26*(5), 333-340.
Rushton, W. A. H., & Baker, H. D. (1964). Red/green sensitivity in normal vision. *Vision research*, *4*(1-2), 75-85.
Sanda, N., Cerliani, L., Authié, C. N., Sabbah, N., Sahel, J.-A., Habas, C., Safran, A. B., & Thiebaut de Schotten, M. (2018). Visual brain plasticity induced by central and peripheral visual field loss. *Brain Structure and Function*, *223*, 3473-3485.
Solomon, S. G., & Lennie, P. (2005). Chromatic gain controls in visual cortical neurons. *Journal of Neuroscience*, *25*(19), 4779-4792.
Tootell, R. B. H., Hadjikhani, N. K., Mendola, J. D., Marrett, S., & Dale, A. M. (1998). From retinotopy to recognition: fMRI in human visual cortex. *Trends in cognitive sciences*, *2*(5), 174-183.
Tootell, R. B. H., Mendola, J. D., Hadjikhani, N. K., Ledden, P. J., Liu, A. K., Reppas, J. B., Sereno, M. I., & Dale, A. M. (1997). Functional analysis of V3A and related areas in human visual cortex. *Journal of Neuroscience*, *17*(18), 7060-7078.
von dem Hagen, E. A. H., Hoffmann, M. B., & Morland, A. B. (2008). Identifying human albinism: a comparison of VEP and fMRI. *Investigative ophthalmology & visual science*, *49*(1), 238-249.
Wade, A., Augath, M., Logothetis, N., & Wandell, B. (2008). fMRI measurements of color in macaque and human. *Journal of Vision*, *8*(10), 6-6.
Wade, A. R., Brewer, A. A., Rieger, J. W., & Wandell, B. A. (2002). Functional measurements of human ventral occipital cortex: retinotopy and colour. *Philosophical Transactions of the Royal Society of London. Series B: Biological Sciences*, *357*(1424), 963-973.
Wald, G., Brown, P. K., & Smith, P. H. (1955). Iodopsin. *The Journal of general physiology*, *38*(5), 623-681.
Wandell, B. A., Dumoulin, S. O., & Brewer, A. A. (2007). Visual field maps in human cortex. *Neuron*, *56*(2), 366-383.
Wandell, B. A., Poirson, A. B., Newsome, W. T., Baseler, H. A., Boynton, G. M., Huk, A., Gandhi, S., & Sharpe, L. T. (1999). Color signals in human motion-selective cortex. *Neuron*, *24*(4), 901-909.

Welbourne, L. E., Morland, A. B., & Wade, A. R. (2018). Population receptive field (pRF) measurements of chromatic responses in human visual cortex using fMRI. *NeuroImage*, *167*, 84-94.

Winawer, J., & Witthoft, N. (2015). Human V4 and ventral occipital retinotopic maps. *Visual neuroscience*, *32*, E020.

Xiao, J. X., Xie, S., Ye, J. T., Liu, H. H., Gan, X. L., Gong, G. L., & Jiang, X. X. (2007). Detection of abnormal visual cortex in children with amblyopia by voxel-based morphometry. *American journal of ophthalmology*, *143*(3), 489-493.

Zeki, S., Watson, J. D., Lueck, C. J., Friston, K. J., Kennard, C., & Frackowiak, R. S. (1991). A direct demonstration of functional specialization in human visual cortex. *Journal of Neuroscience*, *11*(3), 641-649.

Bound thesis paper 1

In primary visual cortex fMRI responses to chromatic and achromatic stimuli are interdependent and predict contrast detection thresholds

Lowndes, R., Aveyard, R., Welbourne, L., Wade, A., & Morland, A.

Vision Research

2024

Vision Research 218 (2024) 108398

Contents lists available at ScienceDirect

Vision Research

journal homepage: www.elsevier.com/locate/visres

In primary visual cortex fMRI responses to chromatic and achromatic stimuli are interdependent and predict contrast detection thresholds

Rebecca Lowndes [a,b,*], Richard Aveyard [b], Lauren E. Welbourne [a,b], Alex Wade [a,b,c], Antony B. Morland [a,b,c]

[a] Department of Psychology, University of York, United Kingdom
[b] York Neuroimaging Centre, University of York, United Kingdom
[c] York Biomedical Research Institute, University of York, United Kingdom

ARTICLE INFO

Keywords:
fMRI
Primary Visual cortex
Chromatic vision
Achromatic vision
Modelling
Interdependence

ABSTRACT

Chromatic and achromatic signals in primary visual cortex have historically been considered independent of each other but have since shown evidence of interdependence. Here, we investigated the combination of two components of a stimulus; an achromatic dynamically changing check background and a chromatic (L-M or S cone) target grating. We found that combinations of chromatic and achromatic signals in primary visual cortex were interdependent, with the dynamic range of responses to chromatic contrast decreasing as achromatic contrast increased. A contrast detection threshold study also revealed interdependence of background and target, with increasing chromatic contrast detection thresholds as achromatic background contrast increased. A model that incorporated a normalising effect of achromatic contrast on chromatic responses, but not vice versa, best predicted our V1 data as well as behavioural thresholds. Further along the visual hierarchy, the dynamic range of chromatic responses was maintained when compared to achromatic responses, which became increasingly compressive.

1. Introduction

Normal human colour vision is trichromatic with three different cone classes tuned to different wavelengths in the visual spectrum (Bowmaker & Dartnall, 1980; Brown & Wald, 1964). The three cone photoreceptors are referred to as L, tuned to long wavelengths, M, tuned to medium wavelengths, and S, tuned to short wavelengths. In the retina, these photoreceptors are combined by specialised bipolar and ganglion cells which receive opponent input from the L and M cones to form the L-M pathway and opponent input of S and the sum of L and M outputs forms the S-(L + M) pathway (Dacey & Lee, 1994). The signals generated in them are relayed along the axons of the ganglion cells to separate layers in the lateral geniculate nucleus (LGN) which has a specific cytoarchitectonic structure. The L-M signal projects to parvocellular layers, while the S opponent signal projects to the koniocellular layers (for review see Martinovic, 2014). A third pathway projects to the magnocellular layers of the LGN and is commonly referred to as L + M + S, though debate remains about the inclusion of S cones (Chatterjee & Callaway, 2002; Sun et al., 2006). While parvocellular and koniocellular layers of the LGN include projections from ganglion cells that are colour opponent (Conway, 2009), it should be noted that not all cells in these layers are colour opponent (Sincich & Horton, 2005). This means that chromatic signals are not totally segregated from achromatic signals as early in the visual system as the thalamus.

From the LGN, the parvo, magno and konio pathways project to primary visual cortex. In the macaque monkey, magnocellular projections terminate in layer 4Cα, parvocellular projections terminate in layer 4Cβ, and koniocellular projections terminate in layer 2/3 blobs (sometimes called patches) (Sincich & Horton, 2005; Van Essen & Gallant, 1994). That each pathway terminates in separate layers of V1 lead early researchers to believe that signals from magno, parvo and konio cellular layers in LGN, remain segregated, and thus, independent, at this cortical level (Livingstone & Hubel, 1988). However, this picture is overly simplistic, as the signals intermingle extensively beyond their input layers. For example, many studies emphasise that magnocellular inputs in layer 4Cα project to layer 4B, but layer 4Cα actually projects more densely to both blobs and interblobs of layers 2/3 which are associated with parvo- and konio- cellular projections respectively,

* Corresponding author.
E-mail address: rebecca.lowndes@york.ac.uk (R. Lowndes).

https://doi.org/10.1016/j.visres.2024.108398
Received 12 December 2023; Received in revised form 24 March 2024; Accepted 24 March 2024
Available online 29 March 2024

implying early mixing of the chromatic (parvo and konio) and achromatic (magno) streams (Callaway & Wiser, 1996).

Most neurons in primate V1 which respond to chromatic stimuli also respond to achromatic stimuli (Johnson et al., 2008; Shapley & Hawken, 2011) meaning that their responses are driven by both chromatic and luminance signals. Solomon and Lennie (2005) found that colour-luminance cells in V1 show normalisation primarily driven by achromatic contrast inputs. This suggests therefore that chromatic responses are influenced by achromatic responses in visual cortex, but perhaps not vice versa. Contrast normalisation is consistently shown to be a property of single cells responding to combinations of signals in the cat primary visual cortex (Bonds, 1991; Heeger, 1992; Ohzawa et al., 1982; Ohzawa et al., 1985). Contrast normalisation, usually modelled as divisive, shifts response sensitivity of a neuron to account for ambient features in the image encoded by other neurons and while this normalisation has been most often shown in the visual domain, it is considered canonical to neural computation across domains as well as species (Carandini & Heeger, 2012). Contrast normalisation therefore offers candidate models to account for interdependence of chromatic and achromatic responses in visual cortex.

Psychophysical studies have long sought to capture the behaviour of chromatic mechanisms independent of achromatic mechanisms. This is normally achieved by presenting isoluminant stimuli to silence achromatic mechanisms. Isoluminance is a challenge to specify, particularly over large areas of the visual field because wavelength dependent pre-receptoral absorption due to macular pigmentation varies over the retina (Chen et al., 2001; Davies & Morland, 2004; Hammond et al., 1997; Ruddock, 1963; Snodderly et al., 1984), as does the morphology of cone outer segments (Goodchild et al., 1996; Smith & Pokorny, 1975; Srinivasan et al., 2008). This led Barbur and colleagues (1994) to present chromatic modulations superimposed on dynamically changing luminance checks to access mechanisms sensitive to chromatic modulations alone. The thresholds for detecting chromatic modulations were largely independent of the contrast of the background checks up to 35 % achromatic contrast, lending support to independence, particularly at threshold. However, there was a linear increase in the contrast detection threshold of achromatic gratings with increasing contrast of the random checked background. That is, the increase in contrast of the random luminance checked background made it progressively more difficult to detect achromatic target stimuli. This shows that the responses to the achromatic target grating and achromatic background are, predictably, interdependent, as a change in one component of the stimulus affects the detection of another, suggestive of a single mechanism processing both the background and target. This is consistent with earlier increment threshold work, which show that increment thresholds increase with overall luminance of the stimulus (Cornsweet & Teller, 1965).

Other psychophysical work has sought to understand how interactions, driven primarily by a presumed contrast normalisation mechanism, can be characterised. Due to the orientation tuning of neurons in V1, cross orientation gratings should be stimulating independent populations of neurons. Thus, dependence of the threshold for detecting target gratings on the contrast of a background grating at a different orientation could indicate contrast normalisation. Psychophysical work on cross-orientation gratings has shown that achromatic gratings of increasing contrast increase the detection threshold of achromatic target gratings and that this effect can be accounted for on the basis of divisive contrast normalisation (Baker et al., 2007; Meese & Holmes, 2010; Petrov et al., 2005). Similarly, the detection threshold of chromatic grating targets cross-oriented with chromatic grating backgrounds also increases with background contrast (Medina & Mullen, 2009). Important for the current study is the further work using spatially identical gratings as background and target that showed increasing contrast modulation along many chromatic directions, including achromatic, can increase the contrast detection threshold along many other chromatic directions (Chen et al., 2000a). This increase in contrast detection threshold points to interdependence of achromatic and chromatic mechanisms. The authors also demonstrated that such interdependencies could be captured by a divisive contrast normalisation mechanism (Chen et al., 2000b). For a review of chromatic and luminance noise masking research, see Eskew (2009).

Much like psychophysical approaches, neuroimaging research on human colour vision has largely sought to examine chromatic and achromatic response properties of the brain separately (for review see Wandell et al., 2006). Previous work has demonstrated that BOLD responses to S cone stimuli are significantly higher relative to their detection threshold compared to responses to L-M stimuli relative to their detection threshold (Lowndes et al., 2023; Mullen et al., 2007). Wade and colleagues (2008) used a random luminance background similar to Barbur (1994) and found that L-M responses were approximately double the responses to L + M + S contrast. A random luminance background method was also used in a recent study in our lab to show that detection thresholds for colour stimuli reflect neural signals found in visual areas V1, V2 and V4, in the case of the longstanding psychophysical effect of increasing spatial frequency decreasing sensitivity to chromatic stimuli (Lowndes et al., 2023).

Relatively fewer fMRI studies have combined achromatic and chromatic responses. Engel, Zhang and Wandell (1997) presented gratings with different degrees of chromatic and achromatic signal varying from chromatic modulations alone to achromatic alone. The results showed that in cone contrast space cortical responses were larger for chromatic than for achromatic modulations in both L against M and S against (L + M) chromatic planes. Similar to our previous work, they showed a tight coupling between behavioural contrast detection thresholds and V1 and V2 responses for most of the stimulus conditions. Another study investigated the V1 response to chromatic directions around the L and M contrast plane (Barnett et al., 2021) and found that V1 was most responsive to modulations in the L-M direction at 0 cycles per degree (CPD) and that the tuning largely followed a quadratic law indicating interactions of chromatic and achromatic signals.

The current study aimed to investigate the nature and extent of interdependence of cortical responses to chromatic and achromatic stimulus components. Our second aim was to investigate whether the way cortical responses combine can predict contrast detection threshold measurements. To achieve these aims we presented chromatic targets (L-M and S cone) at different contrasts superimposed on a background of checks that also varied in contrast, in fMRI. We found an interdependence of achromatic and chromatic cortical responses in V1 demonstrated by a reduction in chromatic responses at high achromatic background contrast. We also conducted a behavioural detection threshold study that showed a significant increase in contrast detection threshold of the chromatic targets with increasing achromatic background contrast, again indicating an interdependence of chromatic and achromatic mechanisms. Both the fMRI and behavioural data were best fitted by a model that included contrast normalisation of chromatic signals. Our examination of extrastriate regions revealed an increasingly compressive response to the achromatic background which was also smaller in magnitude at more anterior regions of the visual hierarchy. However, responses to the colour target did not become any more compressive and in many cases were of the same magnitude up the visual hierarchy. Maintaining a large dynamic range for encoding colour, while reducing it for achromatic variations may offer a useful representation of visual information for perception.

2. Methods

2.1. Participants

2.1.1. fMRI experiment

Seven (seven female) colour-normal trichromats (confirmed with Ishihara's tests for colour blindness, 38 plates edition) with a mean age of 27.17 years (+- 4.58 years) were recruited for four 60-minute experimental fMRI sessions, and one retinotopy session. The ethics

committee at York Neuroimaging centre at the University of York approved the experiment.

2.1.2. Behavioural experiment

12 (9 female) colour-normal trichromats (confirmed with Ishihara's tests for colour blindness, 38 plates edition) with a mean age of 29 years (+- 5.10 years) were recruited for three 50-minute behavioural sessions. The ethics committee at York Neuroimaging centre at the University of York approved the experiment.

2.2. Experiment and stimulus design

All visual stimuli were designed and presented using PsychoPy and PsychToolBox in MATLAB. The delivery system used for the visual stimulus in the scanner was a ViewPixx projector which projected the stimulus onto a custom-made acrylic screen. The participant viewed the screen with a mirror fixed to the head coil in the scanner. Behavioural stimuli were displayed using a ViewPixx monitor. Spectral measurements of the RGB channels of the scanner and behavioural screen were made using a 'Jaz' (Ocean Optics, FL) spectrometer. Chromatic stimuli were defined using the 10-deg cone fundamentals based on the Stiles and Burch 10-deg CMFs described in Stockman and Sharpe (2000). All stimuli were specified in terms of cone contrast. No further accounting for luminance for the individual participants in this study was conducted, so if presented on a uniform background the gratings we generated could contain luminance artefacts. However, the random luminance modulation described is an effective way of rendering many of these artefacts invisible and thus supress any neural responses to achromatic artefacts. There are also some benefits to showing physically identical stimuli to all participants, as this provides consistency across participants and sessions.

2.2.1. Retinotopy stimuli

Of the seven participants that completed the fMRI experiment, six took part in retinotopy scans as described. One participant had good retinotopy previously available from another visual neuroscience experiment (Vernon et al., 2016).

The retinotopy stimulus used was identical to that used in our previous paper (Lowndes et al., 2023) and similar to that described in other work (Alvarez et al., 2015; Binda et al., 2013; Dumoulin & Wandell, 2008; Welbourne et al., 2018). 1.25 degree wide sweeping bars moved in 8 bar directions across a 20 degree diameter circular aperture with four blank periods. The bar moved in steps once for every TR length (2500 ms) in 16 steps per direction, and contained 100 % contrast noise, updating at 2 Hz. Participants preformed a button press when the fixation cross changed as an attentional task to aid fixation. Four repeats were carried out for each participant.

2.2.2. Stimuli - fMRI experiment

The stimuli used for this experiment were adapted from Birch et al (1992) and similar to that used by another study from our lab (Lowndes et al., 2023). The 'background' stimulus consisted of an array of 100x100, 0.2 degree checks, which were each assigned a grayscale value that deviated a random amount from uniform grey between five different values for different trials: ±3.125, 6.25, 12.5, 25 or 50 % L + M + S contrast. The random contrast of each check was updated every 0.05 s (20 Hz). Superimposed target gratings were additional modulations that added either L-M (0 %, 0.3 %, 0.6 %, 1.3 %, 2.7 %) or S cone (0 %, 1.313 %, 2.625 %, 5.25 %, 10.5 %) contrast. This led to 25 compound stimuli for each colour condition which subtended the entire background (20 degrees). Orientation of the target grating was vertical and contrast polarity was reversed at a rate of 1 Hz in a square-wave function. A circular mask (diameter of 20 degrees) was applied to the stimuli. The spatial frequency of the grating was chosen to be 1.25 cpd and was presented in a square-wave pattern. This was the same as the lowest spatial frequency used in a previous study in our lab which used a similar background to investigate spatial frequency differences between S cone and L-M stimuli (Lowndes et al., 2023). In that previous study, we showed BOLD responses were very similar for both chromatic conditions at 1.25 cycles per degree and 2.7 % and 10.5 % contrast for L-M and S cone, respectively. Using the same spatial frequency here, as well as selecting previously used contrasts as our highest contrasts, gives us precedent to predict that responses to each colour direction will be similar. Additionally, the relatively low spatial frequency we have chosen allows us to discount the effects of chromatic aberration, as this has an influence at higher spatial frequencies (Bradley et al., 1992; Murasugi & Cavanagh, 1988).

To further ensure that chromatic aberration would not affect our findings, we used the equation detailed by Strasburger et al (2018) to calculate the diameter of blur given as:

$$b^{\circ} = 0.057PD$$

where P is the pupil diameter in millimetres and D is the defocus in dioptres. Eye recordings were taken of participants while they were taking part in the fMRI experiment. We found that pupil diameter was 3.19 mm on average. D has been calculated as ± 0.5 in previous work over the eccentricities used in this study and over similar wavelengths (458–632 nm) to the projector limits in our study (455–625 nm). We can therefore calculate the diameter of blur to be 0.091 degrees, which would extend 0.045 degrees on either side of grating boundary. With a grating bar width of 0.4 degrees, blur from extending from each boundary is not sufficient to cover the majority of the bar width (2 x 0.045 degrees), leaving 0.309 degrees of each bar unaffected by blur and thus at the specified contrast.

A rapid event-related design was used to present the 25 unique compound stimulus types in each condition (L-M or S), with each stimulus being displayed for 2 s, 10 times in a session. The trial order and the inter-trial intervals were optimised by using Optseq2 (Dale, 1999), which we applied to generate eight unique trial orders that each lasted 1940 s. Participants were randomly assigned one of the eight unique trial orders for each session. As this long run would be arduous for participants, it was split into five, 388 s runs, all to be completed in order in one scan session for each participant. Each trial run was padded with an extra 20 s of fMRI acquisitions at the end to ensure a return to baseline, so each run comprised 408 s. We conducted four sessions (in which 5 runs were presented) per participant; in two sessions we acquired responses to L-M target gratings and in the other two we acquired responses to S target gratings.

2.2.3. Stimuli – Behavioural experiment

Behavioural experiments were performed using a VIEWPIXX display using a two-interval forced choice paradigm. The background, present for the entirety of each run, comprised an array of 100x100 squares (0.2x0.2 degrees squared) with a 20 degree circular mask at five levels of achromatic contrast (3.125, 6.25, 12.5, 25 or 50 %) which changed between runs (see Fig. 1). Target stimuli were chromatic square-wave gratings which subtended the entire background at 1.25 cpd and were either L + M + S, S cone or L-M cone contrast. First, participants used a sliding scale to estimate their threshold (pressing up and down to increase and decrease contrast until they could just see the target grating), and this was used as the starting contrast for a staircase. Target stimuli occurred during one of two potential 0.5 s presentations, with each potential presentation indicated by the fixation changing from a standard fixation (+) to a cross (x). Potential presentations were separated by a 0.5 s interval. One presentation time contained a grating and one did not. If the target grating was present in the first presentation, participants were instructed to press '1′, if it was in the second presentation, they were instructed to press '2′. A standard three-up one-down staircase adjusted the contrast and the task finished after 16 reversals or 100 trials. The ~80 % threshold was calculated as the mean of the contrast during the last 7 reversals. If there were fewer than 7 reversals in a run,

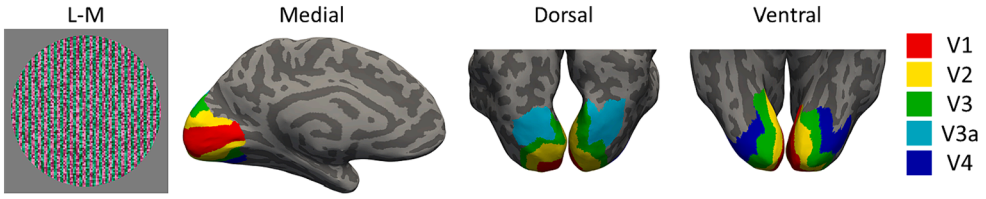

Fig. 1. Leftmost panel: an example of high contrast background stimuli with a high contrast L-M overlay. The L-M contrast has been artificially increased above the maximum used in the experiment for visibility. Right panels: The medial dorsal and ventral views of the ROIs used for one participant.

the participant was asked to return and complete this run again, beginning at a lower contrast.

2.3. MRI protocol

All scans were carried out using a Siemens 3 T MRI scanner, with a 64-channel head coil. The subject's head was positioned in the coil with foam padding to ensure the head was stable.

2.3.1. Retinotopy

76 EPI slices were taken within an FOV of 192x192mm with 1.5 mm isotropic voxels (TR = 2500 ms, TE = 40.8 ms, flip angle = 75°, voxel matrix = 128x128). Scan slices were aligned horizontally and always covered occipital and temporal lobes. Four retinotopy scans were taken for each participant.

2.3.2. fMRI experiments

36 EPI slices were taken within an FOV of 200x200mm with 2.5 mm isotropic voxels (TR = 1000 ms, TE = 30 ms, flip angle = 75°, voxel matrix = 128x128). Scan slices were aligned horizontally and always covered occipital and temporal lobes. A camera was positioned pointing at the participants left eye for blink monitoring and pupil diameter calculations.

2.3.3. Structural

In addition to functional scans, a T1-weighted and T2-weighted structural scan were taken for each subject, at a 0.8x0.8x0.8 mm resolution. The protocol for these scans was taken from the Human Connectome Project (Glasser et al., 2013).

2.4. Data processing

2.4.1. Structural

All structural scans were analysed using the HCP minimal processing pipeline (version 5.0, Glasser et al., 2013) using a combination of FSL (http://fsl.fmrib.ox.ac.uk/fsl/fslwiki/)(Smith et al., 2004) and Freesurfer (https://surfer.nmr.mgh.harvard.edu/) (Dale et al., 1999; Reuter et al., 2012).

2.4.2. Retinotopy

All data processing of retinotopy scans was performed using the 2015 version of the VISTA software (https://web.stanford.edu/group/vista/cgi-bin/wiki/index.php/Software) (Vista Lab, Stanford University), running under MATLAB 2015 (The MathWorks Inc., Natick, MA, USA). We applied pRF modelling to an average of all retinotopy scans (which had been motion corrected between and within scans using a maximum likelihood alignment routine (Nestares & Heeger, 2000)). Functional scans were aligned to individual anatomy scans using FLIRT linear registration (Jenkinson et al., 2002; Jenkinson & Smith, 2001). The retinotopic eccentricities and polar angles extracted by the pRF model were then used to draw boundaries of visual areas V1, V2, V3, V3a and V4 on a flattened representation of visual cortex; for details of the pRF model used and an example of drawn visual area boundaries, see Lowndes et al (2023). These regions of interest (ROIs) were then transformed into NIFTI files using the VISTA function roiSaveAsNifti and compared against an anatomically defined retinotopy atlas to ensure accuracy (Benson et al., 2014).

2.4.3. fMRI experiments

All five runs in a single session were concatenated to form a single run for analysis. All data were pre-processed using FSL version 5.0. Images were skull-stripped using a brain extraction tool (BET Smith, 2002). Motion correction (MCFLIRT; Jenkinson et al., 2002) was followed by spatial smoothing (Gaussian full width half medium 5 mm). Data were high pass temporal filtered (Gaussian-weighted least-squares straight line fitting with sigma = 50.0 s). Individual participant data was registered to their own high resolution structural (generated from T1 and T2 structural images using the HCP processing pipeline) using FLIRT (Jenkinson, 2001, 2002).

Previous work has shown that signals elicited by blinks may be a source of noise in fMRI signals (Gouws et al., 2014; Hupé et al., 2012), so we assessed the eye blinks in each scan to remove them as regressors of no interest. Each eye video was trimmed to the scan length and then split into individual frames. The structural similarity index measure (SSIM) (Wang et al., 2004) was calculated for consecutive image frames, low frequency movement (eg head movement) was excluded by subtracting a five-second windowed moving average from the measures, then instances of SSIM values in the lowest 5 percentiles were labelled as blinks. These were then manually confirmed. Eye blinks were then added as regressors of no interest into further analysis. One participant performed blinks infrequently (~3 blinks during a 7-minute scan), so the lowest 1 percentile was used for this participant, with blinks then manually confirmed again. The eye camera failed to record in 2 of the 42 sessions. Analysis was the same for these sessions but without this regressor of no interest.

Time-series statistical analysis was carried out using FMRIB's Improved Linear Model (FILM) with local autocorrelation correction (Woolrich et al., 2001). fMRI Expert Analysis Tool (FEAT)query was then run for visual areas V1, V2, V3, V3a and V4 with contrast of parameter estimate values converted into mean percentage signal change. For each participant, mean percentage signal change values were then averaged over the two sessions for each colour condition.

2.5. Model development

Our aim was to determine the extent to which responses to the chromatic target were dependent on the achromatic background, and potentially vice versa. We therefore fitted responses to the two components of the stimulus with one model that captured independence and two others that captured interdependence. We deployed the Naka-Rushton relationship in all models, which has been shown in numerous studies to model the achromatic contrast response function accurately in V1 of animals (Albrecht & Hamilton, 1982; DeAngelis et al., 1993) and humans (Rahimi-Nasrabadi et al., 2021). We note also that our form of the equation does not include exponent terms for the variables I and C, which are often introduced and can account for 'dipper functions' that emerge at low background contrasts. We have not removed the terms because we believe they are not useful in general, rather, our background and target contrasts are ones that are unlikely to reveal dipper-like behaviour and therefore we anticipated having little

or no data to inform on the exponent parameters. We adopt the 'exponent-free' form of the Naka-Rushton for all models. Reducing the number of free parameters in the model should also help distinguish between models. Interdependence was captured using divisive contrast normalisation, which has been shown widely in the literature to account for neural and behavioural responses (Chen et al., 2000a, 2000b; Heeger, 1992; Solomon & Lennie, 2005). Additionally, these models assume linear pre-cortical receptive fields, as has been shown to be consistent with previous data (Foley, 1994; Foley & Chen, 1997; Georgeson et al., 2016), although we note there can be early non-linearities.

Our first model assumes that the neurons responding to chromatic and achromatic components of the stimulus are independent, and thus the BOLD response should be as well. If the responses are independent, the responses to each component, chromatic and achromatic should sum linearly. Thus, our first model is a four-parameter model containing two Naka-Rushton equations summed together, henceforth referred to as the independent model:

$$R = RImax\,\frac{I}{I+I50} + RCmax\,\frac{C}{C+C50} \tag{1}$$

Where R is the BOLD response in percent signal change, I is the contrast of the achromatic component of the stimulus, RImax is the maximum response to I, and I50 is the contrast level of the achromatic background at which the achromatic response has reached half of RImax. C is the chromatic contrast, RCmax is the maximum response to C and C50 is the contrast level of C at which the response to colour has reached half of RCmax. This model cannot account for any changes in response to chromatic contrast that depend on achromatic contrast, or vice-versa, and thus, would predict no change in chromatic detection threshold with increasing background contrast in our detection threshold experiment.

A contrast normalisation model has been used before to account for detection thresholds for stimuli combining chromatic and achromatic components (Chen et al., 2000b). In line with this work, we first tested a simplified version of the model originally proposed by Chen and colleagues (2000b) by incorporating divisive normalisation for the response to chromatic contrast dependent on the achromatic contrast as follows:

$$R = RImax\,\frac{I}{I+I50} + RCmax\,\frac{C}{C+kI+C50} \tag{2}$$

Where k is a constant. This model will from now on be referred to as the selective chromatic contrast normalisation model. We also decided to mirror Chen et al.'s approach more closely by allowing achromatic contrast to affect the response to chromatic contrast (as above), and chromatic contrast to affect the response to achromatic contrast, as follows:

$$R = RImax\,\frac{I}{I+jC+I50} + RCmax\,\frac{C}{C+kI+C50} \tag{3}$$

Where j and k are constants. This model will be referred to as the mutual chromatic-achromatic contrast normalisation model. We have therefore defined three models with the first accounting for only independent responses to the two stimulus components and the remaining two accounting for interdependence of responses.

Our detection threshold data will be critical in determining whether the first model, with complete independence of chromatic and achromatic responses, is correct, as the model predicts no change in chromatic detection threshold with increasing background contrast. Models two and three would both allow for some change in chromatic detection threshold with increasing background contrast as has been previously reported by Chen et al., (2000a).

2.6. Assessing model validity

Model fits were calculated using the Matlab function *fminsearch* which allows the minimum values of a multiparameter function to be found. We reran fminsearch with adjusted starting parameters whenever a parameter would be above 1000. Akaike's information criterion (AIC; Akaike, 1974) was then used to evaluate the goodness of fit for each model, taking into account the benefit of any additional parameters. The AIC value for a model is defined as:

$$AIC = 2p - 2\log(L)$$

Where L is the likelihood of the residuals of the model fit and the data, and p is the number of model parameters. AIC values are arbitrary and thus can only be compared for models of the same dataset. The model that enumerates the lowest AIC score for one set of data has the best fit of the models tested. For the fMRI datasets, AIC values were calculated using the residuals of the data averaged across sessions and participants.

We then asked whether the model fits of the BOLD responses in V1 could predict the behavioural thresholds. Using the parameters for model fits found in the fMRI results, we first found the achromatic response alone, with chromatic contrast set to zero. This reduces all three models to the same equation but with different parameter values for RImax and I50 for each model and chromatic direction:

$$R_I = RImax\,\frac{I}{I+I50}$$

Where R_I is the response to achromatic increments only, calculated at each contrast level of I.

The fMRI model of the response (R_I) was then transformed using the following equation:

$$T_I = j\,\frac{1}{\frac{dR_I}{dI}}$$

where T_I is the model predicted detection threshold for achromatic target gratings at each background contrast level of I, j is a constant, and $\frac{dR_I}{dI}$ is the gradient of the modelled fMRI response to achromatic contrast (R_I) with respect to the achromatic contrast (I). Then a further fminsearch was performed in MATLAB with one free parameter (j) to fit on the log of the model predicted threshold and the log of the behaviourally measured thresholds. Note that this new parameter j only shifts the predictions of threshold up or down the vertical axis in figures and does not affect the shape of the predicted curves/lines.

Subsequently, we wanted to investigate whether the models could be used to predict the chromatic responses. Chromatic contrast can be modelled as the following in the independent model:

$$R_C = RCmax\,\frac{C}{C+C50}$$

In the models including chromatic response dependence on achromatic contrast, R_C can be modelled as:

$$R_c = RCmax\,\frac{C}{C+kI+C50}$$

Which is calculated at each level of I.

Again, using the parameters found using the fMRI data, R_C was then calculated for each model then transformed using the following equation:

$$T_C = j\,\frac{1}{\frac{dR_C}{dC}}$$

where T_C is the model predicted threshold and $\frac{dR_C}{dC}$ is the gradient of the modelled fMRI response to chromatic contrast (R_C) increments with respect to chromatic contrast (C) when C is very small, calculated at

each level of I. For the independent model, there is no dependence of chromatic response on achromatic contrast, so this model will predict no change in chromatic contrast detection threshold with increasing achromatic contrast.

AIC values were then calculated on the residuals of the log behavioural threshold data, and the log of the model predicted thresholds. Log values were used to ensure that the higher contrast background (50 %) results were not unduly skewing the results, as this was sometimes an order of magnitude higher than the threshold values with the lowest background contrast, particularly in the achromatic condition.

3. Results

Firstly, we assessed the *reliability of fMRI results (3.1)* we acquired across sessions and conditions, in order to determine whether our responses are consistent. Having ensured internal validity of our fMRI results, we will then be able to average and compare across different sessions and conditions. Secondly, the three models we have proposed will be fitted to our *V1 results (3.2)* to assess the extent of interdependence of responses to achromatic and chromatic stimulus components. We have chosen V1 as the primary area to investigate as it has direct connections to the pathways from the LGN, and may therefore maintain independence, or alternatively exhibit interdependence. Thirdly, statistics will be reported for the *detection thresholds (3.3)* to determine whether there is evidence of interdependence of chromatic and achromatic thresholds. Fourthly, we predicted detection thresholds from V1 responses *(3.4)* using the parameters we derived from V1 (3.2). This will allow us to assess which of the three models best account for behavioural thresholds as well as neural signals. Finally, we will then look at the responses to our stimuli in *extrastriate visual areas (3.5)* to see how signals are processed in more anterior regions.

3.1. Reliability of fMRI results

The first step in analysing the fMRI data is to assess the reliability of our data across sessions, as our intention is to average each participants' results across sessions for each condition. To ensure this is statistically appropriate, we have first correlated the percent signal change values calculated for identical conditions across sessions, the results of which are shown in the first two graphs in Fig. 2. There is a high correlation between results across different scan sessions which were performed on different days. This gives us confidence in averaging the results across sessions for the same condition. Secondly, the L-M and S condition sessions each contain five stimuli that are identical to each other, where achromatic contrast is present at five levels (3.125 %, 6.25 %, 12.5 %, 25 % and 50 %) but chromatic contrast is at zero. The rightmost graph of Fig. 2 shows the correlation between responses to these stimuli during L-M and S sessions. There is also a high correlation found here, showing good internal validity of our results. We also computed an adjusted R^2 value ($N = 25$) for each of the seven participants and for the L-M condition it varied between 0.48 and 0.85 with a mean of 0.67. For the S cone condition adjusted R^2 ($N = 25$) varied between 0.51 and 0.77 with a mean of 0.61. For the achromatic conditions adjusted R^2 ($N = 5$) varied between 0.70 and 0.98 with a mean of 0.86. This gives us confidence that we can further analyse our results, comparing across days and sessions knowing that responses to our stimuli are reproducible.

3.2. V1 Results

The aim of this section is to assess the fit of the three models to V1 responses to our stimuli. V1 has been selected as the first area to be examined since it is the first cortical area that processes visual signals, as well as the largest retinotopic representation of visual space (Dougherty et al., 2003). Also, we know that the LGN passes signals directly to separate layers of V1 for each visual pathway (Derrington et al., 1984) so if any cortical area would show independence of achromatic and chromatic signals, it should be primary visual cortex. Additionally, previous work has shown a coupling between fMRI responses in primary visual cortex and behavioural contrast detection thresholds (Engel et al., 1997; Lowndes et al., 2023).

Fig. 3 shows the result of our analysis of the 25 chromatic and achromatic combinations for both L-M (Fig. 3A) and S (Fig. 3B) responses, averaged across sessions, and across participants. In the upper and lower rows of panels a and b the same data are plotted as a function of the achromatic contrast (grouped by chromatic contrast) and chromatic contrast (grouped by achromatic contrast), respectively. Each column shows the same data repeated, with the lines in the first three columns representing the fits of the different models; independent, selective chromatic contrast normalisation (Selective Normalisation), and mutual chromatic-achromatic contrast normalisation (Mutual Normalisation). Looking solely at the fMRI data (represented by dots), there are robust increases in response in both achromatic (top rows Fig. 3a and b) and chromatic (bottom rows Fig. 3A and B) stimulus directions, with a larger increase in the achromatic direction. In both L-M and S cone conditions, there appears to be a greater dynamic range of chromatic response at low achromatic background levels. This is evidenced by what we refer to

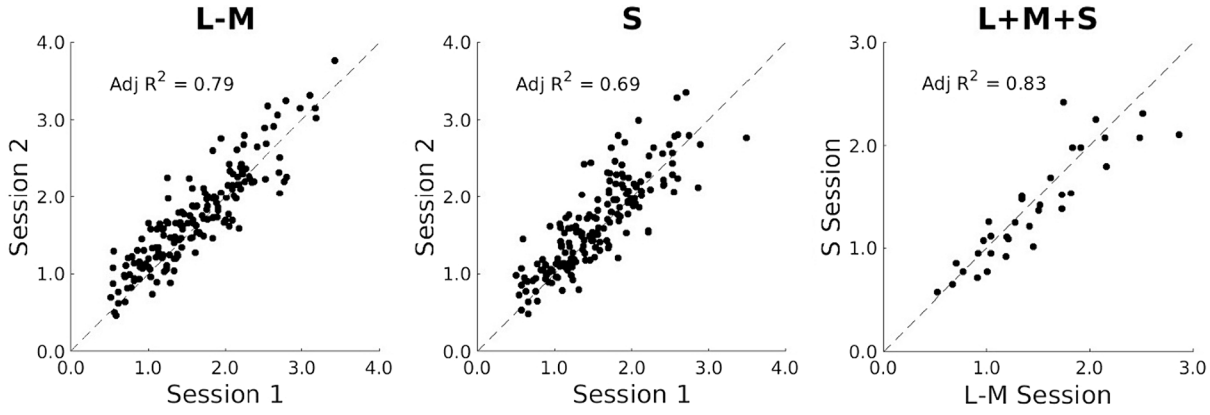

Fig. 2. A scatter graph (left) in which each data point is a percent signal change value in V1 for each stimulus level and participant in L-M session one, plotted against the percent signal change value for that same stimulus level and participant in L-M session two. The dotted diagonal line shows perfect correlation and the value in the top left is adjusted R^2. The middle graph shows a scatter graph plotted as before showing the correlation of each data point for S cone session 1 and S cone session 2. In the rightmost scatter graph each dot is a percent signal change value for each of the achromatic background contrast levels when the chromatic contrast level was zero, averaged across session one and session two for the L-M and S sessions. Since chromatic contrast is zero for these conditions, the stimulus is identical between the L-M and S cone scans, and therefore this plot shows achromatic responses with the same stimulus profile during different scans. Again, adjusted R^2 is shown in the top left. While the data are given here for all participants we also computed correlations for each participant separately (see text for details).

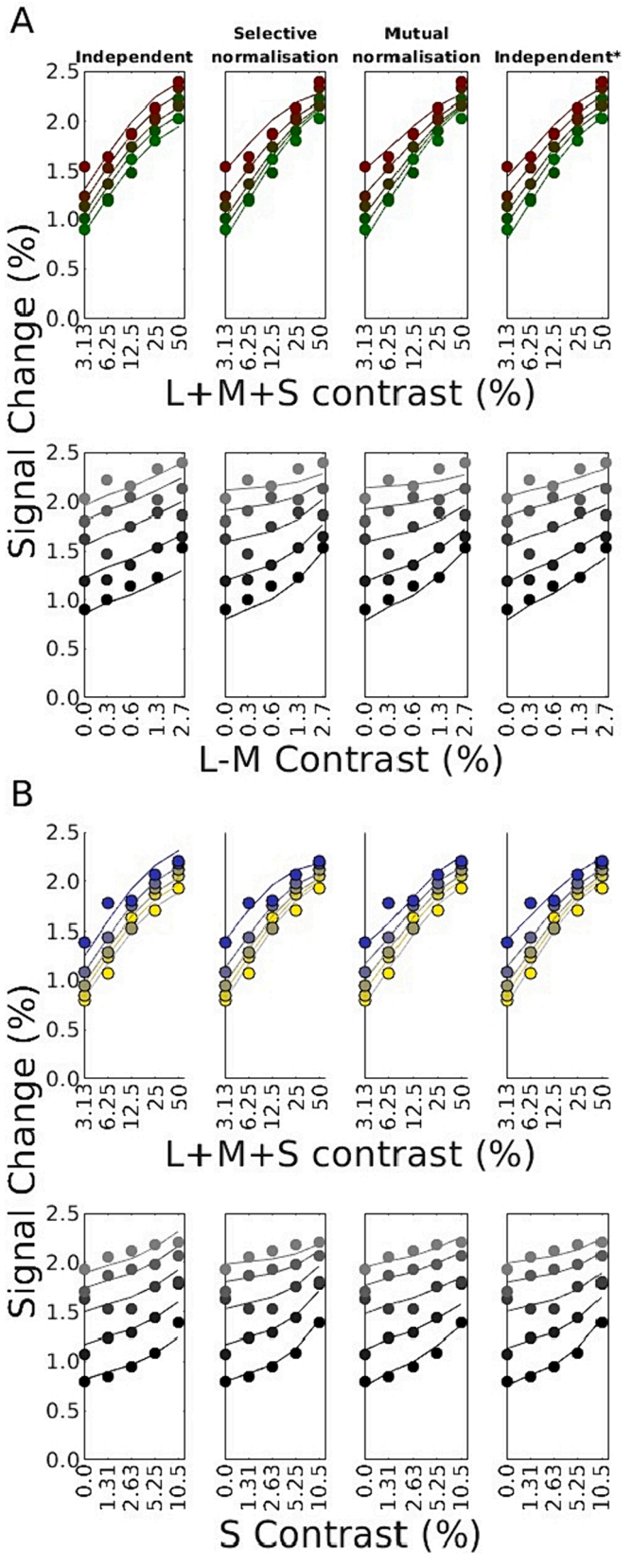

(caption on next column)

Fig. 3. A figure showing the percentage signal change averaged across all participants and both runs for all 25 stimulus conditions in the fMRI sessions. 3A, top panels are responses to L-M plotted along the achromatic contrast axis, with the chromatic contrast increasing from green to red. NB, the colour of these points is arbitrary, for example, the green coloured dot represents the response when the L-M contrast was zero. Fig. 3A, bottom graphs show the same data, this time plotted against the L-M contrast axis with the achromatic contrast increasing as the dots move from black to grey. The graphs in the first column show the independent model fits, the second show the selective chromatic contrast normalisation model fits, the third show the mutual chromatic-achromatic contrast normalisation model fits, and the fourth show the independent neural response with nonlinear BOLD model fits. (For interpretation of the references to colour in this figure legend, the reader is referred to the web version of this article.)

as a 'pinching' of the range of chromatic responses at higher achromatic background contrasts in the top rows of Fig. 3A and B. The corollary of the pinching in the upper data plots is the reduced gradient of chromatic responses as background achromatic contrast is increased in the bottom rows of Fig. 3A and B. These features of the data indicate some interdependence of chromatic and achromatic responses.

Fig. 3B shows the data from the S cone condition sessions in the same way, with the top row showing the achromatic contrast increasing along the x-axis and chromatic contrast going up from yellow to blue. The fourth shows S contrast increasing along the x axis with achromatic contrast going up from black to grey.

The lines in Fig. 3 represent the fit for each model tested. The first model, which assumes the responses to achromatic and chromatic stimulation should be completely independent, accounts for much of the variance quite well in the L-M and S cone condition (Fig. 3A and B, first column), but cannot account for the larger dynamic range of responses to chromatic contrast targets on a low achromatic contrast background compared to the dynamic range on higher achromatic contrast backgrounds. This is most obvious in the L-M condition where achromatic contrast is very low (3.125 %) and L-M contrast is high (2.7 %) which yields a higher response than the model would predict. By definition this model generates lines that are parallel in the plots and therefore cannot account for the observed pinching in the data plots of Fig. 3.

The two models incorporating interdependence using divisive contrast normalisation can account for pinching in the upper plots and correlated reduction in the gradient of the plots in the lower panels. There is a suggestion in the L-M condition that the dynamic range of the chromatic responses may have been compressed too much by the models at high achromatic contrast, which is especially evident in the mutual chromatic-achromatic contrast normalisation model.

AIC values were calculated for each model for L-M and S cone conditions separately, then summed together to show the model performance across conditions. The selective chromatic contrast normalisation model had a lower AIC value (-98.42) compared to the independent (-88.52) model and marginally lower than the mutual chromatic-achromatic contrast normalisation (-98.08) model. This indicates that of these three models, the selective chromatic contrast normalisation model is the most likely to explain our data.

In order to investigate the strength of the normalisation effect, we computed the modelled chromatic responses at each achromatic level, using the selective chromatic contrast normalisation model as an example (Fig. 4). The effect of the modelled normalisation is relatively strong, decreasing L-M responses by a factor of 4.16 and S responses by a factor of 3.03 between 3.13 and 50 % achromatic contrast. When using the mutual chromatic-achromatic contrast normalisation model, the L-M responses were reduced by a factor of 3.67 and S response by a factor of 1.66. It should be noted, however, that these are modelled responses, and the overestimate of pinching shown in Fig. 3 will have translated to these calculations and show a greater change due to contrast normalisation than may be present in the brain data, particularly in the L-M condition, where this effect is stronger.

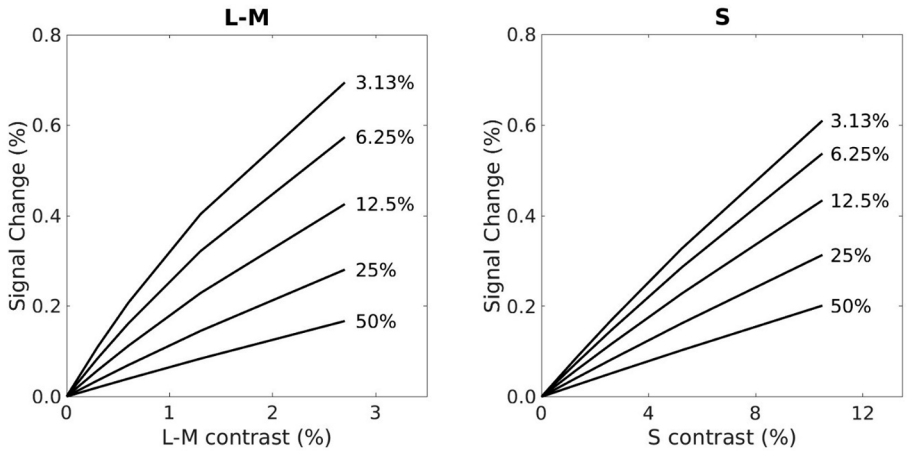

Fig. 4. A graph showing the modelled chromatic response to L-M (left) and S (right) contrast at each achromatic contrast level tested. Each individual line is a mean of the model fit of the chromatic response at the marked achromatic contrast level.

An alternative explanation for our fMRI results in V1 could be that achromatic and chromatic responses are combined independently as in our first model, but that there is some response nonlinearity between the neural response and our measured BOLD response. A nonlinearity is possible, but we note also that there is evidence that it is largely linear in V1 (Boynton et al., 1996). For completeness, however, we have added a fourth model, which assumes linear summation of the achromatic and chromatic responses is representative of the neural response (as shown in our first independent model) and this is followed by a compressive non-linearity of the sum of the neural response (again utilising the Naka-Rushton equation), which is shown in the furthest right column of Fig. 3. As shown, an assumption of non-linearity after combination of achromatic and chromatic neural signals fits the fMRI data in V1 well, in fact the AIC value was significantly lower for this model than any other tested (-113.44) suggesting this model is more likely to explain our data. However, as with the independent model, any model that has no dependence of achromatic contrast on chromatic responses will be unable to account for any changes in behavioural thresholds with increasing achromatic background contrast. As will be shown in section 3.3 and 3.4, we have found significant increases in detection thresholds with increased achromatic contrast, which are well predicted by our contrast normalisation models. Therefore, while investigating non-linearities of the BOLD response is an important avenue for further research, we will focus on the first three models that assume a linear relationship between the neural and BOLD response for the rest of this paper.

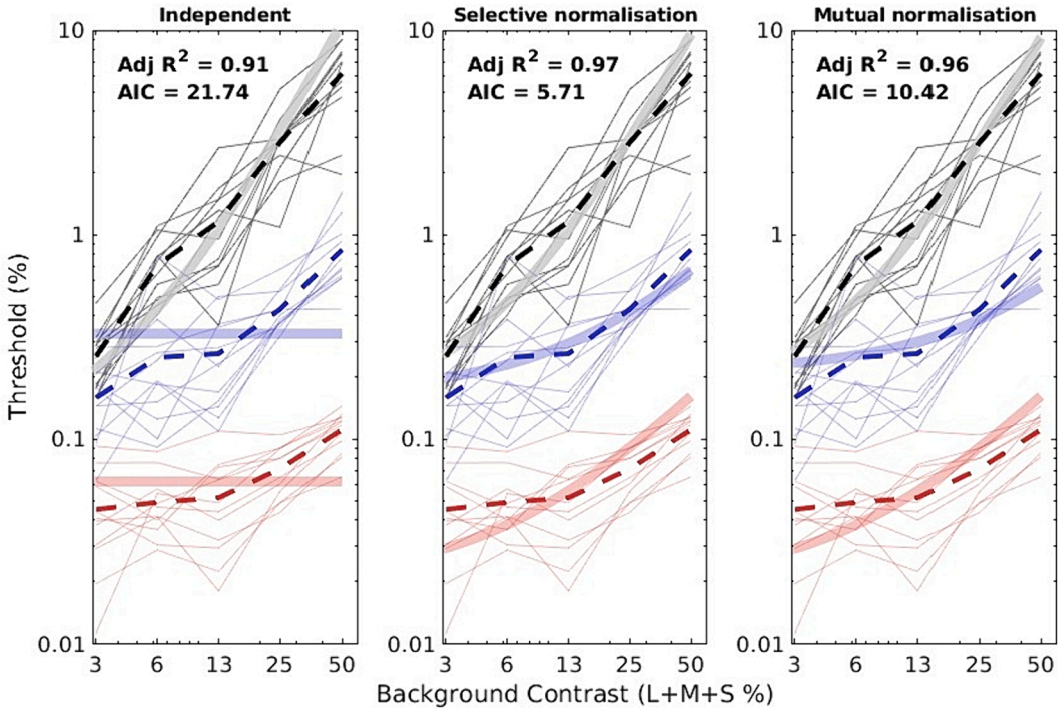

Fig. 5. A figure showing the behavioural thresholds obtained by individuals (thin light grey, blue and red lines) and the mean (dashed lines) for L + M + S, L-M and S colour directions against the different achromatic background contrast levels (3.125–50 %). Each graph displays the same data. The thick transparent lines show the model fit for each model as predicted in *V1 results (3.2)* for the independent, selective chromatic contrast normalisation, and mutual chromatic-achromatic contrast normalisation models. The AIC value at the top of each graph is the sum of the individual AIC values for each colour direction. (For interpretation of the references to colour in this figure legend, the reader is referred to the web version of this article.)

3.3. Detection thresholds

Given the outcome of the modelling above, we anticipate that contrast detection thresholds should vary with background contrast. The contrast detection thresholds are shown in Fig. 5, with three panels showing identical data but different model fits which we will explain in section 3.4. They reveal that the highest thresholds are found for achromatic stimuli, particularly at high achromatic background contrasts. Of the two chromatic directions, S cone detection thresholds were higher than L-M thresholds. The graphs show increases in all behavioural thresholds with increasing background contrast, although, as anticipated, chromatic thresholds increase far less than achromatic thresholds.

We examined whether thresholds changed significantly as a function of background contrast with a 5 by 3 (background contrast level by target colour condition) ANOVA. Greenhouse-Geisser correction to degrees of freedom was applied where sphericity violated. The analysis revealed significant main effects of background contrast ($F(2.62, 28.80) = 125.63$, $p = 4.43x10^{-16}$, $\eta^2 = 0.92$), and colour condition ($F(2, 22) = 611.39$, $p = 5.25x10^{-20}$, $\eta^2 = 0.98$) as well as a significant interaction ($F(8, 88) = 21.34$, $p = 1.20x10^{-17}$, $\eta^2 = 0.66$). This led us to perform subsequent one-way ANOVAs for each colour condition. In the achromatic condition, there was a significant effect of background contrast level ($F(4, 44) = 133.62$, $p = 5.18x10^{-24}$, $\eta^2 = 0.92$). There was also a significant effect of background contrast level in the L-M ($F(2.12, 23.33) = 21.30$, $p = .000004$, $\eta^2 = 0.66$) and S cone ($F(4, 44) = 36.04$, $p = 2.33x10^{-13}$, $\eta^2 = 0.77$). Post-hoc tests revealed that, in both chromatic conditions, this was driven by the two highest levels of achromatic background contrast (25 % and 50 %), as these thresholds were significantly higher than those at the lower background contrasts, and each other. In the achromatic condition, all five levels are significantly different from each other, indicating that the threshold increases significantly with each increase of the background contrast, with the exception of two middling levels of background contrast (6.125 and 12.5 %) not being significantly different from each other ($p = .195$). That there are significant increases in detection thresholds with increasing background contrast in both of the colour directions tested, confirms that there must be some interdependence of the signals from achromatic and chromatic pathways elicited by these stimuli.

3.4. Predicting thresholds from V1 responses

The model parameters found in section 3.2 (*V1 results)* were then used to predict thresholds as described in section 2.6 (*assessing model validity)* and are shown in the transparent coloured lines on Fig. 5. All three models predict the achromatic threshold data well. The independent model, shown in the left panel, cannot account for the changes in chromatic contrast detection threshold. This can be seen in Fig. 5 as flat responses to increasing achromatic background contrast. The selective chromatic contrast normalisation model, shown in the middle panel, predicts achromatic and S cone thresholds very well. The L-M model predictions generate a steeper curve than the detection thresholds we measured. Similarly, the mutual chromatic-achromatic contrast normalisation model, shown in the right panel of Fig. 5, predicts a steeper curve than we find for L-M thresholds, and to a greater extent than for the selective chromatic contrast normalisation model. The mutual chromatic achromatic contrast normalization model also predicts a shallower curve for the S cone thresholds than our detection threshold results show. On inspection of Fig. 5 therefore the detection threshold data appear best fit by the selective chromatic contrast normalisation model (middle column). This is also supported by the AIC values shown the panels of Fig. 5.

3.5. Extrastriate visual areas

In Fig. 6, we plot the contrast response functions for extrastriate visual areas V2, V3, V3A and V4 alongside those for V1. Fig. 6A shows the responses during the L-M condition, and Fig. 6B shows the responses during S cone conditions. The top row of A and B shows responses to achromatic contrast grouped by the chromatic target contrast and the

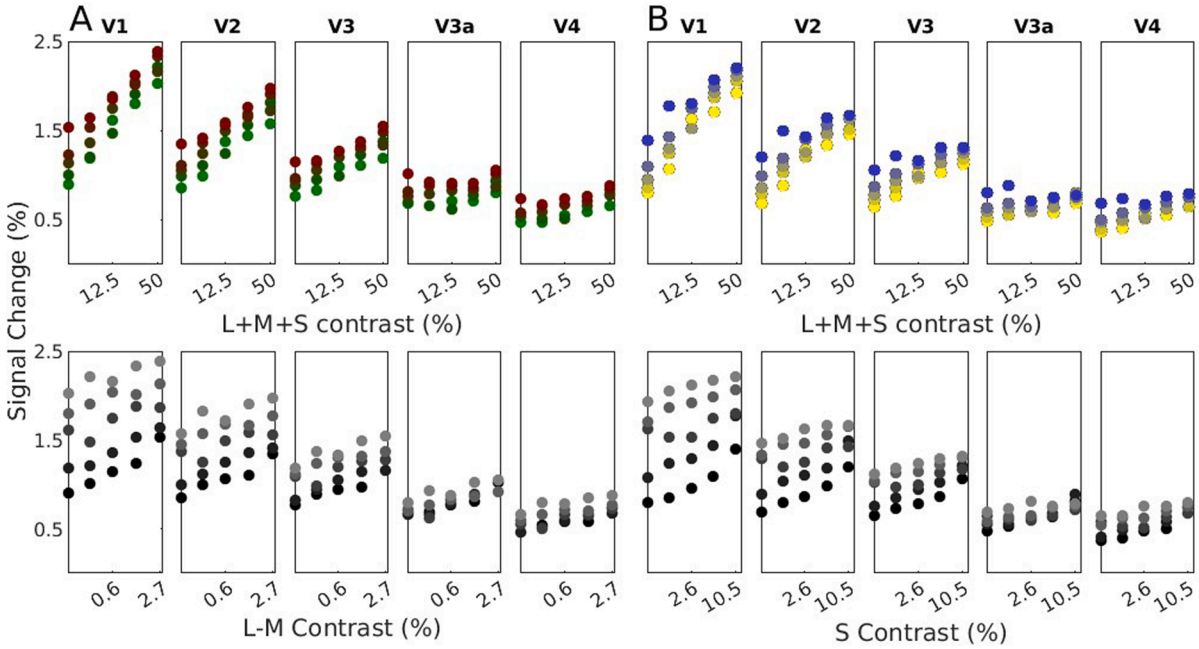

Fig. 6. A) Plots showing the average response to each stimulus in the L-M condition against achromatic contrast (upper) and against L-M contrast (lower) as described in Fig. 3, for each visual area (V1, V2, V3, V3a and V4). In the top panels, L-M contrast increases from green to red. NB, the colour of these points is arbitrary, for example, the green coloured dot represents the response when the L-M contrast was zero. In the bottom graphs, plotted along the L-M contrast axis, achromatic contrast increases as the dots move from black to grey. B) Plots showing the average response to each stimulus in the S cone condition against achromatic contrast (upper) and against S contrast (lower) as in A, with chromatic contrast increasing from yellow to blue. (For interpretation of the references to colour in this figure legend, the reader is referred to the web version of this article.)

bottom row shows responses to chromatic contrast grouped by achromatic background contrast. Inspection of the top rows show that higher up the visual hierarchy the range of response to achromatic contrast falls. This is largely due to the compression of responses to higher background contrasts. The corollary of this in the bottom row plots is the reduction in the vertical spread of the data up the visual hierarchy. The range of response to the target chromatic contrast appears better preserved across visual areas as shown by small changes in the slope of the responses in the lower panels and the relatively well-preserved vertical range of the responses shown by the coloured symbols in the upper panels.

We then plot the mean responses to achromatic contrast across chromatic contrast levels (top row) and the mean responses to chromatic contrast across achromatic contrast levels (bottom row) in each visual area for L-M and S cone conditions in the left column of Figure 7A and B respectively. There is a reduction in the achromatic responses in more anterior regions, coupled with an increasingly compressive response. Conversely, while there is a reduction in responses to chromatic contrast with anterior regions in the bottom plots of Figure 7A and B, the responses measured from each area remain reasonably parallel, maintaining their dynamic range. It must be noted however that all achromatic interactions with the chromatic responses are averaged in these plots.

To minimise the influence of achromatic contrast on the chromatic responses and vice versa we therefore plot achromatic responses in the absence of chromatic targets (top row) and response to the chromatic target in the presence of the lowest contrast achromatic background (bottom row) in the right hand columns of Figure 7A and B. The right column plots are largely similar for the achromatic responses in terms of their shape with compressive characteristics. For the chromatic responses however the gradient of the largely linear responses increases across all areas and appears more parallel, a feature that indicates that the background contrast interacts with the response to the chromatic target contrast in extrastriate cortex as well as V1.

We calculated and plotted (Fig. 7C) the difference between the responses to the highest and lowest achromatic contrasts (in the absence of a chromatic target), alongside the difference to the highest and lowest chromatic contrasts, for L-M (left) and S (right) conditions (for the lowest achromatic background contrast) to provide an empirically derived amplitude of the response range for each visual area to the contrast along different colour directions. The plots show the reduction in responses to achromatic contrast in more anterior visual regions, while the dynamic range of the chromatic responses is better preserved up the visual hierarchy. To assess this statistically, we performed a separate two-way ANOVA for each chromatic condition (visual area by colour direction). In the L-M condition, there was a significant interaction between visual area and colour direction ($F(4,24) = 23.96$, $p = 4.41\text{x}10^{-8}$, $\eta^2 = 0.80$). The interaction was also significant in the S condition ($F(1.93,11.60) = 21.03$, $p = .00065$, $\eta^2 = 0.78$). This led us to preform subsequent one-way ANOVAs for each condition, on achromatic and chromatic results separately. For the achromatic responses, there was a significant effect of visual area during both the LM ($F(4,24) = 21.08$, $p = 1.45\text{x}10^{-7}$, $\eta^2 = 0.78$) and S ($F(4,24) = 47.17$, $p = 4.97\text{x}10^{-11}$, $\eta^2 = 0.89$) conditions with high effect sizes. The effect of visual area was also significant for chromatic responses in both L-M ($F(1.99,11.94) = 8.93$, $p = .004$, $\eta^2 = 0.60$) and S ($F(4,24) = 6.97$, $p = .001$, $\eta^2 = 0.54$) conditions, but with lower effects sizes than were shown for achromatic responses. This shows that while chromatic responses do reduce up the visual hierarchy, this reduction is more dramatic for achromatic responses.

While it may be tempting to model the responses of extrastriate areas and then use those models to fit the behavioural thresholds, there is an issue with this approach. The steeper gradients observed for the achromatic responses in V1 compared to all other areas lead to greater sensitivity and therefore lower thresholds. While the chromatic responses appear more robust over visual areas, it is also true that the

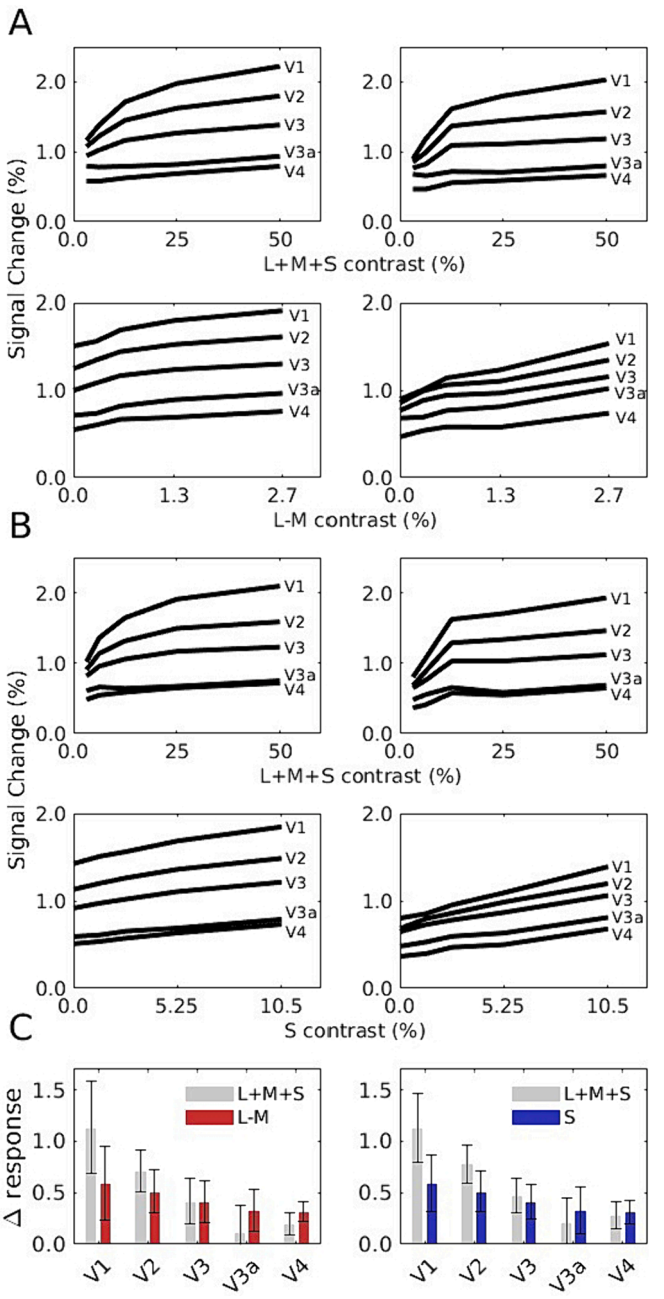

Fig. 7. A) Left column plots show the responses to achromatic contrast averaged across all L-M contrast levels (upper) and the responses to L-M contrast averaged across all achromatic contrast levels (lower) in each visual area. Right column plots show the response to 0% L-M stimulus contrast for each achromatic contrast level for each visual area (upper) and the response to the lowest achromatic contrast at each L-M contrast level (lower). B) As in A, left plots show the mean responses and right plots show the responses to the lowest level contrasts, now for the S cone condition. C) The left graph shows a bar chart displaying the difference (Δ) between the mean response to the maximum (50%) and minimum (3.125%) achromatic contrast for each visual area when L-M contrast is 0% in grey bars. The red bars show the difference in the response to the maximum L-M contrast (2.7%) and the minimum (0%) where achromatic contrast is at its lowest (3.125%). The right graph shows the difference (Δ) between the mean response to the maximum achromatic contrast (50%) and the minimum (3.125%) for each visual area when S contrast is 0% in grey bars. Blue bars show the difference between the maximum S contrast (10.5%) and the minimum (0%) where achromatic response is at its lowest (3.125%). Error bars are 1 standard deviation.

gradient of those responses reduces up the visual hierarchy, so again our model for thresholds would predict lower thresholds from V1 responses compared to those derived from any other visual area. Moreover, given the compressive nature of the achromatic contrast response function, the variance of the data is reduced considerably compared to the measurement error and therefore insights concerning the interdependence of signals and their relationships with thresholds are much more limited for responses from extrastriate areas.

4. Discussion

The aim of this study was to investigate the nature and extent of interdependence of brain responses to chromatic targets on achromatic backgrounds, and how they can explain target detection thresholds. From our fMRI experiment, we found that a model incorporating divisive contrast normalisation of chromatic contrast responses by achromatic contrast best explained our data in V1 out of the three models tested, closely followed by mutual normalisation of achromatic and chromatic responses by chromatic and achromatic contrast. The selective chromatic contrast normalisation model predicted detection thresholds best out of the models tested. We also found that achromatic responses reduced further up the visual hierarchy, while chromatic responses remained more consistent.

In our detection thresholds experiment, we found a clear increase in achromatic contrast detection thresholds with increasing achromatic background contrast. This is in line with the study by Barbur (1994) and suggests that despite differing spatial and temporal frequencies, these two stimulus components are generating responses in similar sets of neurons. Our study found more subtle increases in contrast detection threshold in both chromatic directions that only became significant at high (>= 25 %) background contrast. Barbur et al (1994) reported little change in chromatic contrast detection thresholds as achromatic background contrast increased, but examination of their plots does indicate that thresholds for gratings presented on 35 % compared to 8 % backgrounds were higher, which is consistent with our findings. Chen and colleagues (2000a) investigated the potential for interdependence of chromatic and achromatic thresholds using background masks and pedestal targets of different chromatic directions, but identical spatial and temporal properties. They found an increase in contrast detection thresholds of isoluminant targets corresponding to L-M (red-green) and S cone (blue-yellow) when achromatic backgrounds rose above 10 % contrast. This suggests, along with our work, that achromatic and chromatic responses are interdependent. Chen and colleagues (2000b) used divisive contrast normalisation to explain their findings.

Other psychophysics research has shown chromatic responses consistent with divisive contrast normalisation. Medina and Mullen (2009) showed that cross orientation masking effects are significantly greater for chromatic test stimuli on chromatic masks than for their achromatic counterparts. However, another study found that the cross-orientation masking effect did not occur with achromatic masks and chromatic test stimuli (Mullen et al., 2014). Given that we and Chen et al have found evidence for interdependence for stimuli that are not cross orientated, the normalisation of chromatic by achromatic signals may be specific to the relative orientation of the components.

Single-cell recordings of neurons in the primary visual cortex of macaques showed that V1 combines magnocellular and parvocellular inputs (Li et al., 2015), suggesting interdependence of the responses of these pathways. All chromatic cortical neurons show evidence of divisive contrast normalisation in macaque V1 (Solomon & Lennie, 2005) with the divisive pool being derived from a population representing more diverse response patterns. In humans, there is evidence in electrophysiology for non-linear summing of responses to the combination of chromatic and achromatic stimuli whereby the response to combinations were smaller than predicted by the sum of responses to the parts (Martinovic & Andersen, 2018). Taken together, this research shows that achromatic and chromatic signals are interdependently processed and that this can be shown in physiology. Our measurements of V1 responses are consistent with the physiological studies above and based on previous modelling approaches we explored further the nature of the interdependence of responses to chromatic and achromatic stimuli.

To uncover the source of the interdependence of chromatic and achromatic responses in early visual cortex, we deployed a simplified version of the contrast normalisation model outlined by Chen et al., (2000b) which accounted for mutually inhibitory combinations of chromatic and achromatic responses. Our modelling indicated that inhibition may be unidirectional, as the model that included only the chromatic response dependence on achromatic contrast, but not the achromatic response dependence on chromatic contrast, was found to be the most likely to explain our fMRI results in V1. It is possible that the achromatic stimuli we presented were highly potent, given their spatiotemporal characteristics and high contrast levels, and thus it may have a dominant effect on the normalisation pool, leading to any normalisation from the chromatic targets on achromatic responses to be undetectable. However, single unit recordings of neurons in V1 and V2 of macaques, have shown that among neurons that are responsive to both chromatic and achromatic stimuli, the normalisation pool is primarily driven by colour directions close to achromatic (Solomon & Lennie, 2005). Taken together with our work, there is evidence therefore that the pools used in divisive contrast normalisation can be selective.

We showed that a model of fMRI signals in V1 can predict contrast detection thresholds. The modelled changes in responses to chromatic target gratings with increasing achromatic background contrast predicted the increase in detection threshold of the same gratings with increasing background contrast, although the predictions were better for the S cone than the L-M direction. The modelled response to the background component of the stimulus alone was also able to predict the increases in detection thresholds for achromatic target gratings as background contrast increased, showing that there is a common mechanism for processing the target and background, when they are both achromatic even when they have different spatiotemporal properties. This offers reassurance that luminance artefacts of the chromatic gratings are unlikely to be registered in the brain responses we measured. Other work has also shown correlations between brain response and detection thresholds; contrast detection thresholds at many points of the L-M and S-(L + M) chromatic plane show a coupling with responses in V1 and V2, at temporal frequencies of 4 Hz and below (Engel et al., 1997). Previous work in our lab has shown that V1 responses relate well to the elevation of contrast detection thresholds when the spatial frequency of chromatic stimuli is increased (Lowndes et al., 2023).

We assumed that the relationship between the neural responses and the BOLD response is linear in our modelling framework. However, it is of interest that V1 responses can be modelled well with no interaction between neural responses followed by a compressive non-linearity, which could reflect a compressive non-linear relationship between the neural responses and BOLD. In the domain of vision there is evidence to support that the neural-BOLD response is linear (Boynton et al., 1996) and it is also true that when we introduced the non-linearity, the model would be incapable of predicting chromatic threshold elevations as a function of the achromatic background. So while it is of future interest to understand the relationship between BOLD and the neural responses that drive it (Logothetis et al., 2001), increasing the degrees of freedom to model it here is beyond the scope of our study.

In extrastriate visual areas (V2-V4) we found a smaller and more compressive response to achromatic contrast up the visual hierarchy, consistent with previous literature (Buracas & Boynton, 2007; Gouws et al., 2014; Liu & Wandell, 2005; Tregillus et al., 2021). The compression of responses further up the visual stream is more subtle in our chromatic response data. The results that chromatic information is better preserved relative to achromatic background information likely reflects the value of colour in identification or recognition of visual features that are processed higher up the visual hierarchy. We also found BOLD responses to S cone stimuli were remarkably similar to those

elicited by L-M stimuli. The cone contrasts of the stimuli eliciting these responses were however many more multiples of the psychophysically determined threshold for L-M than for S cone stimuli. S cone contrast has been shown to correlate better with BOLD response than a threshold based metric (Mullen et al., 2007). Similarly, our recent study found similar BOLD responses to S cone stimuli at 6.17 times threshold as L-M stimuli at 20.95 times threshold (Lowndes et al., 2023).

5. Conclusions

This study has provided new insight into the combinations of chromatic and achromatic responses in primary visual cortex of humans, and how they relate to behavioural responses. V1 responses were best predicted by a selective chromatic contrast normalisation model of the three models tested, showing that achromatic and chromatic responses are interdependent. Behavioural responses also showed dependence of the detection threshold for chromatic targets on achromatic background contrast, which was well predicted by the same selective chromatic contrast normalisation model. This study has shown that V1 responses align well with behaviour, suggesting that perception of these stimuli is set at this early cortical stage. A large dynamic range was maintained for encoding colour up the visual hierarchy, while it was reduced for achromatic variations, which may offer a useful representation of visual information for perception of natural images.

CRediT authorship contribution statement

Rebecca Lowndes: Writing – review & editing, Writing – original draft, Software, Methodology, Investigation, Formal analysis, Data curation, Conceptualization. **Richard Aveyard:** Software. **Lauren E. Welbourne:** Investigation. **Alex Wade:** Supervision, Software. **Antony B. Morland:** Writing – review & editing, Supervision, Software, Methodology, Investigation, Formal analysis, Conceptualization.

Declaration of Competing Interest

The authors declare that they have no known competing financial interests or personal relationships that could have appeared to influence the work reported in this paper.

Data availability

Data will be made available on request.

Acknowledgments

Supported by funding from BBSRC (BB/P007252).

References

Akaike, H. (1974). A new look at the statistical model identification. *IEEE Transactions on Automatic Control, 19*(6), 716–723.
Albrecht, D. G., & Hamilton, D. B. (1982). Striate cortex of monkey and cat: Contrast response function. *Journal of Neurophysiology, 48*(1), 217–237.
Alvarez, I., De Haas, B. A., Clark, C. A., Rees, G., & Schwarzkopf, D. S. (2015). Comparing different stimulus configurations for population receptive field mapping in human fMRI. *Frontiers in human neuroscience, 9*, 96.
Baker, D. H., Meese, T. S., & Summers, R. J. (2007). Psychophysical evidence for two routes to suppression before binocular summation of signals in human vision. *Neuroscience, 146*(1), 435–448.
Barbur, J. L., Harlow, J., & Plant, G. T. (1994). Insights into the different exploits of colour in the visual cortex. *Proceedings of the Royal Society of London. Series B: Biological Sciences, 258*(1353), 327-334.
Barnett, M. A., Aguirre, G. K., & Brainard, D. (2021). A quadratic model captures the human V1 response to variations in chromatic direction and contrast. *eLife, 10*, e65590.
Benson, N. C., Butt, O. H., Brainard, D. H., & Aguirre, G. K. (2014). Correction of distortion in flattened representations of the cortical surface allows prediction of V1–V3 functional organization from anatomy. *PLoS Computational Biology, 10*(3), e1003538.
Binda, P., Thomas, J. M., Boynton, G. M., & Fine, I. (2013). Minimizing biases in estimating the reorganization of human visual areas with BOLD retinotopic mapping. *Journal of Vision, 13*(7), 13.
Birch, J., Barbur, J. L., & Harlow, A. J. (1992). New method based on random luminance masking for measuring isochromatic zones using high resolution colour displays. *Ophthalmic and Physiological Optics, 12*(2), 133–136.
Bonds, A. B. (1991). Temporal dynamics of contrast gain in single cells of the cat striate cortex. *Visual neuroscience, 6*(3), 239–255.
Bowmaker, J. K., & Dartnall, H. (1980). Visual pigments of rods and cones in a human retina. *The Journal of physiology, 298*(1), 501–511.
Boynton, G. M., Engel, S. A., Glover, G. H., & Heeger, D. J. (1996). Linear systems analysis of functional magnetic resonance imaging in human V1. *Journal of Neuroscience, 16*(13), 4207–4221.
Bradley, A., Zhang, X., & Thibos, L. (1992). Failures of isoluminance caused by ocular chromatic aberrations. *Applied Optics, 31*(19), 3657–3667.
Brown, P. K., & Wald, G. (1964). Visual pigments in single rods and cones of the human retina. *Science, 144*(3614), 45–52.
Buracas, G. T., & Boynton, G. M. (2007). The effect of spatial attention on contrast response functions in human visual cortex. *Journal of Neuroscience, 27*(1), 93–97.
Callaway, E. M., & Wiser, A. K. (1996). Contributions of individual layer 2–5 spiny neurons to local circuits in macaque primary visual cortex. *Visual neuroscience, 13*(5), 907–922.
Carandini, M., & Heeger, D. J. (2012). Normalization as a canonical neural computation. *Nature Reviews Neuroscience, 13*(1), 51–62.
Chatterjee, S., & Callaway, E. M. (2002). S cone contributions to the magnocellular visual pathway in macaque monkey. *Neuron, 35*(6), 1135–1146.
Chen, C.-C., Foley, J. M., & Brainard, D. H. (2000a). Detection of chromoluminance patterns on chromoluminance pedestals I: Threshold measurements. *Vision research, 40*(7), 773–788.
Chen, C.-C., Foley, J. M., & Brainard, D. H. (2000b). Detection of chromoluminance patterns on chromoluminance pedestals II: Model. *Vision Research, 40*(7), 789–803.
Chen, S.-F., Chang, Y., & Wu, J.-C. (2001). The spatial distribution of macular pigment in humans. *Current Eye Research, 23*(6), 422–434.
Conway, B. R. (2009). Color vision, cones, and color-coding in the cortex. *The Neuroscientist, 15*(3), 274–290.
Cornsweet, T. N., & Teller, D. Y. (1965). Relation of increment thresholds to brightness and luminance. *JOSA, 55*(10), 1303–1308.
Dacey, D. M., & Lee, B. B. (1994). The'blue-on'opponent pathway in primate retina originates from a distinct bistratified ganglion cell type. *Nature, 367*(6465), 731–735.
Dale, A. M. (1999). Optimal experimental design for event-related fMRI. *Human Brain Mapping, 8*(2–3), 109–114.
Dale, A. M., Fischl, B., & Sereno, M. I. (1999). Cortical surface-based analysis: I. Segmentation and surface reconstruction. *NeuroImage, 9*(2), 179–194.
Davies, N. P., & Morland, A. B. (2004). Macular pigments: Their characteristics and putative role. *Progress in Retinal and Eye Research, 23*(5), 533–559.
DeAngelis, G. C., Ohzawa, I., & Freeman, R. D. (1993). Spatiotemporal organization of simple-cell receptive fields in the cat's striate cortex. II. Linearity of temporal and spatial summation. *Journal of neurophysiology, 69*(4), 1118–1135.
Derrington, A. M., Krauskopf, J., & Lennie, P. (1984). Chromatic mechanisms in lateral geniculate nucleus of macaque. *The Journal of physiology, 357*(1), 241–265.
Dougherty, R. F., Koch, V. M., Brewer, A. A., Fischer, B., Modersitzki, J., & Wandell, B. A. (2003). Visual field representations and locations of visual areas V1/2/3 in human visual cortex. *Journal of Vision, 3*(10), 1.
Dumoulin, S. O., & Wandell, B. A. (2008). Population receptive field estimates in human visual cortex. *NeuroImage, 39*(2), 647–660.
Engel, S., Zhang, X., & Wandell, B. (1997). Colour tuning in human visual cortex measured with functional magnetic resonance imaging. *Nature, 388*(6637), 68–71.
Eskew, R. T., Jr (2009). Higher order color mechanisms: A critical review. *Vision research, 49*(22), 2686–2704.
Foley, J. M. (1994). Human luminance pattern-vision mechanisms: Masking experiments require a new model. *JOSA A, 11*(6), 1710–1719.
Foley, J. M., & Chen, C.-C. (1997). Analysis of the effect of pattern adaptation on pattern pedestal effects: A two-process model. *Vision research, 37*(19), 2779–2788.
Georgeson, M. A., Wallis, S. A., Meese, T. S., & Baker, D. H. (2016). Contrast and lustre: A model that accounts for eleven different forms of contrast discrimination in binocular vision. *Vision Research, 129*, 98–118.
Glasser, M. F., Sotiropoulos, S. N., Wilson, J. A., Coalson, T. S., Fischl, B., Andersson, J. L., Xu, J., Jbabdi, S., Webster, M., & Polimeni, J. R. (2013). The minimal preprocessing pipelines for the Human Connectome Project. *NeuroImage, 80*, 105–124.
Goodchild, A. K., Ghosh, K. K., & Martin, P. R. (1996). Comparison of photoreceptor spatial density and ganglion cell morphology in the retina of human, macaque monkey, cat, and the marmoset Callithrix jacchus. *Journal of Comparative Neurology, 366*(1), 55–75.
Gouws, A. D., Alvarez, I., Watson, D. M., Uesaki, M., Rogers, J., & Morland, A. B. (2014). On the role of suppression in spatial attention: Evidence from negative BOLD in human subcortical and cortical structures. *Journal of Neuroscience, 34*(31), 10347–10360.
Hammond, B. R., Wooten, B. R., & Snodderly, D. M. (1997). Individual variations in the spatial profile of human macular pigment. *JOSA A, 14*(6), 1187–1196.
Heeger, D. J. (1992). Normalization of cell responses in cat striate cortex. *Visual Neuroscience, 9*(2), 181–197.
Hupé, J.-M., Bordier, C., & Dojat, M. (2012). A BOLD signature of eyeblinks in the visual cortex. *NeuroImage, 61*(1), 149–161.

Jenkinson, M., Bannister, P., Brady, M., & Smith, S. (2002). Improved optimization for the robust and accurate linear registration and motion correction of brain images. *NeuroImage, 17*(2), 825–841.
Jenkinson, M., & Smith, S. (2001). A global optimisation method for robust affine registration of brain images. *Medical image analysis, 5*(2), 143–156.
Johnson, E. N., Hawken, M. J., & Shapley, R. (2008). The orientation selectivity of color-responsive neurons in macaque V1. *Journal of Neuroscience, 28*(32), 8096–8106.
Li, X., Chen, Y., Lashgari, R., Bereshpolova, Y., Swadlow, H. A., Lee, B. B., & Alonso, J. M. (2015). Mixing of chromatic and luminance retinal signals in primate area V1. *Cerebral Cortex, 25*(7), 1920–1937.
Liu, J., & Wandell, B. A. (2005). Specializations for chromatic and temporal signals in human visual cortex. *Journal of Neuroscience, 25*(13), 3459–3468.
Livingstone, M., & Hubel, D. (1988). Segregation of form, color, movement, and depth: Anatomy, physiology, and perception. *Science, 240*(4853), 740–749.
Logothetis, N. K., Pauls, J., Augath, M., Trinath, T., & Oeltermann, A. (2001). Neurophysiological investigation of the basis of the fMRI signal. *Nature, 412*(6843), 150–157.
Lowndes, R., Welbourne, L., Williams, M., Gouws, A., Wade, A., & Morland, A. (2023). Increasing spatial frequency of S-cone defined gratings reduces their visibility and brain response more than for gratings defined by LM cone contrast. *Vision Research, 207*, Article 108209.
Martinovic, J. (2014). *Magno-, Parvo-,Koniocellular Pathways. Encyclopedia of Color Science and Technology* (pp. 1–5). Berlin, Heidelberg: Springer.
Martinovic, J., & Andersen, S. K. (2018). Cortical summation and attentional modulation of combined chromatic and luminance signals. *NeuroImage, 176*, 390–403.
Medina, J. M., & Mullen, K. T. (2009). Cross-orientation masking in human color vision. *Journal of Vision, 9*(3), 20.
Meese, T. S., & Holmes, D. J. (2010). Orientation masking and cross-orientation suppression (XOS): Implications for estimates of filter bandwidth. *Journal of Vision, 10*(12), 9.
Mullen, K. T., Dumoulin, S. O., McMahon, K. L., De Zubicaray, G. I., & Hess, R. F. (2007). Selectivity of human retinotopic visual cortex to S-cone-opponent, L/M-cone-opponent and achromatic stimulation. *European Journal of Neuroscience, 25*(2), 491–502.
Mullen, K. T., Kim, Y. J., & Gheiratmand, M. (2014). Contrast normalization in colour vision: The effect of luminance contrast on colour contrast detection. *Scientific Reports, 4*(1), 7350.
Murasugi, C. M., & Cavanagh, P. (1988). Anisotropy in the chromatic channel: A horizontal-vertical. *Spatial Vision, 3*(4), 281–291.
Nestares, O., & Heeger, D. J. (2000). Robust multiresolution alignment of MRI brain volumes. *Magnetic Resonance in Medicine: An Official Journal of the International Society for Magnetic Resonance in Medicine, 43*(5), 705–715.
Ohzawa, I., Sclar, G., & Freeman, R. D. (1982). Contrast gain control in the cat visual cortex. *Nature, 298*(5871), 266–268.
Ohzawa, I., Sclar, G., & Freeman, R. D. (1985). Contrast gain control in the cat's visual system. *Journal of neurophysiology, 54*(3), 651–667.
Petrov, Y., Carandini, M., & McKee, S. (2005). Two distinct mechanisms of suppression in human vision. *Journal of Neuroscience, 25*(38), 8704–8707.
Rahimi-Nasrabadi, H., Jin, J., Mazade, R., Pons, C., Najafian, S., & Alonso, J.-M. (2021). Image luminance changes contrast sensitivity in visual cortex. *Cell Reports, 34*(5), Article 108692.
Reuter, M., Schmansky, N. J., Rosas, H. D., & Fischl, B. (2012). Within-subject template estimation for unbiased longitudinal image analysis. *NeuroImage, 61*(4), 1402–1418.
Ruddock, K. H. (1963). Evidence for macular pigmentation from colour matching data. *Vision Research, 3*(9–10), 417–429.
Shapley, R., & Hawken, M. J. (2011). Color in the cortex: Single-and double-opponent cells. *Vision Research, 51*(7), 701–717.
Sincich, L. C., & Horton, J. C. (2005). The circuitry of V1 and V2: Integration of color, form, and motion. *Annual Review of Neuroscience, 28*, 303–326.
Smith, S. M., Jenkinson, M., Woolrich, M. W., Beckmann, C. F., Behrens, T. E. J., Johansen-Berg, H., Bannister, P. R., De Luca, M., Drobnjak, I., & Flitney, D. E. (2004). Advances in functional and structural MR image analysis and implementation as FSL. *NeuroImage, 23*, S208–S219.
Smith, V. C., & Pokorny, J. (1975). Spectral sensitivity of the foveal cone photopigments between 400 and 500 nm. *Vision Research, 15*(2), 161–171.
Snodderly, D. M., Auran, J. D., & Delori, F. C. (1984). The macular pigment. II. Spatial distribution in primate retinas. *Investigative Ophthalmology & Visual Science, 25*(6), 674–685.
Solomon, S. G., & Lennie, P. (2005). Chromatic gain controls in visual cortical neurons. *Journal of Neuroscience, 25*(19), 4779–4792.
Srinivasan, V. J., Monson, B. K., Wojtkowski, M., Bilonick, R. A., Gorczynska, I., Chen, R., Duker, J. S., Schuman, J. S., & Fujimoto, J. G. (2008). Characterization of outer retinal morphology with high-speed, ultrahigh-resolution optical coherence tomography. *Investigative Ophthalmology & Visual Science, 49*(4), 1571–1579.
Stockman, A., & Sharpe, L. T. (2000). Tritanopic color matches and the middle-and long-wavelength-sensitive cone spectral sensitivities. *Vision Research, 40*(13), 1739–1750.
Strasburger, H., Bach, M., & Heinrich, S. P. (2018). Blur unblurred—a mini tutorial. *i-Perception, 9*(2), 2041669518765850.
Sun, H., Smithson, H. E., Zaidi, Q., & Lee, B. B. (2006). Do magnocellular and parvocellular ganglion cells avoid short-wavelength cone input? *Visual Neuroscience, 23*(3–4), 441–446.
Tregillus, K. E. M., Isherwood, Z. J., Vanston, J. E., Engel, S. A., MacLeod, D. I. A., Kuriki, I., & Webster, M. A. (2021). Color compensation in anomalous trichromats assessed with fMRI. *Current Biology, 31*(5), 936–942.
Van Essen, D. C., & Gallant, J. L. (1994). Neural mechanisms of form and motion processing in the primate visual system. *Neuron, 13*(1), 1–10.
Vernon, R. J. W., Gouws, A. D., Lawrence, S. J. D., Wade, A. R., & Morland, A. B. (2016). Multivariate patterns in the human object-processing pathway reveal a shift from retinotopic to shape curvature representations in lateral occipital areas, LO-1 and LO-2. *Journal of Neuroscience, 36*(21), 5763–5774.
Wandell, B. A., Dumoulin, S. O., & Brewer, A. A. (2006). Computational neuroimaging: Color signals in the visual pathways. *Neuro-Ophthalmology, 23*, 324–343.
Wang, Z., Bovik, A. C., Sheikh, H. R., & Simoncelli, E. P. (2004). Image quality assessment: From error visibility to structural similarity. *IEEE Transactions on Image Processing, 13*(4), 600–612.
Welbourne, L. E., Morland, A. B., & Wade, A. R. (2018). Population receptive field (pRF) measurements of chromatic responses in human visual cortex using fMRI. *NeuroImage, 167*, 84–94.
Woolrich, M. W., Ripley, B. D., Brady, M., & Smith, S. M. (2001). Temporal autocorrelation in univariate linear modeling of FMRI data. *NeuroImage, 14*(6), 1370–1386.

Bound thesis paper 2

Increasing spatial frequency of S-cone defined gratings reduces their visibility and brain response more than for gratings defined by L-M cone contrast.

Lowndes, R., Welbourne, L., Williams, M., Gouws, A., Wade, A., & Morland, A.

Vision Research

2023

Vision Research 207 (2023) 108209

Contents lists available at ScienceDirect

Vision Research

journal homepage: www.elsevier.com/locate/visres

Increasing spatial frequency of S-cone defined gratings reduces their visibility and brain response more than for gratings defined by L-M cone contrast

Rebecca Lowndes [a,b,*], Lauren Welbourne [a,b], Molly Williams [a], Andre Gouws [a,b], Alex Wade [a,b,c], Antony Morland [a,b,c]

[a] Department of Psychology, University of York, United Kingdom
[b] York Neuroimaging Centre, University of York, United Kingdom
[c] York Biomedical Research Institute, University of York, United Kingdom

A B S T R A C T

Chromatic sensitivity reduces as spatial frequency increases. Here, we explore the behavioural and neuronal responses to chromatic stimuli at two spatial frequencies for which the difference in sensitivity will be greater for S-cone than L-M stimuli. Luminance artefacts were removed using the Random Luminance Modulation (RLM) technique. As expected, doubling the spatial frequency increased the detection threshold more for S-cone than for isoluminant L-M gratings. We then used fMRI to measure the cortical BOLD responses to the same two chromatic stimuli (S and L-M) at the same two spatial frequencies. Responses were measured in six visual areas (V1, V2, V3, V3a, hV4, TO1/2). We found a significant interaction between spatial frequency in V1, V2 and V4 suggesting that the behaviourally observed increase in contrast threshold for high spatial frequency S-cone stimuli is reflected in these retinotopic areas. Our measurements show that neural responses consistent with psychophysical behaviour in a colour detection task can be observed as early as primary visual cortex.

1. Introduction

It has been long established that human colour vision is trichromatic (Young, 1802, Von Helmholtz, 1867). Long after those historical works, it was found that cone photoreceptors in the human eye had different spectral absorptions (Brown and Wald, 1964; Bowmaker and Dartnall, 1980), having three cone classes tuned to long (L) medium (M) and short (S) wavelengths. These three cones form three visual pathways; L+M (achromatic luminance channel), L-M (red-green) and S-(L+M) (blue-yellow) (MacLeod and Boynton, 1979) demonstrated in the Lateral Geniculate Nucleus (LGN) of primates (Wiesel & Hubel, 1966; Derrington, Krauskopf, & Lennie, 1984). Early psychophysical work investigated contrast sensitivity as a function of spatial frequency along red-green and blue-yellow colour directions and found that sensitivity is reduced as spatial frequency increases (Mullen, 1985). The chromatic pathways in the LGN have since been more accurately described as red-cyan (L-M) and lavender-lime (S-(L+M)) (Conway, 2009). The reduction in sensitivity for high spatial frequency chromatic gratings has been replicated more recently for both L-M and S colour directions (Mullen & Kingdom, 2002, Welbourne, Morland & Wade, 2018, Neitz et al., 2020, Wuerger et al., 2020). Work above threshold in colour matching tasks has shown that pattern sensitivity is lower in S-cone than L-M conditions (Poirson and Wandell, 1993). Other work has confirmed that the difference in threshold between high and low spatial frequencies is more pronounced for gratings defined along the S than the L-M cardinal colour directions (Poirson and Wandell, 1996, Mullen and Kingdom, 2002).

Work by Williams and colleagues (1993) investigated whether these differences were due to optical factors or neural sampling effects. Optical factors are any factors relating to the eye such as chromatic aberration, which causes colour distortion, and differences in quantum catch, which is the effect of the reduced number of S-cones in the human retina when compared to L and M cones. They showed that the reduction in sensitivity caused by optical factors to S-cone and L-M stimuli was largely the same across spatial frequencies, particularly those below 4 cpd. They found that neural factors affected L-M and S-cone sensitivity at similar rates at 4 cpd and above. Between 2 (the lowest spatial frequency tested) and 4 cpd, there is a hint that there is a greater reduction in sensitivity for S-cone compared to L-M stimuli. Other work (Swanson, 1996) has shown that S-cone contrast sensitivity can be relatively independent of non-neural factors when measured between 1 and 5 cpd using an extension of two-colour increment threshold techniques developed by Stiles (1946). Later work has shown using quick contrast

* Corresponding author.
E-mail address: rebecca.lowndes@york.ac.uk (R. Lowndes).

https://doi.org/10.1016/j.visres.2023.108209
Received 19 May 2022; Received in revised form 30 January 2023; Accepted 31 January 2023
Available online 4 March 2023

sensitivity functions that binocular summation of chromatic stimuli depends on neural processing and not optical factors up to 2.5 cpd (Kim et al., 2017). The current study aims to investigate neural factors and has adopted a method inspired by the work of Stiles using backgrounds to ensure targets are detected by single chromatic neural mechanisms.

The human occipital lobe has multiple retinotopic representations, which can be identified with fMRI (DeYoe et al., 1994; Sereno et al., 1995; Engel, Glover & Wandell, 1997). The largest representation is striate cortex (V1) (Dougherty et al., 2003), which receives input from the LGN. Beyond V1, lie V2, V3, V3a and hV4, which have been shown to exhibit preferential responses to different stimuli. Colour appears to drive responses in ventral occipital area hV4, first identified in humans by Zeki and colleagues (1991). Area V3a lies on the dorsal surface and has a similar topography and the same hierarchical position as hV4 in the visual cortex. V3a, is more commonly associated with motion selectivity (Tootell et al., 1997; Klaver et al., 2008; Mikellidou et al., 2018) and has shown a significant preference for achromatic stimuli (Mullen et al., 2007) as well as high temporal frequency flicker (Liu and Wandell, 2005). However, other work has shown dorsal involvement in colour processing, including V3a (Liu & Wandell, 2005; Mullen, Thompson and Hess, 2010; D'Souza et al., 2011, Castaldi et al., 2013). Further along the dorsal stream lie TO1 and TO2, the retinotopic analogue of MT+ (Amano, Wandell, & Dumoulin, 2009), the human motion area. These visual field maps are considered to be motion selective and show lower responses to chromatic stimuli than achromatic stimuli (Mullen et al., 2007; Wandell et al., 1999).

While many studies have shown that ventral visual areas, including hV4, are very sensitive to colour stimuli (Zeki et al., 1991; McKeefry & Zeki, 1997; Wade, Brewer, Rieger & Wandell, 2002; Goddard et al., 2011; Mullen, Chang and Hess, 2015; Mullen, 2019), the findings do not mean that substantive chromatic processing is not undertaken in earlier visual areas such as V1 (Mullen et al., 2007). In fact, studies have shown chromatic processing is a common feature in early visual areas (Railo et al., 2012; Mullen et al., 2015; Mullen, 2019); an fMRI adaptation study showed all early visual areas showed responses to both coloured and achromatic stimuli (Mullen, Chang and Hess, 2015; Mullen, 2019). Careful examination of responses to colour modulations in V1 and V2 (Engel, Zhang and Wandell, 1997) showed a coupling between fMRI BOLD responses to coloured gratings and psychophysical detection thresholds, for some, but not all stimulus conditions.

Using fMRI to link neuronal responses and perception is challenging. To optimise signal quality in fMRI, stimuli are normally presented above threshold and over a relatively large spatial area. The former means that inaccurate specification of cone stimulation values can result in small but significant luminance artefacts. The latter means that accurate specification of cone stimulation is challenging because of the spatial variations of spectrally selective absorption in the macular pigments (Ruddock, 1963; Snodderly, Auran & Delori, 1984; Hammond, Wooten, & Snodderly, 1997; Chen, Chang and Wu, 2001; Davies and Morland, 2004) and morphology of cone outer segments (Goodchild, Ghosh and Martin, 1996; Srinivasan et al., 2008) across eccentricities of the retina. Chromatic aberration can also induce luminance artefacts, particularly at high spatial frequencies (Murasugi and Cavanagh, 1988; Bradley, Zhang and Thibos, 1992). To overcome these challenges, we adopted the approach taken by Birch, Barbur and Harlow (1992), who presented colour stimuli superimposed on a rapidly updating grid of checks with random luminance values. This Random Luminance Modulation (RLM) reduces the sensitivity of the achromatic pathways. This renders luminance artefacts undetectable and therefore allows responses to chromatic content of stimuli to be isolated. This specific technique has not yet been used fMRI experiments, though Wade and colleagues (2008) used a similar technique to demonstrate robust responses to colour stimuli in human ventral cortex.

In this study we first aimed to determine whether the lower sensitivity to high spatial frequency S-cone grating stimuli compared to their L-M counterparts could be established psychophysically in the presence of an RLM background. We measured sensitivity to square wave gratings on an RLM background at two spatial frequencies (1.25 and 2.5 cycles per degree (cpd)) for two colour directions (S-cone and L-M). Relatively low spatial frequencies were chosen to reduce the effects of longitudinal chromatic aberration, which are more pronounced as spatial frequency increases (Murasugi and Cavanagh, 1988; Bradley, Zhang and Thibos, 1992). We found grating contrast sensitivity at 2.5 cpd was reduced compared to 1.25 cpd grating and that this reduction in sensitivity was greater for S-cone than L-M gratings. Suprathreshold versions of the four grating stimuli were presented to participants during acquisition of fMRI data. We assessed responses from six retinotopic representations (V1, V2, V3, V3a, hV4 and TO1/2) to determine at what levels of the cortical hierarchy we might observe processing consistent with the contrast sensitivities we measured. We found an interaction between spatial frequency and colour direction - that followed our contrast sensitivity measures - in V1, V2 and, in one experiment V4, which was driven by the greater difference between responses to high and low spatial frequency stimuli defined along the S-cone compared to L-M colour directions. The responses we measured in these areas were therefore consistent with the behavioural data and likely indicate that the mechanism limiting detection of coloured gratings is set at or before primary visual cortex.

2. Methods

2.1. Participants

2.1.1. Behavioural experiment

Six (four female) colour-normal trichromats (confirmed with a Rayleigh match) with a mean age of 33.5 years (+- 11.00 years) were recruited for a single 40-minute psychophysics session in the scanner. The ethics committee at York Neuroimaging centre at the University of York approved this experiment.

2.1.2. FMRI experiments

Six (four female) colour-normal trichromats (confirmed with a Rayleigh match) with a mean age of 25.7 years (+- 5.47 years) were recruited. All participants took part in five hour-long fMRI sessions. The ethics committee at York Neuroimaging centre at the University of York approved these experiments.

2.2. Experiment and stimulus design

2.2.1. Target stimuli

Target stimuli (Fig. 1) were square wave gratings in the central 10x10 degrees squared of either low spatial frequency (1.25 cpd) or high spatial frequency (2.5 cpd). The spatial frequencies tested in this experiment were carefully chosen to ensure that any results found could not be explained exclusively by the effects of longitudinal chromatic aberration, which has a strong influence at high spatial frequencies (Murasugi and Cavanagh, 1988; Bradley, Zhang and Thibos, 1992). Some evidence suggests that the effects of longitudinal chromatic aberration are negligible below 4 cpd (Pefferkorn, Chiron & Vienot., 1997) which is beyond the highest spatial frequency of the current study at 2.5 cpd. To examine this more thoroughly, we used the equation detailed by Strasburger et al (2018) to calculate the diameter of blur given as:

$$b^{\circ} = 0.057PD$$

where P is the pupil diameter in millimetres and D is the defocus in diopters. A different project in our lab used the same contrast RLM background as the current project, but recorded videos of the eyes of participants. We found in 6 participants that pupil diameter was 3.19 mm on average. Rynders, Navarro, and Losada (1998) calculated D over similar wavelengths (458–632 nm) to the limits of the projector used in the current study (455–625 nm) and found D to be equal to ±0.5 over the eccentricities used in our stimuli. Therefore, the diameter of blur is

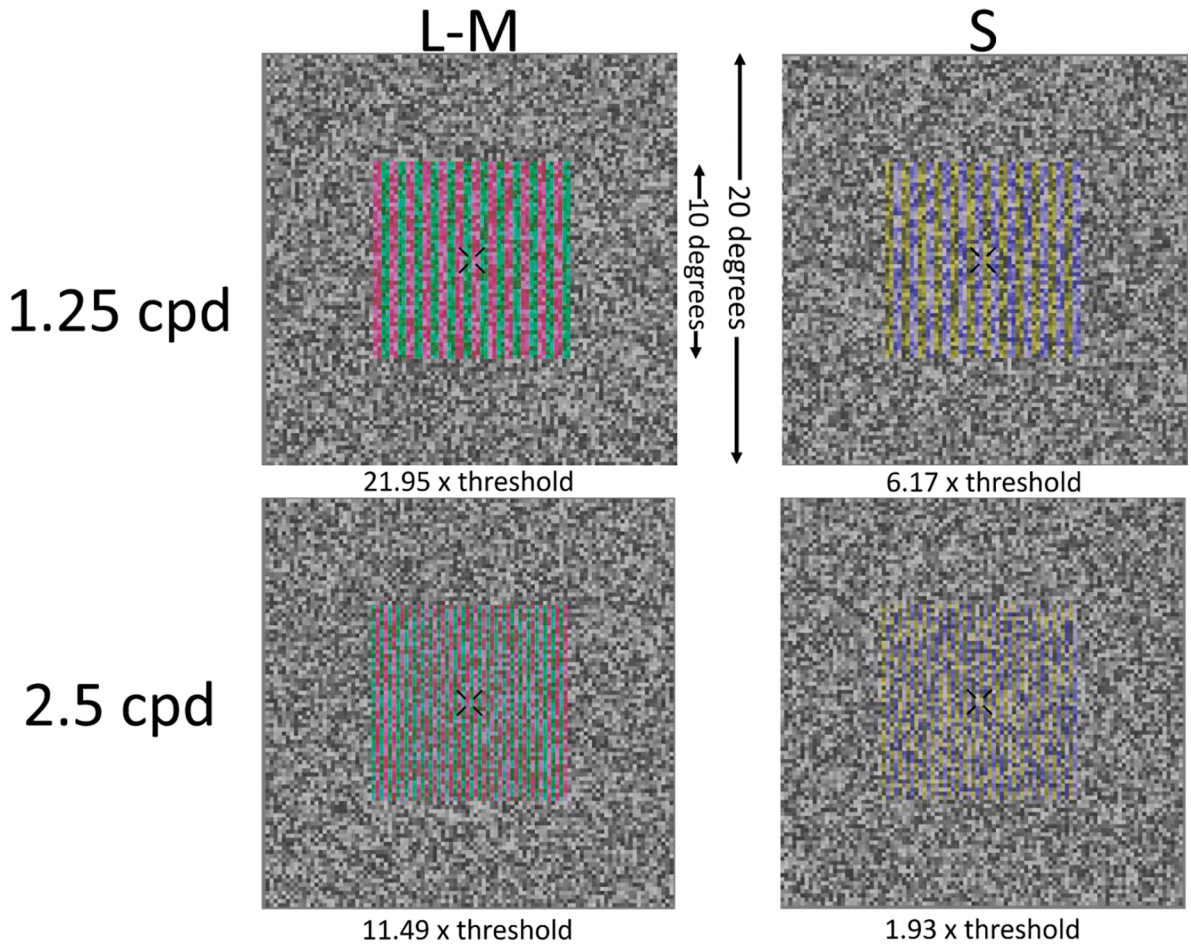

Fig. 1. Images of the stimuli that were presented during experiments. Note that target gratings are shown at a higher contrast for demonstration purposes. The multiples of threshold shown below are based on the mean threshold found for each condition from the behavioural experiment described in 2.2.4 and 3.1, with a contrast of 2.7% in the L-M condition and 10.5% in the S-cone condition. Fixation is shown here as was present during the fMRI experiments.

equal to 0.091. The blur would therefore extend 0.045 degrees on either side of the grating boundary. Given that the grating bar width has a minimum of 0.2 degrees, blur extending from each boundary (2 × 0.045 degrees) leaves the majority of the bar, 0.109 degrees, unaffected by blurr and therefore at the specified contrast.

Chromatic contrasts of the targets (2.7% L-M and 10.5% S-cone) were chosen for the fMRI experiments based on multiples of the behavioural thresholds found in the behavioural experiment outlined in 2.2.4 and 3.1. An fMRI study by Mullen et al (2007) found surprisingly high responses to S-cone stimuli at lower (5x) multiples of threshold in comparison with similarly high responses to L-M stimuli at much higher (31x) multiples of threshold. We reasoned therefore that selecting stimulus contrasts that should elicit similar fMRI responses for L-M and S-cone stimuli at 1.25 cycles per degree would offer the best way to examine effects associated with doubling spatial frequency. We therefore chose values of ~ 22x (21.95) multiples of threshold for L-M (equating to 2.7%) and ~ 6x (6.17) multiples of threshold for S-cone (equating to 10.5%). We erred on the side of caution insofar as relative to Mullen et al (2007) our S-cone stimuli may be anticipated to yield greater response than those to L-M stimuli. Moreover, these values were also high enough that our high spatial frequency targets (2.5 cpd) in both chromatic conditions were still visible (11.49 multiples of threshold for L-M and 1.93 multiples of threshold for S-cone).

2.2.2. Random luminance modulation (RLM) stimuli

The stimuli used for the RLM background were adapted from Birch and colleagues (1992). The background stimulus consisted of an array of squares, in which each check was assigned a greyscale value between ±50% L+M contrast from the uniform grey field at random every 0.05 s (20 Hz). This background subtended 20x20 degrees square of visual angle and remained on for the duration of each scan. The rationale for the design is to have a rapidly updating, relatively high luminance (mean luminance 177 cd/m^2) contrast component to the stimulus, to which luminance sensitive mechanisms will respond robustly. Any small luminance artefacts resulting from colour modulations superimposed on the background should therefore be undetected by luminance sensitive mechanisms.

2.2.3. Stimulus presentation

The visual stimuli were designed and presented using PsychoPy and PsychToolBox in MATLAB. The delivery system used for the visual stimulus in the scanner was a ViewPixx projector, which projected the stimulus onto a custom-made acrylic screen. The participant viewed the screen with a mirror fixed to the head coil in the scanner. Spectral measurements of the RGB channels of the scanner screen were made using a 'Jaz' (Ocean Optics, FL) spectrometer. Chromatic stimuli were defined using the 10-deg cone fundamentals based on the Stiles and Burch 10-deg colour matching functions described in Stockman and Sharpe (2000). These values allowed us to specify isoluminant S and L-M cone stimuli for the average observer using silent substitution. No further accounting for luminance for the individual participants in this study was conducted, so if presented on a uniform background the gratings we generated could contain luminance artefacts. However, the random luminance modulation described in 2.2.2 is an effective way of

rendering many of these artefacts invisible.

2.2.4. Behavioural experiment

Behavioural experiments were performed inside the scanner bore using a two-interval forced choice paradigm. The RLM background comprised an array of 100x100 squares (0.2x0.2 degrees squared) (Fig. 1) which remained on throughout the duration of the experiment. Target stimuli were chromatic gratings in the central 10x10 degrees squared of either low spatial frequency (1.25 cpd, comprising bars of width equal to two background checks) or high spatial frequency (2.5 cpd, comprising bars of width equal to one background check). Fixation changed from standard (+) to cross (x) for 0.5 s when the target stimulus could be present. Targets were separated by a 2 s interval, with one target containing a chromatic grating, and one without but still showing the RLM background. Participants were asked to press '1′ if the target was in the first presentation of 'x' and '2′ if it was in the second presentation. A standard three-up one-down staircase was used to adjust the target contrast. The task finished after 16 reversals or 100 trials. The ~ 80% threshold was calculated as the mean of the contrast during the last 7 reversals.

2.2.5. fMRI experiment 1: RLM background (0.2x0.2 squared degree checks)

In the first fMRI experiment, the background comprised an array of squares (100x100) covering an area of 20x20 degrees squared (Fig. 1) - identical to that used in the behavioural experiments. Each element of the array subtended 0.2 × 0.2 degrees of visual angle. Target gratings were superimposed over the RLM background which added either chromatic contrast (L-M contrast at 2.7%, S-cone contrast at 10.5%) or, in a control experiment, achromatic contrast (L+M contrast at 15%), in a square wave pattern. As before, stimuli at two spatial frequencies were presented; 1.25 cpd and 2.5 cpd. The orientation of the target grating was vertical and contrast polarity was reversed at 1 Hz. The choice of reversal rate of the target stimulus increases the likelihood that colour specific mechanisms dominate the response to the colour modulations, as they have sluggish temporal response properties (Regan and He, 1996, Wade et al., 2008), particularly for S-cone stimuli (Liu & Wandell, 2005). Each block-design fMRI run consisted of a single combination of three potential chromatic conditions and two potential spatial frequency conditions presented eight times with a cycle time of 30 s. Each cycle contained a 15 s grating presentation with RLM background and fixation marker and 15 s of RLM only with a fixation marker. In each session, lasting approximately one hour, all six combinations of stimulus spatial frequency and colour direction were presented. Each participant completed three sessions resulting in 18 h of scan data.

To help participants maintain fixation during the fMRI experiments, they performed a demanding attentional task (button press when the fixation cross changed width) which was not locked to the timing of the stimuli.

2.2.6. fMRI experiment 2: RLM background (0.4x0.4 squared degree checks)

In order to establish whether any effects were due to the change in spatial frequency, or the change in spatial concordance with the RLM background, all participants also completed a further one-hour scan session with the background checks set to 0.4 deg rather than the original 0.2 deg. This meant that the 1.25 cpd grating matched the RLM background spatially. The target gratings followed the same colour directions (L-M, S-cone and L+M) at one spatial frequency of 1.25 cycles per degree. Participants completed the same fixation task as described in 2.2.5. Each chromatic condition was presented in two runs in one scanning session leading to six scans in a session. Each run followed the block design described above.

2.2.7. Retinotopy stimuli

The retinotopy scans used a sweeping bar stimulus, which were similar to those described in other experiments (Dumoulin and Wandell 2008; Binda, Thomas, Boynton, & Fine, 2013; Alvarez et al., 2015; Welbourne, Morland & Wade, 2018). Specifically, our bars were 1.25 degrees of visual angle wide, and moved in 16 steps across a 20 degrees diameter circular aperture, for 8 bar directions (with four blank periods); the order of the bar directions and positions of the blank periods was as described in Welbourne, Morland and Wade (2018). Each bar step lasted for the length of one TR (2500 ms), and contained a 100% contrast white noise stimulus, which had been scaled by a factor of 8 to reduce the average spatial frequency in the texture. The texture updated at 2 Hz. Participants carried out four repeats of these scans in one scan session. To aid participants in maintaining central fixation, participants performed an attentional task (button press when the fixation point changed colour) that was not locked to the timing of the stimuli. The scan session for the retinotopy lasted for approximately 40 min and comprised four runs.

2.3. MRI protocol

All scans were carried out using a Siemens 3 T MRI scanner, with a 64-channel head coil. The participant's head was positioned in the coil with foam padding to ensure the head was stable. For the functional scans, 76 EPI slices were taken within an FOV of 192x192mm with 1.5 mm isotropic voxels (TR = 2500 ms, TE = 40.8 ms, flip angle = 75 degrees, voxel matrix = 128x128). Scan slices were aligned axially and always covered occipital and temporal lobes.

In addition to the functional scans, three T1-weighted and two T2-weighted structural scans were taken for each participant, at a 0.8x0.8x0.8 mm resolution. The protocol for these scans was taken from the Human Connectome Project (Glasser et al., 2013).

2.4. Data processing

2.4.1. Structural - data processing

All structural scans were analysed using the HCP minimal processing pipeline (version 5.0, (Glasser et al., 2013) using a combination of FSL (http://fsl.fmrib.ox.ac.uk/fsl/fslwiki/ (Smith et al., 2004) and Freesurfer (http://surfer.nmr.mgh.harvard.edu/ (Dale, Fischl & Sereno, 1999; Reuter, Schmansky, Rosas, & Fischl, 2012)).

TO1 and TO2 were derived using the anatomically defined retinotopy atlas (Benson et al., 2014) implemented in the python analysis toolbox 'neuropythy' (Benson and Winawer, 2018). The atlas then predicted several Freesurfer-based maps (visual area, eccentricity, polar angle, and pRF size), which were used to delineate the central 5 degrees of TO1 and TO2 which were then combined into a single ROI referred to as TO1/2 for further analysis.

2.4.2. Retinotopy - data processing

Population receptive field (pRF) mapping was performed using the 2015 version of the VISTA software (https://web.stanford.edu/group/vista/cgi-bin/wiki/index.php/Software) (Vista Lab, Stanford University), running under MATLAB 2015 (The MathWorks Inc., Natick, MA, USA). We applied pRF modelling to an average of all retinotopy scans which had been motion corrected between and within scans using a maximum likelihood alignment routine (Nestares and Heeger, 2000). Functional scans were aligned to individual anatomy scans using FLIRT linear registration (Jenkinson and Smith 2001; Jenkinson, Bannister, Brady, & Smith, 2002). The retinotopic eccentricities and polar angles extracted by the pRF model were then used to draw boundaries of visual areas V1, V2, V3, V3a and hV4 on a flattened representation of visual cortex (see Fig. 2); for details of the pRF model used see Welbourne et al (2018). These regions of interest (ROIs) were then restricted to the central 5 degrees of eccentricity to best fit the stimuli (10 deg diameter) and transformed into NIFTI files using the VISTA function roiSaveAsNifti for use in the rest of the analysis, which was performed in FSL (see below).

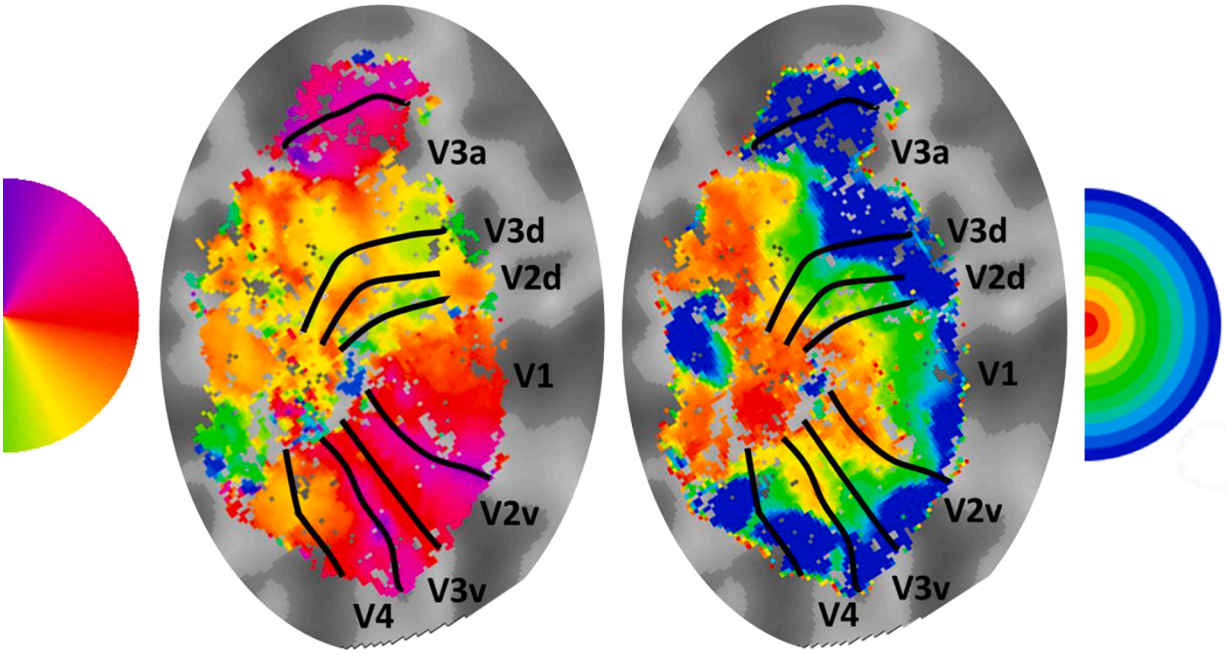

Fig. 2. The retinotopic maps used to delineate ROIs for one participant with phase map (left) and eccentricity map (right) for the left hemisphere. Visual area boundaries are overlaid on the maps.

2.4.3. fMRI experiments - data processing

The data for all fMRI experiments other than retinotopy detailed in 2.4.2 were pre-processed using FEAT (FMRI Expert Analysis Tool) version 6.00, part of FSL (FMRIB's Software Library) version 5.0. Images were skull-stripped using a brain extraction tool (BET (Smith, 2002)). Motion correction (MCFLIRT; (Jenkinson, Bannister, Brady, & Smith, 2002)) was followed by spatial smoothing (Gaussian full width half maximum 2 mm). Data were high pass temporal filtered (Gaussian-weighted least-squares straight line fitting with sigma = 15.0 s). Individual participant data was registered to their own high resolution structural (generated from T1 and T2 structural images using the HCP processing pipeline) using FLIRT (12 DOF, Jenkinson and Smith, 2001; Jenkinson, Bannister, Brady, & Smith, 2002). Time-series statistical analysis was carried out using FILM with autocorrelation correction (Woolrich, Ripley, Brady, & Smith, 2001).

For each run for each participant, two explanatory variables were defined. The first modelled our target as 15 s on and 15 s of blank. The second modelled each time the task appeared on screen. The target model was our main effect and the task was modelled as a variable of no interest. Percentage signal change was then computed for each run, each visual area and in each participant individually using FeatQuery. Signal change values for runs of the identical conditions were then averaged for each participant.

3. Results

3.1. Behavioural results

We first assessed whether a doubling of the spatial frequency of the chromatic gratings from 1.25 to 2.5 cpd reduced the sensitivity more to S compared to L-M contrast. The sensitivity (1/cone contrast threshold) for detecting chromatic gratings superimposed on the luminance-modulated background are shown in Fig. 3. Doubling the spatial frequency decreased sensitivity to gratings modulated along both cardinal colour directions (Fig. 3 left panel). Every participant tested demonstrated greater difference between S-cone than L-M contrast sensitivity (Fig. 3 right panel). A 2x2 ANOVA revealed a significant interaction between colour condition and contrast threshold ($F(1, 5) = 7.83$, $p = .038$, $\eta^2 = 0.61$) which is driven by the greater loss of sensitivity to high spatial frequency S-cone stimuli consistent with the literature (Mullen, 1985; Mullen and Kingdom, 2002; Poirson and Wandell, 1993; 1996; Welbourne, Morland and Wade, 2018). Brain regions that perform chromatic processing that underpin the behavioural measures should therefore show an interaction in the BOLD response between the spatial frequency and colour axis of the gratings.

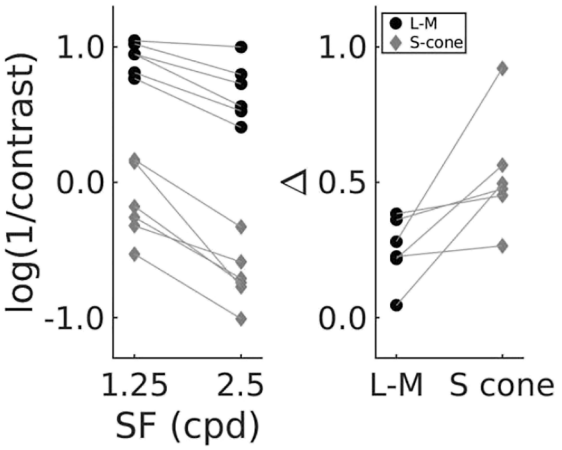

Fig. 3. Left panel: A graph to show the inverse log of the cone contrast thresholds (~80% correct) for L-M and S-cone conditions at the test spatial frequencies of 1.25 and 2.5 cpd. The dots and diamonds represent each participant's individual threshold and lines are drawn between each participant's threshold at each spatial frequency. Right panel: A graph showing the difference (Δ) between sensitivities shown in the left panel at 1.25 cpd and 2.5 cpd for L-M and S-cone conditions. Dots represent the difference for each participant and lines are drawn between their L-M and S-cone Δ values.

3.2. fMRI results

Based on the behavioural data, we hypothesised that the effect of doubling spatial frequency would be more pronounced for BOLD

responses to S-cone targets compared to L-M targets. Given that different visual areas have different sensitivities to both colour and spatial frequencies, we also asked whether this interaction might also depend on the cortical location from which we record responses. Such an effect would be indicated by a three-way interaction between visual field map, chromaticity and spatial frequency.

Responses to the four chromatic stimulus conditions acquired for each visual field map are shown in Fig. 4. It appears that the reduction in response resulting from a doubling of spatial frequency is greater for S than L-M stimuli in all regions of interest apart from TO1/2. To assess whether effects varied by visual field map, we ran a three-way repeated measures ANOVA (see table 1) which revealed a significant three way interaction between visual area, colour direction and spatial frequency. There was a significant two-way interaction between colour direction and spatial frequency, likely driven by the fact that all but one (TO1/2) visual area showed the same pattern of response. Also noted is the interaction between visual area and spatial frequency, again likely caused by the responses in TO1/2.

To follow-up on the three-way interaction we performed two-way ANOVAs on the responses from each visual field map. Significant interactions between colour axis and spatial frequency were found in V1 ($F(1, 5) = 11.26$, $p = .020$, $\eta^2 = 0.69$;) and V2 ($F(1, 5) = 9.75$, $p = .026$, $\eta^2 = 0.66$) but not in V3 ($F(1, 5) = 3.30$, $p = .129$, $\eta^2 = 0.40$), V3a ($F(1, 5) = 1.50$, $p = .275$, $\eta^2 = 0.23$) or TO1/2 ($F(1, 5) = 0.76$, $p = .422$, $\eta^2 = 0.13$) with V4 ($F(1, 5) = 6.34$, $p = .053$, $\eta^2 = 0.56$) approaching significance.

Given the markedly small responses from TO1/2 we checked to see whether they differed from zero with single sample t-tests. The TO1/2 response only differed from zero for the high spatial frequency L-M condition ($T(5) = 3.14$, $p = .026$).

While the responses we recorded to gratings defined along cardinal colour axes fitted with our predictions in some visual field maps we still wanted to check that the modulation of the background minimised the chance of detecting responses to luminance artefacts in our stimuli. To do this, we presented gratings defined by L+M contrast superimposed on the modulating background. The gratings were at a contrast that was high (15%) relative to any expected luminance artefact. The responses to target gratings at 1.25 and 2.5 cpd are shown for each visual field map in Fig. 5. The responses at 2.5 cpd were not significantly different from zero, but responses to the low spatial frequency grating appear larger, although notably smaller than responses we recorded to coloured gratings of the same spatial frequency. The results indicate that small luminance artefacts are unlikely to register responses that would unduly affect the responses we attribute to chromatic modulations of our targets. To investigate potential effects we applied a two-way repeated measures ANOVA, which showed a significant interaction between the effect of spatial frequency and visual field map ($F(5,25) = 6.31$, $p = .020$, $\eta^2 = 0.56$). There could be an issue therefore in terms of how the difference between the spatial frequency of the target and background reduces the masking of the background. Pairwise comparisons reveal that this effect appears to be driven by V1 ($F(1, 5) = 9.73$, $p = .026$, $\eta^2 = 0.66$) and V2 ($F(1, 5) = 7.08$, $p = .045$, $\eta^2 = 0.59$) as all other areas showed a non-significant effect of the spatial frequency of achromatic stimuli (V3: $F(1, 5) = 2.04$, $p = .212$, $\eta^2 = 0.29$; V3a: $F(1, 5) = 0.50$, $p = .512$, $\eta^2 = 0.09$; hV4: $F(1, 5) = 1.01$, $p = .360$, $\eta^2 = 0.17$; TO1/2: $F(1, 5) = 2.10$, $p = .207$, $\eta^2 = 0.30$). It is reassuring that in the high spatial frequency condition there is no significant response to 15% contrast L+M gratings as a source of a luminance artefact in chromatic conditions is chromatic aberration, which is increasingly problematic as spatial frequency increases (Murasugi and Cavanagh, 1988; Bradley, Zhang and Thibos, 1992).

To check whether the partial release from the masking of the background (when target and background are not matched) could have caused the interaction between chromatic condition and spatial frequency we performed an experiment in which we increased the size of the background checks to 0.4 squared degrees, which matched the width of the coarser (1.25 cpd) target grating's bars. We compared the target related responses to this stimulus configuration with those originally obtained with the background check size of 0.2 squared degrees as shown in Fig. 6. In all visual field maps the responses obtained with the smaller background checks were greater than those obtained with background checks that matched the width of the target gratings irrespective of the colour of those gratings. However, if the change in response to the target resulting from the change in the background varied by colour direction, this could contribute to the interaction between spatial frequency and colour direction we detected earlier. We therefore ran a three-way repeated measures ANOVA (Table 2), which showed no significant interaction between colour direction and spatial frequency of the background and no significant three-way interaction between colour direction, spatial frequency and visual area which shows that the different target and background spatial properties that we originally used are unlikely to be the cause of the interaction between colour direction and spatial frequency that we observed earlier (Table 1).

In the knowledge that increasing the background check size reduced the response to the low spatial frequency target grating, notwithstanding the absence of an interaction between background check size and colour direction, we chose to be cautious and compare responses to target grating of different spatial frequencies and colour directions under conditions where the background checks matched the bar widths of the target gratings. The spatial frequency of the target gratings are therefore identical to those shown in Fig. 4. The responses obtained under these matched conditions are shown in Fig. 7. The reduction in response caused by the doubling of spatial frequencies is still clearly evident for S-cone stimuli, but is now less clear for L-M stimuli. It appears therefore, that the larger cost of increasing spatial frequency for S-cone than L-M cone defined grating persists. To check this we ran a three-way ANOVA as we did before (Table 3). There was a significant three-way interaction between visual field map, spatial frequency and colour axis and the same two-way interaction between spatial frequency and colour axis as found for the main experiment. Follow-up two-way ANOVAs applied for each visual field map - to investigate the source of the three-way interaction - showed significant interactions between colour axis and spatial frequency in all visual field maps apart from V3a

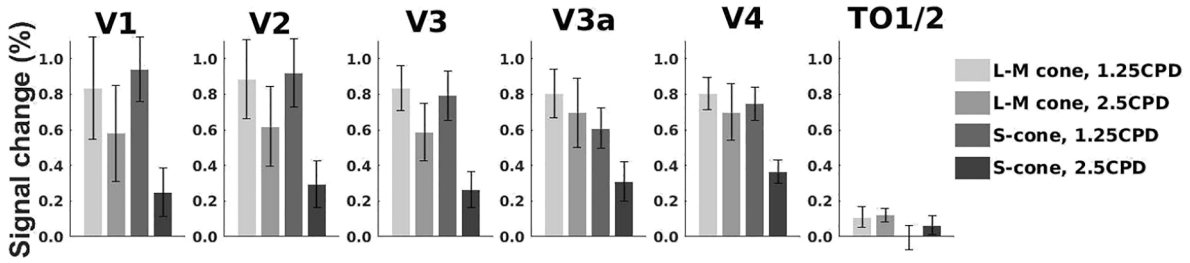

Fig. 4. A bar graph to show the mean percent signal change to each spatial frequency (1.25 and 2.5 cpd) for each colour direction (L-M and S-cone) for each visual area. Error bars are one standard error of the mean (SEM).

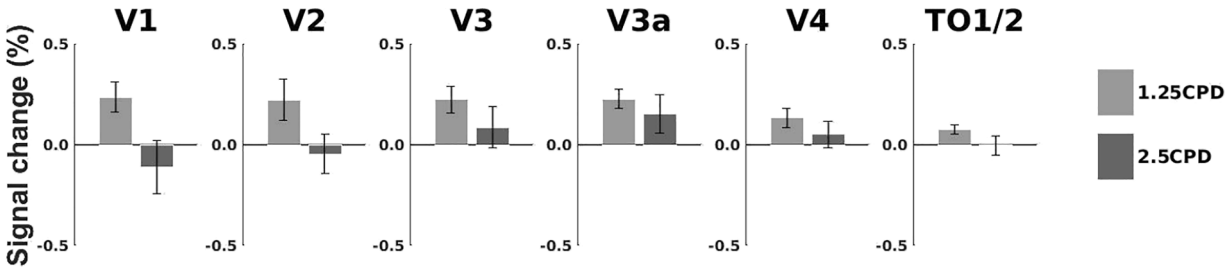

Fig. 5. Bar graphs to show the percentage signal change to achromatic stimuli at both spatial frequencies (1.25 and 2.5 cpd). Error bars are one SEM.

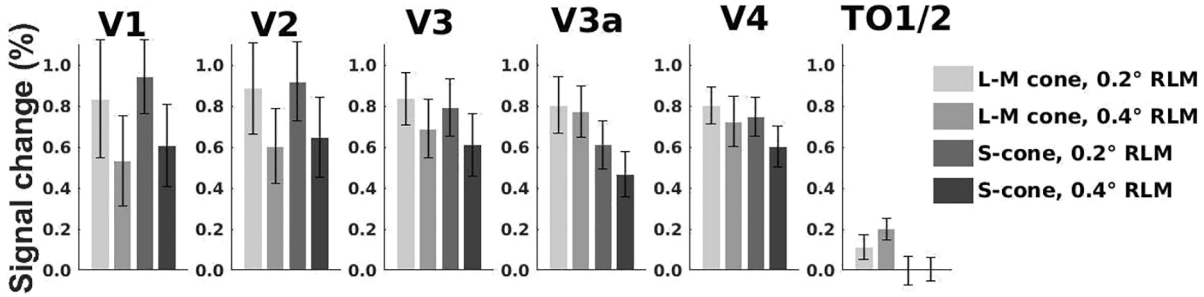

Fig. 6. A bar graph to show the mean percent signal change to the lower spatial frequency target (1.25 cpd) on the high spatial frequency and low spatial frequency background (0.2 and 0.4 degrees squared checks) for each colour direction (L-M and S-cone) for each visual area. Error bars are one SEM.

Table 1
Results of the ANOVA to investigate effects of visual areas (V1, V2, V3, V3a, hV4 and TO1/2), chromatic condition (L-M and S-cone) and spatial frequency (1.25 and 2.5 cpd) on the BOLD response. Greenhouse-Geisser correction is applied when sphericity is violated.

Source	Mauchly's *p*	df1, df2	F	*p*	Effect Size
Area (A)	0.099	5, 25	7.57	**<0.001**	0.60
Chromatic Condition (B)	.	1, 5	8.05	**0.036**	0.62
Spatial Frequency (C)	.	1, 5	41.71	**0.001**	0.89
A × B	**0.012**	1.52, 7.60	1.37	0.299	0.22
A × C	0.073	5, 25	10.88	**<0.001**	0.69
B × C	.	1, 5	6.67	**0.049**	0.57
A × B × C	0.203	5, 25	3.92	**0.009**	0.44

Table 2
Results of the ANOVA to investigate effects of visual areas (V1, V2, V3, V3a, hV4 and TO1/2), chromatic condition (L-M and S-cone) and spatial frequency of the RLM background (0.2 and 0.4 degrees squared checks, 1.25 cpd target grating) on the BOLD response. Greenhouse-Geisser correction is applied when sphericity is violated.

Source	Mauchly's *p*	df1, df2	F	*p*	Effect Size
Area (A)	**0.009**	1.37, 6.86	8.59	**<0.001**	0.63
Chromatic Condition (B)	.	1, 5	2.17	0.201	0.30
Background Spatial Frequency (C)	.	1, 5	8.85	**0.031**	0.64
A × B	0.169	5, 25	7.44	**<0.001**	0.60
A × C	**<0.001**	1.51, 7.56	6.93	**0.024**	0.58
B × C	.	1, 5	0.26	0.631	0.05
A × B × C	0.053	5, 25	0.38	0.920	0.05

and TO1/2 (V1: $F(1, 5) = 6.82$, $p = .048$, $\eta^2 = 0.58$; V2: $F(1, 5) = 7.90$, $p = .038$, $\eta^2 = 0.61$; V3: $F(1, 5) = 7.13$, $p = .044$, $\eta^2 = 0.59$; V3a: $F(1, 5) = 2.10$, $p = .207$, $\eta^2 = 0.30$; hV4: $F(1, 5) = 19.24$, $p = .007$, $\eta^2 = 0.79$; TO1/2: $F(1, 5) = 5.81$, $p = .061$, $\eta^2 = 0.54$). The significant interactions are driven by the lower responses elicited by the high spatial frequency S gratings compared to their lower spatial frequency counterparts and gratings defined by modulation along the L-M colour axis. The results indicate again that the doubling of the target grating's spatial frequency reduces responses to stimuli defined by modulations along the S more than those defined by modulations along the L-M axis.

4. Discussion

The aim of this study was to uncover the effects of spatial frequency on both behavioural and neural responses to chromatic stimuli. We found reduced contrast sensitivity for high compared to low spatial frequency coloured gratings. Moreover, the decrease in sensitivity at high spatial frequencies was greater for gratings defined by S compared to L-M cone contrast. The BOLD responses we recorded from V1, V2 and V4 showed a significant interaction between spatial frequency of the target and chromatic condition, mirroring the behavioural results. This study suggests that neural responses to colour align well with behaviour in these areas.

The contrast sensitivity measures we obtained replicate a long-standing interaction between L-M and S-cone defined gratings and their spatial frequency (Mullen, 1985; Mullen and Kingdom, 2002; Poirson and Wandell, 1993, 1996, Welbourne, Morland and Wade, 2018). This shows that the RLM technique is capable of isolating chromatic mechanisms of human vision as others who devised the approach have shown in the past (Birch, Barbur & Harlow, 1992; Barbur, Birch and Harlow, 1993; Barbur, Harlow and Plant, 1994). We went further when we applied the RLM technique to measure brain responses. Measuring brain responses always comes with greater challenges because stimuli are presented at many times threshold and over a large area of visual field. For colour, this means that there is the potential for relatively large chromatic contrasts to generate small achromatic artefacts. Moreover, chromatic aberration can also play a role in generating luminance artefacts of coloured gratings, particularly at high spatial frequency

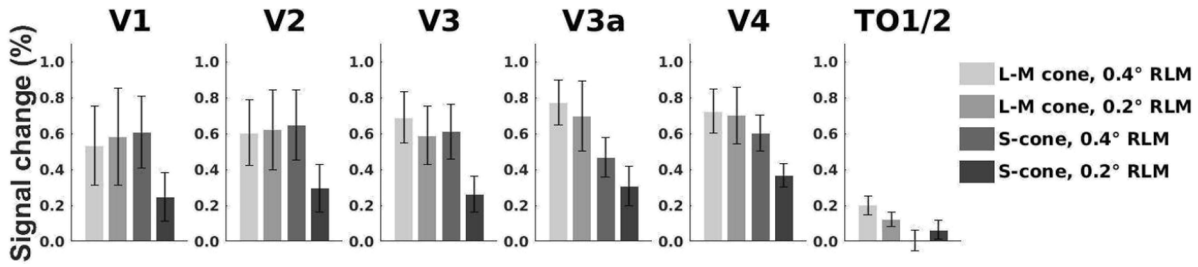

Fig. 7. A bar graph to show the mean percent signal change to the low spatial frequency target (1.25 cpd) on the low spatial frequency background (0.4 degrees squared checks) and the higher spatial frequency target (2.5 cpd) on the high spatial frequency background (0.2 degrees squared checks) for each colour direction (L-M and S-cone) for each visual area. Error bars are one SEM.

Table 3
Results of the ANOVA to investigate effects of visual areas (V1, V2, V3, V3a, hV4 and TO1/2), chromatic condition (L-M and S-cone) and spatial frequency when both targets were concordant with the RLM background (0.4 degrees squared checks with 1.25 cpd target and 0.2 degrees squared checks with 2.5 cpd target). Greenhouse-Geisser correction is applied when sphericity is violated.

Source	Mauchly's *p*	df1, df2	F	*p*	Effect Size
Area (A)	0.052	5, 25	6.10	**0.001**	0.55
Chromatic Condition (B)	.	1, 5	7.73	**0.039**	0.61
Spatial Frequency (C)	.	1, 5	4.19	0.096	0.46
A × B	**0.017**	1.86, 9.31	2.57	0.131	0.34
A × C	0.356	5, 25	5.22	**0.002**	0.51
B × C	.	1, 5	6.76	**0.048**	0.58
A × B × C	0.152	5, 25	7.06	**<0.001**	0.59

(Murasugi and Cavanagh, 1988, Bradley, Zhang and Thibos, 1992). Our result that gratings defined by a relatively high (15%) increment of achromatic contrast generated undetectable brain signals when presented on the randomly changing backgrounds suggests that any achromatic artefacts would not generate significant responses from cortex. This shows therefore that the RLM approach is well suited to studies of chromatic mechanisms, particularly for suprathreshold stimuli presented over a large area of the visual field. We note however that we did not account for each individual's macular pigment density, which could rotate the vector of the S-cone stimuli. However, this rotation is likely very small as variations in white points as a function of macular pigment density align closely with tritan confusion lines (Wright 1928–29, Ruddock, 1963).

Returning to the behavioural results, we replicated the lasting finding that there is lower sensitivity to S-cone stimuli than L-M stimuli in general and even more so at high spatial frequencies (Mullen, 1985; Mullen & Kingdom, 2002; Poirson & Wandell, 1993, 1996; Welbourne, Morland & Wade, 2018). Previous studies have suggested that S-cones have a lower response at all spatial frequencies due to a reduced quantum catch (Williams, Sekiguchi, & Brainard, 1993), but this does not explain the spatial frequency differences. Swanson (1996) showed that non-neural factors do not affect S-cone contrast sensitivity between 1 and 5 cpd, so these differences must be due to neural factors. The brain responses to coloured gratings depended both on their spatial frequency and colour as demonstrated by the interaction we have reported. This feature was most consistently observed in visual areas V1 and V2, but was also observed in hV4 in one but not another test. Previous work in our lab (Welbourne, Morland & Wade, 2018) has demonstrated decreased activity in V1 in high spatial frequency S-cone conditions when compared to L-M, but only at more peripheral eccentricities. Engel, Zhang and Wandell (1997) showed that responses in V1 aligned well with behaviour at 1 Hz temporal frequency, which is the same frequency we have used. There is also evidence that V1 is functionally linked with V2 and hV4 in a way that could explain the consistent interaction found in these areas in the current study. For example Nakamura and colleagues (1993) showed that in macaques, whilst V4 primarily receives input from V2, it also receives information directly from V1, bypassing V2. It also sends feedback projections to V1 and V2, as well as V3 (for review see Pasupathy, Popovkina & Kim, 2020). In humans, Wade and colleagues (2008, 2002) found significant responses to chromatic contrast across the ventral surface.

Although V3a exhibited a strong response to chromatic conditions, the interaction between chromatic condition and spatial frequency was not shown. V3a has been shown to have preference for achromatic stimuli and an enhanced response to flicker stimuli (Liu and Wandell, 2005). Therefore, the interaction between chromatic condition and spatial frequency may not be as salient in this area. In contrast to our work, previous work using an luminance modulated background found that chromatic responses were confined to the ventral surface (Wade et al., 2008), with no activation by chromatic stimuli of human dorsal areas like V3a. However, this study differed from ours in important ways that may explain the strong response we demonstrate in V3a. Firstly, the chromatic stimuli used in Wade and colleagues (2008) were defined as patches of colour and luminance, and had no spatial coherence unlike the gratings used in our study. Secondly, the chromatic target and achromatic background updated together at 1 Hz, so the temporal frequency of their achromatic and chromatic components were the same. V3a has been shown to be responsible for structure in motion processing (Koyama et al., 2005), so it is possible that our use of spatially structured grating and a temporally disparate stimulus has caused the colour to be perceived as a coherent separate stimulus that led to the response from V3a we have shown in this study.

TO1/2 showed very little response to any of our conditions, consistent with a motion selective and colour invariant area (Zeki et al., 1991). Previous work has shown fMRI responses in MT + to s-cone stimuli (Wandell et al., 1999), but this was 10 times lower than responses to achromatic stimuli, and the stimulus used in their experiment was low spatial frequency (0.5 cpd) and fast moving (8 degrees/second). In contrast, our stimuli were not moving, but phase shifting at a much lower rate (1 Hz) and our lowest spatial frequency grating was higher and thus not optimised for MT+. The research on MT+ is contentious about whether this area receives chromatic input at all (Zeki et al., 1991; Liu and Wandell, 2005) and our study suggests that it might not, or only when the chromatic information is at much lower spatial, but higher temporal, frequencies. Indeed, psychophysical studies have shown that when moving chromatic gratings are equated in luminance there is no visual perception of motion (Ramachandran and Gregory, 1978), lending support to the idea that MT+ does not receive chromatic input. Previous work relied on no, or suboptimal luminance masking to isolate chromatic stimuli (Wandell et al., 1999). Since MT+ is highly sensitive to even very low achromatic contrast, it is feasible that these previous results have been influenced by small luminance artefacts and chromatic aberration, which our study has accounted for using RLM.

hV4 has often been found to be a colour-specific area (Zeki et al., 1991; McKeefry & Zeki, 1997; Goddard et al., 2011) so it is interesting

that we did not find anything special about hV4 in this experiment. This research provides support for the suggestion that chromatic vision is more generally processed across the cortex, with some preferential processing in early areas V1 and V2 and ventral hV4. That we observed an interaction between spatial frequency and chromatic condition in V1, the lowest level of the cortical hierarchy, suggests that the neural mechanism could be set before the cortex, perhaps in the LGN or even colour opponent ganglion cells.

Psychophysical research has shown that colour perception is spatially low-pass at detection threshold (Mullen, 1985; Mullen and Kingdom, 2002; Poirson and Wandell, 1996; Welbourne, Morland and Wade, 2018) and for suprathreshold stimulus matching (Poirson and Wandell, 1993). In fMRI, V1 has also been shown to have spatially low-pass responses to colour stimuli when luminance is absent (Schluppeck and Engel, 2002). Both the behavioural and imaging studies are thought to be consistent with a low-pass single-opponent mechanism and our results add weight to this argument. It is also noted that there are double opponent cells in V1 that respond to both colour and luminance, but these exhibit band-pass characteristics, peaking at 2.56 cpd (Schluppeck and Engel, 2002). Such band pass mechanisms have recently been suggested to underpin the appearance of some structured chromatic stimuli (Shapley, Nunez and Gordon, 2019). However, our responses are far less likely to reflect these double opponent mechanisms because we record lower, not greater, responses to the 2.5 than the 1.25 cpd gratings.

We noted BOLD responses to S-cone stimuli at low spatial frequency were remarkably similar to those elicited by L-M stimuli. The cone contrasts of the stimuli eliciting these responses were however many more multiples of the psychophysically determined threshold for L-M than for S-cone stimuli. Mullen and colleagues (2007) also found surprisingly high S-cone responses in early visual areas relative to threshold, and found that cone contrast correlated better with BOLD response than a threshold based metric. Specifically, they found fMRI responses were just as robust for S-cone stimuli at 5 times threshold as L-M stimuli at 31 times threshold. Similarly, the current study has found similar BOLD responses to low spatial frequency S-cone stimuli at 6.17 times threshold as L-M stimuli at 20.95 times threshold. These results support the hypothesis that some contrast normalisation must be implemented for S-cone stimuli, leading to responses being amplified in V1 (Georgeson & Sullivan 1975, Heeger, 1992, Mullen et al., 2007, Carandini and Heeger, 2012).

5. Conclusions

This study has used RLM to provide support for previous work on colour contrast sensitivity, showing that colour vision is spatially low-pass, a finding which is reflected in fMRI BOLD responses in visual cortex. In V1, V2 and hV4, BOLD responses mirror behavioural data most consistently, showing that these areas are likely involved with colour perception. There is also some normalisation of S-cone signals across visual areas to make them more visible. The spatially low-pass nature of colour vision shown in this study provides support for work indicating that colour vision utilises single-opponent mechanisms. We have also found signals in the brain in early visual cortex that align well with behaviour, showing that chromatic responses are set early in the visual pathway, perhaps in the LGN.

CRediT authorship contribution statement

Rebecca Lowndes: Conceptualization, Methodology, Software, Investigation, Formal analysis, Data curation, Writing – original draft, Writing – review & editing. **Lauren Welbourne:** Formal analysis, Visualization. **Molly Williams:** Investigation. **Andre Gouws:** Software. **Alex Wade:** Supervision, Software, Writing – review & editing. **Antony Morland:** Conceptualization, Writing – review & editing, Methodology, Software, Investigation, Formal analysis, Supervision.

Declaration of Competing Interest

The authors declare that they have no known competing financial interests or personal relationships that could have appeared to influence the work reported in this paper.

Data availability

Data will be made available on request.

Acknowledgments

Supported by funding from BBSRC (BB/P007252).

References

Alvarez, I., De Haas, B. A., Clark, C. A., Rees, G., & Schwarzkopf, D. S. (2015). Comparing different stimulus configurations for population receptive field mapping in human fMRI. *Frontiers in Human Neuroscience, 9*(96), 1–16.

Amano, K., Wandell, B. A., & Dumoulin, S. O. (2009). Visual field maps, population receptive field sizes, and visual field coverage in the human MT+ complex. *Journal of Neurophysiology, 102*(5), 2704–2718.

Barbur, J. L., Birch, J., & Harlow, A. J. (1993). Colour vision testing using spatiotemporal luminance masking. In *Colour vision deficiencies XI* (pp. 417–426). Dordrecht: Springer.

Barbur, J. L., Harlow, J., & Plant, G. T. (1994). Insights into the different exploits of colour in the visual cortex. *Proceedings of the Royal Society of London. Series B: Biological Sciences*, *258*(1353), 327-334.

Benson, N. C., Butt, O. H., Brainard, D. H., & Aguirre, G. K. (2014). Correction of distortion in flattened representations of the cortical surface allows prediction of V1–V3 functional organization from anatomy. *PLoS Computational Biology, 10*(3), 1–9.

Benson, N. C., & Winawer, J. (2018). Bayesian analysis of retinotopic maps. *elife, 7*, 1–29.

Binda, P., Thomas, J. M., Boynton, G. M., & Fine, I. (2013). Minimizing biases in estimating the reorganization of human visual areas with BOLD retinotopic mapping. *Journal of Vision, 13*(7), 1–16.

Birch, J., Barbur, J. L., & Harlow, A. J. (1992). New method based on random luminance masking for measuring isochromatic zones using high resolution colour displays. *Ophthalmic and Physiological Optics, 12*(2), 133–136.

Bowmaker, J. K., & Dartnall, H. (1980). Visual pigments of rods and cones in a human retina. *The Journal of Physiology, 298*(1), 501–511.

Bradley, A., Zhang, X., & Thibos, L. (1992). Failures of isoluminance caused by ocular chromatic aberrations. *Applied Optics, 31*(19), 3657–3667.

Brown, P. K., & Wald, G. (1964). Visual pigments in single rods and cones of the human retina. *Science, 144*(3614), 45–52.

Carandini, M., & Heeger, D. J. (2012). Normalization as a canonical neural computation. *Nature Reviews Neuroscience, 13*(1), 51–62.

Castaldi, E., Frijia, F., Montanaro, D., Tosetti, M., & Morrone, M. C. (2013). BOLD human responses to chromatic spatial features. *European Journal of Neuroscience, 38*(2), 2290–2299.

Chen, S. F., Chang, Y., & Wu, J. C. (2001). The spatial distribution of macular pigment in humans. *Current Eye Research, 23*(6), 422–434.

Conway, B. R. (2009). Color vision, cones, and color-coding in the cortex. *The Neuroscientist, 15*(3), 274–290.

Dale, A. M., Fischl, B., & Sereno, M. I. (1999). Cortical surface-based analysis: I. Segmentation and surface reconstruction. *Neuroimage, 9*(2), 179–194.

Davies, N. P., & Morland, A. B. (2004). Macular pigments: Their characteristics and putative role. *Progress in Retinal and Eye Research, 23*(5), 533–559.

Derrington, A. M., Krauskopf, J., & Lennie, P. (1984). Chromatic mechanisms in lateral geniculate nucleus of macaque. *The Journal of physiology, 357*(1), 241–265.

DeYoe, E. A., Bandettini, P., Neitz, J., Miller, D., & Winans, P. (1994). Functional magnetic resonance imaging (FMRI) of the human brain. *Journal of Neuroscience Methods, 54*(2), 171–187.

Dougherty, R. F., Koch, V. M., Brewer, A. A., Fischer, B., Modersitzki, J., & Wandell, B. A. (2003). Visual field representations and locations of visual areas V1/2/3 in human visual cortex. *Journal of Vision, 3*(10), 586–598.

D'Souza, D. V., Auer, T., Strasburger, H., Frahm, J., & Lee, B. B. (2011). Temporal frequency and chromatic processing in humans: An fMRI study of the cortical visual areas. *Journal of Vision, 11*(8), 1–17.

Dumoulin, S. O., & Wandell, B. A. (2008). Population receptive field estimates in human visual cortex. *NeuroImage, 39*(2), 647–660.

Engel, S. A., Glover, G. H., & Wandell, B. A. (1997). Retinotopic organization in human visual cortex and the spatial precision of functional MRI. *Cerebral cortex (New York, NY: 1991)*, *7*(2), 181-192.

Engel, S., Zhang, X., & Wandell, B. (1997). Colour tuning in human visual cortex measured with functional magnetic resonance imaging. *Nature, 388*(6637), 68–71.

Georgeson, M. A., & Sullivan, G. D. (1975). Contrast constancy: Deblurring in human vision by spatial frequency channels. *The Journal of Physiology, 252*(3), 627–656.

Glasser, M. F., Sotiropoulos, S. N., Wilson, J. A., Coalson, T. S., Fischl, B., Andersson, J. L., ... & Wu-Minn HCP Consortium. (2013). The minimal preprocessing pipelines for the Human Connectome Project. *Neuroimage*, *80*, 105-124.

Goddard, E., Mannion, D. J., McDonald, J. S., Solomon, S. G., & Clifford, C. W. (2011). Color responsiveness argues against a dorsal component of human V4. *Journal of Vision, 11*(4), 1–21.
Goodchild, A. K., Ghosh, K. K., & Martin, P. R. (1996). Comparison of photoreceptor spatial density and ganglion cell morphology in the retina of human, macaque monkey, cat, and the marmoset Callithrix jacchus. *Journal of Comparative Neurology, 366*(1), 55–75.
Hammond, B. R., Wooten, B. R., & Snodderly, D. M. (1997). Individual variations in the spatial profile of human macular pigment. *JOSA A, 14*(6), 1187–1196.
Heeger, D. J. (1992). Normalization of cell responses in cat striate cortex. *Vis. Neurosci., 9*, 181–197.
Jenkinson, M., & Smith, S. (2001). A global optimisation method for robust affine registration of brain images. *Medical Image Analysis, 5*(2), 143–156.
Jenkinson, M., Bannister, P., Brady, M., & Smith, S. (2002). Improved optimization for the robust and accurate linear registration and motion correction of brain images. *Neuroimage, 17*(2), 825–841.
Kim, Y. J., Reynaud, A., Hess, R. F., & Mullen, K. T. (2017). A normative data set for the clinical assessment of achromatic and chromatic contrast sensitivity using a qCSF approach. *Investigative Ophthalmology & Visual Science, 58*(9), 3628–3636.
Klaver, P., Lichtensteiger, J., Bucher, K., Dietrich, T., Loenneker, T., & Martin, E. (2008). Dorsal stream development in motion and structure-from-motion perception. *Neuroimage, 39*(4), 1815–1823.
Koyama, S., Sasaki, Y., Andersen, G. J., Tootell, R. B., Matsuura, M., & Watanabe, T. (2005). Separate processing of different global-motion structures in visual cortex is revealed by FMRI. *Current Biology, 15*(22), 2027–2032.
Liu, J., & Wandell, B. A. (2005). Specializations for chromatic and temporal signals in human visual cortex. *The Journal of Neuroscience, 25*, 3459–3468.
MacLeod, D. I., & Boynton, R. M. (1979). Chromaticity diagram showing cone excitation by stimuli of equal luminance. *JOSA, 69*(8), 1183–1186.
McKeefry, D. J., & Zeki, S. (1997). The position and topography of the human colour centre as revealed by functional magnetic resonance imaging. *Brain: A Journal of Neurology, 120*(12), 2229–2242.
Mikellidou, K., Frijia, F., Montanaro, D., Greco, V., Burr, D. C., & Morrone, M. C. (2018). Cortical BOLD responses to moderate-and high-speed motion in the human visual cortex. *Scientific Reports, 8*(1), 1–12.
Mullen, K. T. (1985). The contrast sensitivity of human colour vision to red-green and blue-yellow chromatic gratings. *The Journal of Physiology, 359*(1), 381–400.
Mullen, K. T. (2019). The response to colour in the human visual cortex: The fMRI approach. *Current Opinion in Behavioral Sciences, 30*, 141–148.
Mullen, K. T., Dumoulin, S. O., McMahon, K. L., De Zubicaray, G. I., & Hess, R. F. (2007). Selectivity of human retinotopic visual cortex to S-cone-opponent, L/M-cone-opponent and achromatic stimulation. *European Journal of Neuroscience, 25*(2), 491–502.
Mullen, K. T., & Kingdom, F. A. A. (2002). Differential distributions of red–green and blue–yellow cone opponency across the visual field. *Visual Neuroscience, 19*(1), 109–118.
Mullen, K. T., Thompson, B., & Hess, R. F. (2010). Responses of the human visual cortex and LGN to achromatic and chromatic temporal modulations: An fMRI study. *Journal Vision, 10*(13), 1–19.
Mullen, K. T., Chang, D. H., & Hess, R. F. (2015). The selectivity of responses to red-green colour and achromatic contrast in the human visual cortex: An fMRI adaptation study. *European Journal of Neuroscience, 42*(11), 2923–2933.
Murasugi, C. M., & Cavanagh, P. (1988). Anisotropy in the chromatic channel: A horizontal-vertical. *Spatial Vision, 3*(4), 281–291.
Neitz, A., Jiang, X., Kuchenbecker, J. A., Domdei, N., Harmening, W., Yan, H., … Sabesan, R. (2020). Effect of cone spectral topography on chromatic detection sensitivity. *JOSA A, 37*(4), 1–24.
Nestares, O., & Heeger, D. J. (2000). Robust multiresolution alignment of MRI brain volumes. *Magnetic Resonance in Medicine: An Official Journal of the International Society for Magnetic Resonance in Medicine, 43*(5), 705–715.
Pasupathy, A., Popovkina, D. V., & Kim, T. (2020). Visual functions of primate area V4. *Annual Review of Vision Science, 6*, 363–385.
Pefferkorn, S., Chiron, A., & Viénot, F. (1997). *Effect of longitudinal chromatic aberration on photometric matches using a heterochromatic square-wave grating. In Colour Vision Deficiencies XIII* (pp. 403–407). Dordrecht: Springer.
Poirson, A. B., & Wandell, B. A. (1993). Appearance of colored patterns: Pattern–color separability. *JOSA A, 10*(12), 2458–2470.
Poirson, A. B., & Wandell, B. A. (1996). Pattern—color separable pathways predict sensitivity to simple colored patterns. *Vision Research, 36*(4), 515–526.
Railo, H., Salminen-Vaparanta, N., Henriksson, L., Revonsuo, A., & Koivisto, M. (2012). Unconscious and conscious processing of color rely on activity in early visual cortex: A TMS study. *Journal of Cognitive Neuroscience, 24*(4), 819–829.
Ramachandran, V. S., & Gregory, R. L. (1978). Does colour provide an input to human motion perception? *Nature, 275*(5675), 55–56.
Regan, D., & He, P. (1996). Magnetic and electrical brain responses to chromatic contrast in human. *Vision Research, 36*(1), 1–18.
Reuter, M., Schmansky, N. J., Rosas, H. D., & Fischl, B. (2012). Within-subject template estimation for unbiased longitudinal image analysis. *Neuroimage, 61*(4), 1402–1418.
Ruddock, K. H. (1963). Evidence for macular pigmentation from colour matching data. *Vision Research, 3*(9–10), 417–429.
Rynders, M. C., Navarro, R., & Losada, M. A. (1998). Objective measurement of the off-axis longitudinal chromatic aberration in the human eye. *Vision Research, 38*(4), 513–522.
Schluppeck, D., & Engel, S. A. (2002). Color opponent neurons in V1: A review and model reconciling results from imaging and single-unit recording. *Journal of Vision, 2*(6), 480–492.
Sereno, M. I., Dale, A. M., Reppas, J. B., Kwong, K. K., Belliveau, J. W., Brady, T. J., … Tootell, R. B. H. (1995). Borders of multiple visual areas in humans revealed by functional magnetic resonance imaging. *Science, 268*(5212), 889–893.
Shapley, R., Nunez, V., & Gordon, J. (2019). Cortical double-opponent cells and human color perception. *Current Opinion in Behavioral Sciences, 30*, 1–7.
Smith, S. M. (2002). Fast robust automated brain extraction. *Human Brain Mapping, 17*(3), 143–155.
Smith, S. M., Jenkinson, M., Woolrich, M. W., Beckmann, C. F., Behrens, T. E., Johansen-Berg, H., … Matthews, P. M. (2004). Advances in functional and structural MR image analysis and implementation as FSL. *Neuroimage, 23*, S208–S219.
Snodderly, D. M., Auran, J. D., & Delori, F. C. (1984). The macular pigment. II. Spatial distribution in primate retinas. *Investigative Ophthalmology & Visual Science, 25*(6), 674–685.
Srinivasan, V. J., Monson, B. K., Wojtkowski, M., Bilonick, R. A., Gorczynska, I., Chen, R., … Fujimoto, J. G. (2008). Characterization of outer retinal morphology with high-speed, ultrahigh-resolution optical coherence tomography. *Investigative Ophthalmology & Visual Science, 49*(4), 1571–1579.
Stiles, W. S. (1946). Separation of the 'blue'and 'green'mechanisms of foveal vision by measurements of increment thresholds. *Proceedings of the Royal Society of London. Series B-Biological Sciences, 133*(873), 418-434.
Stockman, A., & Sharpe, L. T. (2000). Tritanopic color matches and the middle-and long-wavelength-sensitive cone spectral sensitivities. *Vision Research, 40*(13), 1739–1750.
Strasburger, H., Bach, M., & Heinrich, S. P. (2018). Blur unblurred—a mini tutorial. *i-Perception, 9*(2), 1–15.
Swanson, W. H. (1996). S-cone spatial contrast sensitivity can be independent of pre-receptoral factors. *Vision Research, 36*(21), 3549–3555.
Tootell, R. B., Mendola, J. D., Hadjikhani, N. K., Ledden, P. J., Liu, A. K., Reppas, J. B., … Dale, A. M. (1997). Functional analysis of V3A and related areas in human visual cortex. *Journal of Neuroscience, 17*(18), 7060–7078.
Von Helmholtz, H. (1867). *Treatise on Physiological Optics* (vol. iii). translated by J. P. C. Southall, Opt.Soc. Am., 1924–5.
Wade, A. R., Brewer, A. A., Rieger, J. W., & Wandell, B. A. (2002). Functional measurements of human ventral occipital cortex: Retinotopy and colour. *Philosophical Transactions of the Royal Society of London. Series B: Biological Sciences, 357*(1424), 963–973.
Wade, A., Augath, M., Logothetis, N., & Wandell, B. (2008). fMRI measurements of color in macaque and human. *Journal of vision, 8*(10), 1–19.
Wandell, B. A., Poirson, A. B., Newsome, W. T., Baseler, H. A., Boynton, G. M., Huk, A., … Sharpe, L. T. (1999). Color signals in human motion-selective cortex. *Neuron, 24*(4), 901–909.
Wiesel, T. N., & Hubel, D. H. (1966). Spatial and chromatic interactions in the lateral geniculate body of the rhesus monkey. *Journal of Neurophysiology, 29*(6), 1115–1156.
Welbourne, L. E., Morland, A. B., & Wade, A. R. (2018). Population receptive field (pRF) measurements of chromatic responses in human visual cortex using fMRI. *NeuroImage, 167*, 84–94.
Williams, D., Sekiguchi, N., & Brainard, D. (1993). Color, contrast sensitivity, and the cone mosaic. *Proceedings of the National Academy of Sciences, 90*(21), 9770–9777.
Woolrich, M. W., Ripley, B. D., Brady, M., & Smith, S. M. (2001). Temporal autocorrelation in univariate linear modeling of FMRI data. *Neuroimage, 14*(6), 1370–1386.
Wright, W. D. (1928-29) A re-determination of the trichromatic coefficients of the spectral colours. *Transactions of the Optical Society 30*(4), 141-164.
Wuerger, S., Ashraf, M., Kim, M., Martinovic, J., Pérez-Ortiz, M., & Mantiuk, R. K. (2020). Spatio-chromatic contrast sensitivity under mesopic and photopic light levels. *Journal of Vision, 20*(4), 1–26.
Young, T. (1802). II. The Bakerian Lecture. On the theory of light and colours. *Philosophical transactions of the Royal Society of London, 92*, 12–48.
Zeki, S., Watson, J. D., Lueck, C. J., Friston, K. J., Kennard, C., & Frackowiak, R. S. (1991). A direct demonstration of functional specialization in human visual cortex. *Journal of Neuroscience, 11*(3), 641–649.

Bound thesis paper 3

Structural differences across multiple visual cortical regions in the absence of cone function in congenital achromatopsia.

Lowndes, R., Molz, B., Warriner, L., Herbik, A., De Best, P.B., Raz, N., Gouws, A., Ahmadi, K., McLean, R.J., Gottlob, I., Kohl, S., Choritz, L., Maguire, J., Kanowski, M., Käsmann-Kellner, B., Wieland, I., Banin, E., Levin, N., Hoffmann, M.B., Morland, A.B., and Baseler, H.A.

Frontiers in Neuroscience

2021

frontiers in Neuroscience

ORIGINAL RESEARCH
published: 14 October 2021
doi: 10.3389/fnins.2021.718958

Structural Differences Across Multiple Visual Cortical Regions in the Absence of Cone Function in Congenital Achromatopsia

Rebecca Lowndes[1,2], Barbara Molz[1,3†], Lucy Warriner[1], Anne Herbik[4], Pieter B. de Best[5†], Noa Raz[5†], Andre Gouws[2†], Khazar Ahmadi[4†], Rebecca J. McLean[6], Irene Gottlob[6], Susanne Kohl[7], Lars Choritz[4], John Maguire[8], Martin Kanowski[9], Barbara Käsmann-Kellner[10], Ilse Wieland[11], Eyal Banin[12], Netta Levin[5‡], Michael B. Hoffmann[4,13‡], Antony B. Morland[1,14‡] and Heidi A. Baseler[1,14,15‡]*

[1] Department of Psychology, University of York, York, United Kingdom, [2] York Neuroimaging Centre, Department of Psychology, University of York, York, United Kingdom, [3] Language and Genetics Department, Max Planck Institute for Psycholinguistics, Nijmegen, Netherlands, [4] Department of Ophthalmology, University Hospital, Otto von Guericke University, Magdeburg, Germany, [5] MRI Unit, Department of Neurology, Hadassah Medical Center, Jerusalem, Israel, [6] University of Leicester Ulverscroft Eye Unit, University of Leicester, Leicester Royal Infirmary, Leicester, United Kingdom, [7] Molecular Genetics Laboratory, Institute for Ophthalmic Research, Centre for Ophthalmology, University Clinics Tübingen, Tübingen, Germany, [8] School of Optometry and Vision Sciences, University of Bradford, Bradford, United Kingdom, [9] Department of Neurology, University Hospital, Otto von Guericke University, Magdeburg, Germany, [10] Department of Ophthalmology, Saarland University Hospital and Medical Faculty of the Saarland University Hospital, Homburg, Germany, [11] Department of Molecular Genetics, Institute for Human Genetics, University Hospital, Otto von Guericke University, Magdeburg, Germany, [12] Degenerative Diseases of the Retina Unit, Department of Ophthalmology, Hadassah Medical Center, Jerusalem, Israel, [13] Center for Behavioral Brain Sciences, Magdeburg, Germany, [14] York Biomedical Research Institute, University of York, York, United Kingdom, [15] Hull York Medical School, University of York, York, United Kingdom

OPEN ACCESS

Edited by:
Holly Bridge,
University of Oxford, United Kingdom

Reviewed by:
Tessa Dekker,
University College London, United Kingdom
Manzar Ashtari,
University of Pennsylvania, United States

***Correspondence:**
Heidi A. Baseler
heidi.baseler@york.ac.uk

[†]NextGenVis Consortium Members

[‡]These authors have contributed equally to this work and share senior authorship

Specialty section:
This article was submitted to Perception Science, a section of the journal Frontiers in Neuroscience

Received: *01 June 2021*
Accepted: *16 September 2021*
Published: *14 October 2021*

Citation:
Lowndes R, Molz B, Warriner L, Herbik A, de Best PB, Raz N, Gouws A, Ahmadi K, McLean RJ, Gottlob I, Kohl S, Choritz L, Maguire J, Kanowski M, Käsmann-Kellner B, Wieland I, Banin E, Levin N, Hoffmann MB, Morland AB and Baseler HA (2021) Structural Differences Across Multiple Visual Cortical Regions in the Absence of Cone Function in Congenital Achromatopsia. Front. Neurosci. 15:718958. doi: 10.3389/fnins.2021.718958

Most individuals with congenital achromatopsia (ACHM) carry mutations that affect the retinal phototransduction pathway of cone photoreceptors, fundamental to both high acuity vision and colour perception. As the central fovea is occupied solely by cones, achromats have an absence of retinal input to the visual cortex and a small central area of blindness. Additionally, those with complete ACHM have no colour perception, and colour processing regions of the ventral cortex also lack typical chromatic signals from the cones. This study examined the cortical morphology (grey matter volume, cortical thickness, and cortical surface area) of multiple visual cortical regions in ACHM (n = 15) compared to normally sighted controls (n = 42) to determine the cortical changes that are associated with the retinal characteristics of ACHM. Surface-based morphometry was applied to T1-weighted MRI in atlas-defined early, ventral and dorsal visual regions of interest. Reduced grey matter volume in V1, V2, V3, and V4 was found in ACHM compared to controls, driven by a reduction in cortical surface area as there was no significant reduction in cortical thickness. Cortical surface area (but not thickness) was reduced in a wide range of areas (V1, V2, V3, TO1, V4, and LO1). Reduction in early visual areas with large foveal representations (V1, V2, and V3) suggests that the lack of foveal input to the visual cortex was a major driving factor in morphological changes in ACHM. However, the significant reduction in ventral area V4 coupled with the lack

of difference in dorsal areas V3a and V3b suggest that deprivation of chromatic signals to visual cortex in ACHM may also contribute to changes in cortical morphology. This research shows that the congenital lack of cone input to the visual cortex can lead to widespread structural changes across multiple visual areas.

Keywords: achromatopsia, congenital visual impairment, anatomical brain regions, visual areas, structural plasticity, parallel visual pathways, ventral and dorsal pathways

INTRODUCTION

Congenital achromatopsia (ACHM; also known as rod monochromacy) is a largely stationary, genetically heterogeneous and predominantly autosomal recessive retinal disorder with a prevalence of approximately ∼1 in 30,000 people (Francois, 1961; Kohl et al., 2004; Aboshiha et al., 2016). Most cases are caused by mutations in one of the several genes expressed in the retinal phototransduction pathway of the cone photoreceptor. As a result, ACHM is characterised by a lack of function in all three cone photoreceptors from birth. The functional integrity of cone photoreceptors is fundamental for the mediation of photopic (bright light) vision, high visual acuity and colour perception. In the normally-sighted, the central fovea of the retina is composed exclusively of cone photoreceptors providing high visual acuity. With only functioning rods, individuals with complete ACHM have a central scotoma where rods are absent and a complete loss of colour vision from birth, along with reduced visual acuity (Haegerstrom-Portnoy et al., 1996a,b; Remmer et al., 2015; Hirji et al., 2018). In normally-sighted individuals, the foveal region of the visual field dominated by cones is overrepresented in the visual cortex (cortical magnification). Crucially, this means that in ACHM a disproportionately large area of the visual cortex receives atypical input due to the defective cone photoreceptors. Thus, it is possible that the lack of visual input to foveal representations within visual regions throughout the cortex may influence the structural characteristics of the visual cortex within this patient population.

The brain contains multiple representations of the visual field, becoming functionally specialised along the visual processing hierarchy. Beyond early occipital areas V1, V2, and V3, higher areas in the ventral stream are important for colour, pattern and shape/form processing (Zeki et al., 1991; McKeefry and Zeki, 1997; Wade et al., 2002; Goddard et al., 2011; Winawer and Witthoft, 2015), while dorsal areas are involved in the analysis of spatial characteristics such as object motion, position, depth and visually guided grasping (Ungerleider and Mishkin, 1982; Goodale and Milner, 1992). In particular, human ventral area V4 responds most strongly to chromatic stimuli (Zeki et al., 1991; Wade et al., 2002; Goddard et al., 2011), and responses in ventral occipital cortex (VO) have been correlated with the perceptual experience of colour (Jiang et al., 2007). Furthermore, damage to ventral areas such as V4 leads to a loss of colour perception (cerebral achromatopsia) (Zeki, 1990). Given the importance of cones for colour perception and high acuity vision needed for processing shape/form, it is possible that lack of cone input in ACHM might affect ventral visual areas more significantly than dorsal areas. Indeed, a behavioural study by Burton et al. (2016) supports this hypothesis, reporting that individuals with ACHM are more impaired in global form perception relative to global motion and biological motion perception.

To date, at least five genes, GNAT2, PDE6C, PDE6H, CNGA3, and CNGB3, have been identified as responsible for over 90% of congenital ACHM cases (Wissinger et al., 2001; Johnson et al., 2004; Varsányi et al., 2005; Thiadens et al., 2009; Liang et al., 2015; Zelinger et al., 2015; Sun et al., 2020). Of these, the vast majority are caused by mutations in either CNGA3 or CNGB3 genes (Kohl et al., 2004; Liang et al., 2015; Zelinger et al., 2015; Sun et al., 2020). Current clinical trials are testing gene-therapeutic interventions to treat congenital ACHM by restoring cone function in the eye (Fischer et al., 2020; Reichel et al., 2021; NCT03758404, NCT03001310, NCT03278873, NCT02935517, NCT02599922, and NCT02610582).

The consequences of potential cortical changes in ACHM on efforts to restore vision are currently unknown. However, we can draw on changes to the posterior visual pathway that have been documented in other visual deficits to provide some context (Prins et al., 2016). Previous research has reported significant structural changes in visual processing pathways in the brain both in individuals with congenital blindness (Ptito et al., 2008; Jiang et al., 2009; Park et al., 2009; Aguirre et al., 2016; Bridge and Watkins, 2019) and acquired defects (Boucard et al., 2009; Hernowo et al., 2014; Brown et al., 2016; Prins et al., 2016; Hanson et al., 2019). Functional changes have been identified in another ophthalmological disorder, i.e., amblyopia, in higher visual areas including V4 and MT+ (Wong, 2012). Structural changes have also been reported in totally blind individuals specifically in connectivity to the ventral visual areas (Reislev et al., 2016a,b). In models of glaucoma, it is evident that the posterior visual pathway undergoes degeneration, which would likely prevent full restoration of vision (Yucel and Gupta, 2015). If cortical atrophy is detected in ACHM, it is possible that degeneration has occurred and could limit restoration of vision.

Efforts to restore vision in different disorders have been cautiously optimistic, but have produced mixed results. In late-onset disorders such as age-related cataract, visual acuity immediately improves following corrective surgery, and this is associated with an increase in grey matter volume of visual brain areas (Lou et al., 2013; Lin et al., 2018). Similarly, in late-blind participants with retinitis pigmentosa, motion detection and BOLD responses to visual stimuli were enhanced following implantation of a retinal prosthesis even after years of deprivation (Castaldi et al., 2016). However, visual recovery evident in these studies may have been strictly dependent on the presence of early visual experience during childhood (Hadad et al., 2015). In early-onset disorders, such visual experience is

absent. Even when the optical image has been fully restored following surgery, vision is not always restored to normal. In cases of early blindness due to corneal opacity, after corneal replacement participants still perform poorly on higher level visual tasks requiring shape, object and face processing (Fine et al., 2003) or colour discrimination (Ackroyd et al., 1974). Following surgery to correct congenital cataract, the degree of vision restoration is inversely related to the extent of changes in visual cortex (Guerreiro et al., 2015, 2016). Overall, these studies suggest that restoring vision to normal must involve normal cortical function and that anatomical biomarkers could provide a valuable indicator of the extent to which function may return to normal, particularly in the case of a congenital deficit.

Using gene therapeutic interventions, such as those well established in Leber's Congenital Amaurosis, visual and behavioural outcomes have also been variable (for review see: Chiu et al., 2021). However, evidence that cortical plasticity is still possible later in life was provided by an fMRI study reporting increased responses in visual cortex following gene therapy when participants with Leber's Congenital Amaurosis were treated in adulthood (Mowad et al., 2020). In ACHM, early studies also report promising but variable results following gene therapy (Farahbakhsh et al., 2020; Fischer et al., 2020; Reichel et al., 2021). In a study of two adult ACHM participants, minor improvements in visual acuity and a reduction in levels of photoaversion were found following treatment (McKyton et al., 2021). Furthermore, population receptive field sizes were reduced in early visual areas following treatment, suggesting that some restoration of cortical function is possible. However, although participants were now able to detect differences in the red end of the spectrum, there was no improvement in colour discrimination nor were fMRI responses detectable in colour-specific brain areas. The absence of improved colour discrimination could be due to insufficient restoration of retinal function or due to limitations in visual cortex. Nevertheless, a lack of colour responses in extrastriate brain areas along with an inability to discriminate colours suggest that long-term deficits may persist.

The aim of the current study was to evaluate how the deprivation of foveal and chromatic vision in participants with ACHM affect the development and structural integrity of multiple visual regions in striate and extrastriate cortex. Given the absence of functioning cones in ACHM, we hypothesised that ventral visual areas would be more affected than dorsal areas. We found that early visual areas V1 to V3 exhibit atrophic changes in ACHM. Similar changes were also present in ventral region V4, but not in dorsal areas V3a and V3b at an equivalent level in the visual hierarchy. We provide evidence therefore that the structural development of visual brain areas driven predominantly by cone input is particularly affected in ACHM.

MATERIALS AND METHODS

Participants

High resolution structural scans were collected at three sites from 42 control participants with normal or corrected to normal vision (mean age ± SD: 30.29 ± 9.72 years; 19 males) and 15 participants with both genetically confirmed ACHM (biallelic CNGA3 (n = 10) or CNGB3 (n = 5) mutations; see **Table 1**) and electroretinographically confirmed absence of cone function (mean age ± SD: 36.73 ± 10.95 years; 9 males). An independent samples t-test between groups found no significant age difference between groups [$t(55) = -2.02$. $p = 0.056$]. However, given the difference in mean age was close to the $p < 0.05$ cut-off, a subsequent analysis assessed age as a possible confound, along with scanner site, gender, and global metrics (see section "Results").

Experimental protocols received approval from the site-specific ethics committees and were in accordance with the Declaration of Helsinki.

MRI Protocol

University of York (10 Controls, 4 Achromatopsia)

A single, high resolution, anatomical, T1-weighted scan (TR, 2500 ms; TE, 2.26ms; TI, 900 ms; voxel size, 1 × 1 × 1 mm^3; flip angle, 7°; matrix size, 256 × 256 × 176, total acquisition time, 306 s) was acquired on each participant using a 64-channel head coil on a SIEMENS MAGNETOM Prisma 3T scanner at the York Neuroimaging Centre (YNiC).

Hadassah Medical Centre (24 Controls, 6 Achromatopsia)

A single, high resolution, anatomical, T1-weighted scan (TR, 2300 ms; TE, 1.5 ms; TI, 900 ms; voxel size, 1 × 1 × 1 mm^3; flip angle, 9°; matrix size, 256 × 256 × 160, total acquisition time, 278 s) was acquired on each participant using a 32-channel head coil on a SIEMENS MAGNETOM Skyra 3T scanner at the Edmond & Lily Safra Centre for Brain Sciences, Hebrew University of Jerusalem.

University of Magdeburg (8 Controls, 5 Achromatopsia)

A single, high resolution, anatomical, T1-weighted scan (TR, 2500 ms; TE, 2.82 ms; TI, 1100 ms; voxel size, 1 × 1 × 1 mm^3; flip angle, 7°; matrix size, 256 × 256 × 192, total acquisition time, 560 s) was acquired on each participant using a 64-channel head coil on a SIEMENS MAGNETOM Prisma 3T scanner at the University Hospital, Magdeburg, Germany.

Data Pre-processing

Cortical reconstruction and volumetric segmentation of the T1-weighted scans and surface-based morphology analysis were performed using the Freesurfer analysis suite Version 6.0 (Dale et al., 1999; Fischl et al., 1999). This included the removal of non-brain tissue (Ségonne et al., 2004), automated Talairach transformation, intensity normalisation (Sled et al., 1998), tessellation of the grey/white matter and pial boundaries (grey/cerebrospinal fluid) with automated topology correction and surface deformation (Dale et al., 1999; Fischl et al., 1999; Ségonne et al., 2007). Subsequently, the cortical surface was inflated and registered to a sphere (Fischl et al., 1999) and the surface parcellated according to gyral and sulcal structures (Ségonne et al., 2004; Desikan et al., 2006).

TABLE 1 | Summary of patient demographics showing participant group (ACHM, participants with congenital achromatopsia; C, control participants), gender (m, male; f, female), age, scanner site (HMC, Hadassah Medical Centre; UM, University of Magdeburg; UY, University of York), and genotype.

Participant	Gender	Age	Site	Genotype
ACHM	m	34	HMC	*CNGA3*
ACHM	m	41	HMC	*CNGA3*
ACHM	m	35	HMC	*CNGA3*
ACHM	f	41	HMC	*CNGA3*
ACHM	f	42	HMC	*CNGA3*
ACHM	m	28	HMC	*CNGA3*
ACHM	m	18	UM	*CNGB3*
ACHM	f	55	UM	*CNGA3*
ACHM	f	29	UM	*CNGB3*
ACHM	m	45	UM	*CNGB3*
ACHM	m	22	UM	*CNGA3*
ACHM	f	40	UY	*CNGB3*
ACHM	m	28	UY	*CNGB3*
ACHM	m	34	UY	*CNGA3*
ACHM	f	51	UY	*CNGA3*
C	m	25	HMC	–
C	f	33	HMC	–
C	m	19	HMC	–
C	f	22	HMC	–
C	f	24	HMC	–
C	m	34	HMC	–
C	f	27	HMC	–
C	m	26	HMC	–
C	m	29	HMC	–
C	f	29	HMC	–
C	f	24	HMC	–
C	f	32	HMC	–
C	f	46	HMC	–
C	f	30	HMC	–
C	f	22	HMC	–
C	f	57	HMC	–
C	f	23	HMC	–
C	m	23	HMC	–
C	m	50	HMC	–
C	m	43	HMC	–
C	f	25	HMC	–
C	f	27	HMC	–
C	m	26	HMC	–
C	m	25	HMC	–
C	m	33	UM	–
C	f	58	UM	–
C	m	29	UM	–
C	m	27	UM	–
C	f	32	UM	–
C	f	53	UM	–
C	f	35	UM	–
C	m	27	UM	–
C	f	26	UY	–
C	f	26	UY	–
C	m	35	UY	–
C	m	29	UY	–
C	f	23	UY	–
C	m	24	UY	–
C	f	30	UY	–
C	m	23	UY	–
C	f	19	UY	–
C	m	22	UY	–

The final surface reconstruction was inspected for potential cortical segmentation errors (for example areas where dura mater was incorrectly included in the grey matter surface during the initial automated segmentation) and, when necessary, manually corrected using the FreeView Visualisation GUI. Manual editing was split between two expert observers who were blind to participant identity and group to avoid bias. Minor edits to the pial surface were made in 50% of ACHM and 50% of control participants. Edits were primarily of the skull and dura mater located at parietal, motor and frontal cortical regions with only a small minority of participants requiring edits in the occipital cortex. All manually corrected reconstructions were rerun ('autoreconall2') utilising the edited brainmask.mgz files.

Data Analysis

A subsequent region-of-interest (ROI)-based analysis was applied where we compared differences in three surface-based measures between ACHM and their demographically matched controls: mean cortical volume (mm^3), cortical thickness (mm) and surface area (mm^2).

Cortical volume was computed as described in Winkler et al. (2018). Briefly, three vertices defining a face in the white surface and three matching vertices in the pial surface form an oblique truncated triangular pyramid; the volumes of these are subsequently computed and summed together for the whole ROI. Cortical thickness was defined as the shortest distance between each grey/white matter boundary vertex and the pial surface (grey matter/cerebrospinal fluid boundary) and vice versa. The final value depicted the average of the two thickness values measured, and thickness values were then averaged across each ROI (Fischl and Dale, 2000). Surface area was measured by calculating the summed surface area across each ROI of each triangle of the surface mesh, the unit used to connect the cortical surface between each vertex.

Regions-of-interest used for this analysis stream were derived using the anatomically defined retinotopy atlas (Benson et al., 2014) implemented in the python analysis toolbox 'neuropythy' (Benson and Winawer, 2018). The atlas then predicted several Freesurfer-based maps (visual area, eccentricity, polar angle, and pRF size), which were used to delineate twelve ROI labels for each participant. The ROIs encompass the entire cortical field representations of areas V1, V2, V3, V3a, V3b, TO1, TO2, V4, VO1, VO2, LO1, and LO2 (**Figure 1A**).

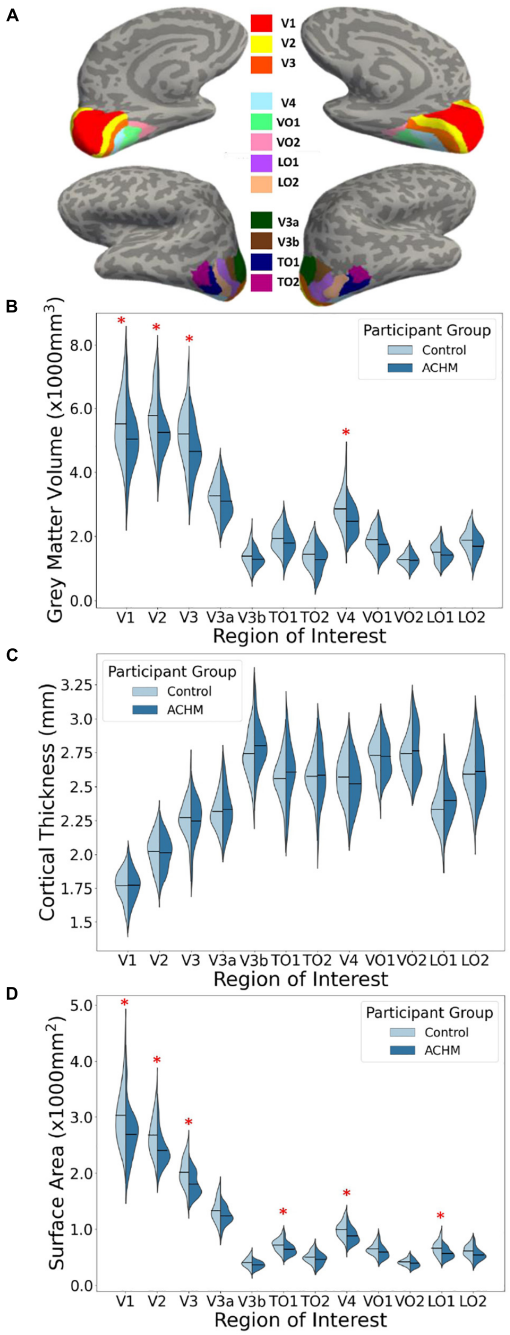

FIGURE 1 | Regions of interest and mean grey matter volume, cortical thickness and surface area for ACHM and controls. **(A)** An inflated surface of one control participant showing the cortical surface of the atlas-defined brain areas used in analysis (Benson et al., 2014; Benson and Winawer, 2018; https://osf.io/knb5g/). **(B)** A violin plot showing the distribution of mean grey matter volume averaged across the two hemispheres of controls and ACHM for each ROI. Horizontal lines within the violins indicate means for each group. Red stars indicate significant differences between groups in *post hoc* comparisons ($p < 0.05$). **(C)** A violin plot showing the distribution of mean cortical thickness averaged across the two hemispheres of controls and ACHM for each ROI. Details as in **(B)**. **(D)** A violin plot showing the distribution of mean cortical surface area averaged across the two hemispheres of controls and ACHM for each ROI. Details as in **(B)**. Red stars indicate significant differences between groups in *post hoc* comparisons ($p < 0.05$).

RESULTS

First, the data were evaluated from each hemisphere separately. A 2 × 2 × 12 mixed measures ANOVA was performed with between-subjects factor participant group (2 levels – ACHM and controls), and within-subjects factors of hemisphere (2 levels – left and right) and ROI (12 levels). Huynh-Feldt correction was applied to correct for sphericity of the data. There was no significant interaction between participant group, hemisphere, and ROI in any of the three metrics (**Supplementary Table 1**). Since hemisphere will have no effect on any interaction found between participant group and ROI, the data were combined across hemispheres. Extracted values of surface area and volume were averaged for each ROI and for each participant. For cortical thickness, the values were weighted by the respective surface area value and the mean cortical thickness. Values were derived by summing the product of the thickness and surface areas on the right and left hemispheres, respectively, and dividing this by the sum of the right and left surface area.

$$\frac{(lh.Thickness \times lh.SurfaceArea) + (rh.Thickness \times rh.SurfaceArea)}{lh.SurfaceArea + rh.SurfaceArea} \quad (1)$$

Results of the data averaged across hemispheres are shown in **Figures 1B–D**. To determine whether the effects of age, scanner site, gender, and global brain metrics influenced any of the three outcome measures, these variables were entered as potential confounds using analysis of covariance (ANCOVA). Repeated measures ANCOVAs were performed for each measurement type (grey matter volume, cortical thickness, and cortical surface area) including the two main variables of interest: participant group (2 levels) and ROI (12 levels). Huynh-Feldt correction was applied to correct for sphericity of the data.

There was no significant main effect of age, gender, scanner site or global brain metrics, and no interactions between any of these variables and participant group. The only significant interaction between the potential confounds and variables of interest was in grey matter volume for ROI × scanner site × gender [$F(8.44, 181.56) = 2.64$, $p = 0.008$]. This may reflect the differing number of each gender at each scanner site. All potential confounds are nevertheless accounted for in the remaining results (see **Table 2**).

The main effect of participant group was significant for grey matter volume [$F(1,43) = 4.87$, $p = 0.033$] and surface area [$F(1,43) = 7.52$, $p = 0.009$] but was not significant for cortical thickness [$F(1,43) < 0.01$, $p = 0.962$]. This indicates that mean volume and surface area are reduced overall in all visual areas tested here in ACHM compared to controls, as seen in **Figure 1**. The main effect of ROI was significant for grey matter volume [$F(4.22, 181.56) = 3.63$, $p = 0.006$] but not for cortical thickness [$F(11, 473) = 1.11$, $p = 0.352$] or surface area [$F(2.26, 97.28) = 0.064$]. This is expected, as differences in visual area size are well documented in the literature (Wandell et al., 2007). Critically, however, the interaction between ROI and participant group was also significant for volume [$F(4.22, 181.56) = 4.85$, $p = 0.001$] and surface area [$F(2.26, 97.28) = 6.62$, $p = 0.001$],

TABLE 2 | Results of analysis of covariance to assess effects of possible confounds age, scanner site, gender and global metrics.

Source	df1, df2	*F*	*p*	Effect size
Grey matter volume				
Participant group (A)	1, 43	4.87	**0.033**	0.10
ROI (B)	4.22, 181.56	3.63	**0.006**	0.08
Scanner site (C)	2, 43	0.61	0.549	0.03
Age (D)	1, 43	1.10	0.299	0.03
Gender (E)	1, 43	0.30	0.587	0.01
Global volume (F)	1, 43	0.95	0.335	0.02
A × B	4.22, 181.56	4.85	**0.001**	0.10
A × C	2, 43	0.02	0.976	0.00
A × E	1, 43	0.00	0.963	0.00
A × B × C	8.44, 181.56	0.39	0.934	0.02
A × B × E	4.22, 181.56	0.86	0.492	0.02
A × C × E	2, 43	0.08	0.920	0.00
A × B × C × E	8.44, 181.56	0.30	0.968	0.01
B × C	8.44, 181.56	1.19	0.308	0.05
B × D	4.22, 181.56	2.14	0.074	0.05
B × E	4.22, 181.56	0.53	0.723	0.01
B × F	4.22, 181.56	0.48	0.764	0.01
B × C × E	8.44, 181.56	2.64	**0.008**	0.11
C × E	2, 43	0.77	0.471	0.03
Cortical thickness				
Participant group (A)	1, 43	0.00	0.962	0.00
ROI (B)	11.00, 473.00	1.11	0.352	0.03
Scanner site (C)	2, 43	0.86	0.432	0.04
Age (D)	1, 43	0.03	0.861	0.00
Gender (E)	1, 43	0.20	0.658	0.01
Global thickness (F)	1, 43	0.51	0.478	0.01
A × B	11.00, 473.00	1.55	0.112	0.04
A × C	2, 43	0.66	0.522	0.03
A × E	1, 43	0.00	0.948	0.00
A × B × C	22.00, 473.00	0.85	0.666	0.04
A × B × E	11.00, 473.00	0.61	0.823	0.01
A × C × E	2, 43	2.94	0.064	0.12
A × B × C × E	22.00, 473.00	0.68	0.862	0.03
B × C	22.00, 473.00	0.79	0.746	0.04
B × D	11.00, 473.00	0.65	0.783	0.02
B × E	11.00, 473.00	0.54	0.875	0.01
B × F	11.00, 473.00	0.86	0.582	0.02
B × C × E	22.00, 473.00	0.50	0.975	0.02
C × E	2, 43	3.68	**0.033**	0.15
Cortical surface area				
Participant group (A)	1, 43	7.52	**0.009**	0.15
ROI (B)	2.26, 97.28	2.72	0.064	0.06
Scanner site (C)	2, 43	0.34	0.712	0.02
Age (D)	1, 43	1.79	0.188	0.04
Gender (E)	1, 43	0.20	0.656	0.01
Global surface area (F)	1, 43	0.71	0.403	0.02
A × B	2.26, 97.28	6.62	**0.001**	0.13
A × C	2, 43	0.03	0.968	0.00
A × E	1, 43	0.10	0.749	0.00
A × B × C	4.53, 97.28	0.10	0.989	0.01
A × B × E	2.26, 97.28	0.81	0.459	0.02
A × C × E	2, 43	0.62	0.542	0.03
A × B × C × E	4.53, 97.28	0.46	0.788	0.02
B × C	4.53, 97.28	0.71	0.601	0.03
B × D	2.26, 97.28	2.89	0.054	0.06
B × E	2.26, 97.28	0.05	0.967	0.00
B × F	2.26, 97.28	0.61	0.565	0.01
B × C × E	4.53, 97.28	2.35	0.052	0.10
C × E	2, 43	0.27	0.765	0.01

Effect size shown is partial eta-squared. Huynh-Feldt correction applied to correct for violation of sphericity. Significance is illustrated by boldface.

but was not significant for cortical thickness [$F(11,473) = 1.55$, $p = 0.112$]. Considering these interactions, we performed *post hoc* pairwise comparisons to determine if there was a significant difference between ACHM participants and controls in grey matter volume and surface area for each of the 12 ROIs, adjusting for multiple comparisons using Bonferroni correction (**Table 3**). This analysis revealed four areas which showed a significant difference between ACHM and controls for grey matter volume (V1: $p = 0.006$, V2: $p = 0.019$, V3: $p = 0.024$, V4, $p = 0.029$) and six areas for surface area (V1: $p = 0.008$, V2: $p = 0.004$, V3: $p = 0.007$, V4: $p = 0.0333$, LO1: $p = 0.015$, TO1: $p = 0.046$).

DISCUSSION

The aim of this study was to investigate any potential morphological changes in visual regions of the brain in participants with ACHM compared to normally sighted controls. Significant reductions were found in ACHM relative to controls for both volume and surface area, but not for thickness. Decreased volume appears to be driven largely by reductions in surface area rather than thickness. Our results reveal widespread morphological alterations throughout the visual cortex, consistent with previous neuroimaging studies of congenitally blind adults (Ptito et al., 2008; Aguirre et al., 2016; Bridge and Watkins, 2019). It appears that ventral visual area V4 is disproportionately affected by reductions in surface area and volume compared to the dorsal pathway areas V3a and V3b. Higher visual areas LO1 and TO1 also are reduced in surface area in ACHM, although not enough to drive differences in volume measurements.

Early Visual Area Results

All early visual areas (V1, V2, and V3) showed significant decreases in grey matter volume and surface area for ACHM. These areas all have particularly large foveal representations (Wandell et al., 2007), suggesting that the substantial reduction in input to these regions in ACHM may explain the decrease in size. All of these areas also process colour information (Mullen et al., 2007; Railo et al., 2012; Hurme et al., 2020), which could contribute further reductions in these areas. In a separate study, we have extended our analysis to investigate more specifically the eccentricity dependence of structural changes

TABLE 3 | *Post hoc* between group comparisons following analysis of variance in **Table 2**, Bonferroni-corrected.

Area	Grey matter volume *p*-Value	Surface area *p*-Value
V1	**0.006**	**0.008**
V2	**0.019**	**0.004**
V3	**0.024**	**0.007**
V3a	0.317	0.091
V3b	0.339	0.175
TO1	0.438	**0.046**
TO2	0.117	0.101
V4	**0.029**	**0.033**
VO1	0.297	0.224
VO2	0.939	0.580
LO1	0.170	**0.015**
LO2	0.156	0.076

Significance is illustrated by boldface.

within primary visual cortex and shows that cortical changes are most pronounced in central visual field representations (manuscript submitted and under review; preprint available under Molz et al., 2021).

V4 and V3a/b Differences

Ventral area V4 was significantly lower in both surface area and volume in ACHM compared to controls. No such difference is found in dorsal areas V3a and V3b, however. This may be driven by the reduction in foveal input in ACHM, which is largely dominated by cone photoreceptors in normally-sighted adults. Previous research has demonstrated a preferential response bias to stimuli from the central visual field in ventral visual areas including V4, VO-1, and VO-2 (Brewer et al., 2005; Arcaro et al., 2009; Winawer and Witthoft, 2015). In contrast, dorsal areas appear to have an increasingly peripheral bias as one moves up the visual processing hierarchy away from primary visual cortex (Tootell et al., 1997; Wandell et al., 2007; Fattori et al., 2009). Areas with a more peripheral bias should therefore be less affected by ACHM, since peripheral vision is relatively preserved in these participants and rod function is intact. Our results showing no significant differences in ACHM in dorsal areas V3a and V3b support this hypothesis.

Ventral areas such as V4 have also been associated with chromatic vision (Bartels and Zeki, 2000; Wade et al., 2002; Brewer et al., 2005; Mullen et al., 2007, 2015; Bannert and Bartels, 2018), while dorsal regions V3a and V3b have been more aligned with motion processing (Tootell et al., 1997; Wandell et al., 2007; Fattori et al., 2009). Therefore, both the lack of chromatic signals and the reduction of foveal inputs caused by the absence of functional cones are likely to contribute to differences observed in V4 (but not V3a or V3b) in ACHM.

Higher Visual Areas

LO1 was also significantly reduced in surface area in ACHM participants. This area is commonly associated with processing of shape and object recognition (Malach et al., 1995; Larsson and Heeger, 2006; Silson et al., 2013) a skill assisted by chromatic vision (Bramão et al., 2011, 2016). LO1 also exhibits a foveal bias (Larsson and Heeger, 2006). Therefore, the cortical deprivation thought to cause this morphological difference may be related to both the lack of foveal and chromatic input to this area.

TO1 also shows a lower surface area in ACHM. This area is part of human area MT+, is most commonly associated with visual motion processing, and has a large foveal representation (Amano et al., 2009). Individuals with ACHM often report problems with motion perception, which is generally impaired when mediated by rods compared to cones (Gegenfurtner et al., 1999), possibly due to lower temporal resolution of the rods (Hess and Nordby, 1986). Thus, both reduced foveal inputs as well as impaired motion processing may explain differences in TO1 in ACHM. This is in contrast to TO2, which has a greater emphasis of the peripheral visual field (Amano et al., 2009) and did not differ significantly between groups.

Surprisingly, ventral areas VO1 and VO2 do not show significant differences in any metric, an unexpected result as both have been associated with chromatic vision (Brewer et al., 2005; Jiang et al., 2007; Arcaro et al., 2009) and have large foveal representations (Brewer et al., 2005). It is unexpected that we failed to detect group differences in VO1 and VO2, which likely receive predominant cone input because of their role in colour processing. Unlike larger areas V1, V2, V3, V3a/b, and V4, smaller regions such as VO1 and VO2 are more likely to be prone to type two errors, which might explain the lack of sensitivity in revealing differences here, although we did detect differences in similarly sized areas such as LO1 and TO1. However, research has suggested that it is more difficult to map areas along the ventral surface accurately due to potential vessel artifacts (the 'venous eclipse'), which might have introduced some uncertainty to area boundaries (Winawer et al., 2010; Benson and Winawer, 2018). Such factors could have contributed to the null result we found in small ventral areas such as VO1 and VO2 using an atlas-based approach.

Cortical Thickness

We found no significant differences in cortical thickness in ACHM in any visual area. This is in contrast to increased cortical thickness reported in primary visual cortex in participants with total congenital blindness (Jiang et al., 2009; Park et al., 2009; Aguirre et al., 2016; Bridge and Watkins, 2019). However, it is important to note that participants with ACHM are still sighted, with an area of absolute blindness restricted only to the central fovea. Our prediction therefore would be that cortical thickening would be observed only in representations of the central visual field. Indeed, our preliminary analysis has found increased cortical thickness in the most central representations of primary visual cortex in ACHM (Molz et al., 2021). It remains to be seen if a total absence of input from the central fovea results in thickening of the foveal representation within higher visual areas.

CONCLUSION

In summary, this study provides an overview of the structural changes present in visual cortex in ACHM compared to

normally-sighted controls. This study has revealed widespread reduction in the surface area and volume of many visual areas. Differences are found particularly in areas that typically have large representations of the fovea and areas associated with chromatic vision, suggesting that both characteristics of cone vision that are absent in ACHM can affect brain morphology. It is important to remember drawing conclusions from this data that atlas-defined ROIs are based on neurotypical individuals. Therefore, when applying an atlas to brains that may differ structurally there may be limitations on the precision of defining the ROIs. However, this technique has been used successfully in the past and there does appear to be some specificity in the ROIs where group differences are found (Norman and Thaler, 2019). Also, there is evidence that topographical organisation of visual cortex follows retinotopic principles, even in congenitally blind individuals (Striem-Amit et al., 2015). An atlas-based approach can therefore be effective in identifying differences between groups, particularly when comparing with a neurotypical control group.

Structural differences in visual cortex in ACHM are important to consider when planning treatment, such as gene therapy to restore cone function to the eye. By adulthood, it is clear that deprivation of chromatic and foveal information has resulted in cortical remodelling, and it is difficult to establish from the literature whether this will limit the success of treatment or if sufficient plasticity remains into adulthood to permit the restoration of function. Research has shown that the volume and surface area of primary visual cortex mature earlier than other brain areas (Leuba and Kraftsik, 1994), completed by the end of the first postnatal year. Less is known about the rate of development of higher cortical areas, or whether structural changes in these areas will affect their ability to perform specialised visual functions. Given the rapid maturation of primary visual cortex, however, it seems advisable to apply any therapeutic interventions as early as possible.

DATA AVAILABILITY STATEMENT

The raw data supporting the conclusions of this article will be made available by the authors, following appropriate data protection guidelines.

ETHICS STATEMENT

The study was in accordance with the Declaration of Helsinki, and was reviewed and approved by each of the site-specific ethics committees: the York Neuroimaging Centre Research Ethics Committee (York), the Hadassah Hebrew University Medical Centre Ethics Committee (Jerusalem), and the Ethical Committee of the Otto von Guericke University Magdeburg, Germany (Magdeburg). The participants provided their written informed consent to participate in this study.

AUTHOR CONTRIBUTIONS

HB, NL, MH, AM, and BM conceived and designed the experiments. BM, PB, AH, RL, NL, NR, AG, KA, RM, IG, SK, LC, JM, MK, BK-K, IW, and EB data acquisition. BM, AH, and PB performed the experiments. RL, LW, and BM analysed the data. RL and LW wrote the paper. HB, RL, LW, BM, AM, MH, PB, AH, NL, NR, AG, KA, RM, IG, SK, LC, JM, MK, BK-K, IW, and EB revised the manuscript. All authors contributed to the article and approved the submitted version.

FUNDING

This project was supported by European Union's Horizon 2020 Research and Innovation Programme under the Marie Sklodowska-Curie grant agreement (No. 641805) and the German Research Foundation (DFG, HO 2002/12-1).

ACKNOWLEDGMENTS

We thank the German patient association 'Achromatopsie Selbsthilfe e.V.' for support in participant recruitment. We also thank Elisa Zamboni for her helpful advice on the use of the Benson atlas and figure preparation.

SUPPLEMENTARY MATERIAL

The Supplementary Material for this article can be found online at: https://www.frontiersin.org/articles/10.3389/fnins.2021.718958/full#supplementary-material

REFERENCES

Aboshiha, J., Dubis, A. M., Carroll, J., Hardcastle, A. J., and Michaelides, M. (2016). The cone dysfunction syndromes. *Br. J. Ophthalmol.* 100, 115–121.

Ackroyd, C., Humphrey, N. K., and Warrington, E. K. (1974). Lasting effects of early blindness: a case study. *Q. J. Exp. Psychol.* 26, 114–124.

Aguirre, G. K., Datta, R., Benson, N. C., Prasad, S., Jacobson, S. G., Cideciyan, A. V., et al. (2016). Patterns of individual variation in visual pathway structure and function in the sighted and blind. *PLoS One* 11:e0164677.

Amano, K., Wandell, B. A., and Dumoulin, S. O. (2009). Visual field maps, population receptive field sizes, and visual field coverage in the human MT+ complex. *J. Neurophysiol.* 102, 2704–2718. doi: 10.1152/jn.00102.2009

Arcaro, M. J., McMains, S. A., Singer, B. D., and Kastner, S. (2009). Retinotopic organization of human ventral visual cortex. *J. Neurosci.* 29, 10638–10652.

Bannert, M. M., and Bartels, A. (2018). Human V4 activity patterns predict behavioral performance in imagery of object color. *J. Neurosci.* 38, 3657–3668. doi: 10.1523/JNEUROSCI.2307-17.2018

Bartels, A., and Zeki, S. (2000). The architecture of the colour centre in the human visual brain: new results and a review. *Eur. J. Neurosci.* 12, 172–193. doi: 10.1046/j.1460-9568.2000.00905.x

Benson, N. C., Butt, O. H., Brainard, D. H., and Aguirre, G. K. (2014). Correction of distortion in flattened representations of the cortical surface allows prediction of V1-V3 functional organization from anatomy. *PLoS Comput. Biol.* 10:e1003538. doi: 10.1371/journal.pcbi.1003538

Benson, N. C., and Winawer, J. (2018). Bayesian analysis of retinotopic maps. *Elife* 6:e40224. doi: 10.7554/eLife.40224

Boucard, C. C., Hernowo, A. T., Maguire, R. P., Jansonius, N. M., Roerdink, J. B., Hooymans, J. M., et al. (2009). Changes in cortical grey matter density associated with long-standing retinal visual field defects. *Brain* 132, 1898–1906. doi: 10.1093/brain/awp119

Bramão, I., Reis, A., Petersson, K. M., and Faísca, L. (2011). The role of color information on object recognition: a review and meta-analysis. *Acta Psychol. (Amst.)* 138, 244–253. doi: 10.1016/j.actpsy.2011.06.010

Bramão, I., Reis, A., Petersson, K. M., and Faísca, L. (2016). Knowing that strawberries are red and seeing red strawberries: the interaction between surface colour and colour knowledge information. *J. Cogn. Psychol.* 28, 641–657. doi: 10.1080/20445911.2016.1182171

Brewer, A. A., Liu, J., Wade, A. R., and Wandell, B. A. (2005). Visual field maps and stimulus selectivity in human ventral occipital cortex. *Nat. Neurosci.* 8, 1102–1109. doi: 10.1038/nn1507

Bridge, H., and Watkins, K. E. (2019). Structural and functional brain reorganisation due to blindness: the special case of bilateral congenital anophthalmia. *Neurosci. Biobehav. Rev.* 107, 765–774. doi: 10.1016/j.neubiorev.2019.10.006

Brown, H. D., Woodall, R. L., Kitching, R. E., Baseler, H. A., and Morland, A. B. (2016). Using magnetic resonance imaging to assess visual deficits: a review. *Ophthalmic Physiol. Opt.* 36, 240–265. doi: 10.1111/opo.12293

Burton, E., Wattam-Bell, J. S., Rubin, G., Aboshiha, J., Michaelides, M., Atkinson, J., et al. (2016). Dissociations in coherence sensitivity reveal atypical development of cortical visual processing in congenital achromatopsia. *Invest. Ophthalmol. Vis. Sci.* 57, 2251–2259. doi: 10.1167/iovs.15-18414

Castaldi, E., Cicchini, G. M., Cinelli, L., Biagi, L., Rizzo, S., and Morrone, M. C. (2016). Visual BOLD response in late blind subjects with Argus II retinal prosthesis. *PLoS Biol.* 14:e1002569.

Chiu, W., Lin, T.-Y., Chang, Y.-C., Isahwan-Ahmad Mulyadi Lai, H., Lin, S.-C., Ma, C., et al. (2021). An update on gene therapy for inherited retinal dystrophy: experience in leber congenital amaurosis clinical trials. *Int. J. Mol. Sci.* 22:4534.

Dale, A. M., Fischl, B., and Sereno, M. I. (1999). Cortical surface-based analysis. I. Segmentation and surface reconstruction. *Neuroimage* 9, 179–194. doi: 10.1006/nimg.1998.0395

Desikan, R. S., Ségonne, F., Fischl, B., Quinn, B. T., Dickerson, B. C., Blacker, D., et al. (2006). An automated labeling system for subdividing the human cerebral cortex on MRI scans into gyral based regions of interest. *Neuroimage* 31, 968–980. doi: 10.1016/j.neuroimage.2006.01.021

Farahbakhsh, M., Anderson, E. J., Rider, A., Greenwood, J. A., Hirji, N., Zaman, S., et al. (2020). A demonstration of cone function plasticity after gene therapy in achromatopsia. *medRxiv* [Preprint]. doi: 10.1101/2020.12.16.20246710

Fattori, P., Pitzalis, S., and Galletti, C. (2009). The cortical visual area V6 in macaque and human brains. *J. Physiol. Paris* 103, 88–97. doi: 10.1016/j.jphysparis.2009.05.012

Fine, I., Wade, A., Brewer, A., May, M. G., Goodman, D. F., Boynton, G. M., et al. (2003). Long-term deprivation affects visual perception and cortex. *Nat. Neurosci.* 6, 915–916. doi: 10.1038/nn1102

Fischer, M. D., Michalakis, S., Wilhelm, B., Zobor, D., Muehlfriedel, R., Kohl, S., et al. (2020). Safety and vision outcomes of subretinal gene therapy targeting cone photoreceptors in achromatopsia: a nonrandomized controlled trial. *JAMA Ophthalmol.* 138, 643–651. doi: 10.1001/jamaophthalmol.2020.1032

Fischl, B., and Dale, A. M. (2000). Measuring the thickness of the human cerebral cortex from magnetic resonance images. *Proc. Natl. Acad. Sci. U. S. A.* 97, 11050–11055. doi: 10.1073/pnas.200033797

Fischl, B., Sereno, M. I., and Dale, A. M. (1999). Cortical surface-based analysis. II: inflation, flattening, and a surface-based coordinate system. *Neuroimage* 9, 195–207. doi: 10.1006/nimg.1998.0396

Francois, J. (1961). *Heredity in Ophthalmology*. St. Louis: Mosby, 497–512.

Gegenfurtner, K., Mayser, H., and Sharpe, L. (1999). Seeing movement in the dark. *Nature* 398, 475–476. doi: 10.1038/19004

Goddard, E., Mannion, D. J., McDonald, J. S., Solomon, S. G., and Clifford, C. W. (2011). Color responsiveness argues against a dorsal component of human V4. *J. Vis.* 11:3. doi: 10.1167/11.4.3

Goodale, M. A., and Milner, A. D. (1992). Separate visual pathways for perception and action. *Trends Neurosci.* 15, 20–25. doi: 10.1016/0166-2236(92)90344-8

Guerreiro, M. J., Erfort, M. V., Henssler, J., Putzar, L., and Röder, B. (2015). Increased visual cortical thickness in sight-recovery individuals. *Hum Brain Mapp.* 36, 5265–5274. doi: 10.1002/hbm.23009

Guerreiro, M. J. S., Putzar, L., and Röder, B. (2016). Persisting cross-modal changes in sight-recovery individuals modulate visual perception. *Curr. Biol.* 26, 3096–3100. doi: 10.1016/j.cub.2016.08.069

Hadad, B., Schwartz, S., Maurer, D., and Lewis, T. L. (2015). Motion perception: a review of developmental changes and the role of early visual experience. *Front. Integr. Neurosci.* 9:49. doi: 10.3389/fnint.2015.00049

Haegerstrom-Portnoy, G., Schneck, M. E., Verdon, W. A., and Hewlett, S. E. (1996a). Clinical vision characteristics of the congenital achromatopsias. I. Visual acuity, refractive error, and binocular status. *Optom. Vis. Sci.* 73, 446–456. doi: 10.1097/00006324-199607000-00001

Haegerstrom-Portnoy, G., Schneck, M. E., Verdon, W. A., and Hewlett, S. E. (1996b). Clinical vision characteristics of the congenital achromatopsias. II. Color vision. *Optom. Vis. Sci.* 73, 457–465. doi: 10.1097/00006324-199607000-00002

Hanson, R. L. W., Gale, R. P., Gouws, A. D., Airody, A., Scott, M. T. W., Akthar, F., et al. (2019). Following the status of visual cortex over time in patients with macular degeneration reveals atrophy of visually deprived brain regions. *Invest. Ophthalmol. Vis. Sci.* 60, 5045–5051. doi: 10.1167/iovs.18-25823

Hernowo, A. T., Prins, D., Baseler, H. A., Plank, T., Gouws, A. D., Hooymans, J. M., et al. (2014). Morphometric analyses of the visual pathways in macular degeneration. *Cortex* 56, 99–110. doi: 10.1016/j.cortex.2013.01.003

Hess, R. F., and Nordby, K. (1986). Spatial and temporal limits of vision in the achromat. *J. Physiol.* 371, 365–385. doi: 10.1113/jphysiol.1986.sp015981

Hirji, N., Aboshiha, J., Georgiou, M., Bainbridge, J., and Michaelides, M. (2018). Achromatopsia: clinical features, molecular genetics, animal models and therapeutic options. *Ophthalmic Genet.* 39, 149–157. doi: 10.1080/13816810.2017.1418389

Hurme, M., Koivisto, M., Henriksson, L., and Railo, H. (2020). Neuronavigated TMS of early visual cortex eliminates unconscious processing of chromatic stimuli. *Neuropsychologia* 136:107266. doi: 10.1016/j.neuropsychologia.2019.107266

Jiang, J., Zhu, W., Shi, F., Liu, Y., Li, J., Qin, W., et al. (2009). Thick visual cortex in the early blind. *J. Neurosci.* 29, 2205–2211. doi: 10.1523/JNEUROSCI.5451-08.2009

Jiang, Y., Zhou, K., and He, S. (2007). Human visual cortex responds to invisible chromatic flicker. *Nat. Neurosci.* 10, 657–662. doi: 10.1038/nn1879

Johnson, S., Michaelides, M., Aligianis, I. A., Ainsworth, J. R., Mollon, J. D., Maher, E. R., et al. (2004). Achromatopsia caused by novel mutations in both CNGA3 and CNGB3. *J. Med. Genet.* 41:e20. doi: 10.1136/jmg.2003.011437

Kohl, S., Jägle, H., Wissinger, B., and Zobor, D. (2004). "Achromatopsia," in *GeneReviews® [Internet]*, eds M. P. Adam, H. H. Ardinger, R. A. Pagon, S. E. Wallace, L. J. H. Bean, K. Stephens, et al. (Seattle, WA: University of Washington), 1993–2020.

Larsson, J., and Heeger, D. J. (2006). Two retinotopic visual areas in human lateral occipital cortex. *J. Neurosci.* 26, 13128–13142. doi: 10.1523/JNEUROSCI.1657-06.2006

Leuba, G., and Kraftsik, R. (1994). Changes in volume, surface estimate, three-dimensional shape and total number of neurons of the human primary visual cortex from midgestation until old age. *Anat. Embryol. (Berl.)* 190, 351–366. doi: 10.1007/BF00187293

Liang, X., Dong, F., Li, H., Li, H., Yang, L., and Sui, R. (2015). Novel CNGA3 mutations in Chinese patients with achromatopsia. *Br. J. Ophthalmol.* 99, 571–576. doi: 10.1136/bjophthalmol-2014-305432

Lin, H., Zhang, L., Lin, D., Chen, W., Zhu, Y., Chen, C., et al. (2018). Visual restoration after cataract surgery promotes functional and structural brain recovery. *EBioMedicine* 30, 52–61.

Lou, A. R., Madsen, K. H., Julian, H. O., Toft, P. B., Kjaer, T. W., Paulson, O. B., et al. (2013). Postoperative increase in grey matter volume in visual cortex after unilateral cataract surgery. *Acta Ophthalmol.* 91, 58–65.

Malach, R., Reppas, J. B., Benson, R. R., Kwong, K. K., Jiang, H., Kennedy, W. A., et al. (1995). Object-related activity revealed by functional magnetic resonance

imaging in human occipital cortex. *Proc. Natl. Acad. Sci. U. S. A.* 92, 8135–8139. doi: 10.1073/pnas.92.18.8135

McKeefry, D. J., and Zeki, S. (1997). The position and topography of the human colour centre as revealed by functional magnetic resonance imaging. *Brain* 120, 2229–2242. doi: 10.1093/brain/120.12.2229

McKyton, A., Averbukh, E., Marks Ohana, D., Levin, N., and Banin, E. (2021). Cortical visual mapping following ocular gene augmentation therapy for achromatopsia. *J. Neurosci.* 41, 7363–7371. doi: 10.1523/JNEUROSCI.3222-20.2021

Molz, B., Herbik, A., Baseler, H. A., de Best, P. B., Vernon, R., Raz, N., et al. (2021). Structural changes to primary visual cortex in the congenital absence of cone input in achromatopsia. *medRxiv* [Preprint]. doi: 10.1101/2021.07.19.21260427

Mowad, T. G., Willett, A. E., Mahmoudian, M., Lipin, M., Heinecke, A., Maguire, A. M., et al. (2020). Compensatory cross-modal plasticity persists after sight restoration. *Front. Neurosci.* 14:291. doi: 10.3389/fnins.2020.00291

Mullen, K. T., Chang, D. H., and Hess, R. F. (2015). The selectivity of responses to red-green colour and achromatic contrast in the human visual cortex: an fMRI adaptation study. *Eur. J. Neurosci.* 42, 2923–2933. doi: 10.1111/ejn.13090

Mullen, K. T., Dumoulin, S. O., McMahon, K. L., de Zubicaray, G. I., and Hess, R. F. (2007). Selectivity of human retinotopic visual cortex to S-cone-opponent, L/M-cone-opponent and achromatic stimulation. *Eur. J. Neurosci.* 25, 491–502. doi: 10.1111/j.1460-9568.2007.05302.x

Norman, L. J., and Thaler, L. (2019). Retinotopic-like maps of spatial sound in primary 'visual'cortex of blind human echolocators. *Proc. Royal Soc. B* 286:20191910.

Park, H. J., Lee, J. D., Kim, E. Y., Park, B., Oh, M. K., Lee, S., et al. (2009). Morphological alterations in the congenital blind based on the analysis of cortical thickness and surface area. *Neuroimage* 47, 98–106. doi: 10.1016/j.neuroimage.2009.03.076

Prins, D., Hanekamp, S., and Cornelissen, F. W. (2016). Structural brain MRI studies in eye diseases: are they clinically relevant? A review of current findings. *Acta Ophthalmol.* 94, 113–121. doi: 10.1111/aos.12825

Ptito, M., Schneider, F. C., Paulson, O. B., and Kupers, R. (2008). Alterations of the visual pathways in congenital blindness. *Exp. Brain Res.* 187, 41–49. doi: 10.1007/s00221-008-1273-4

Railo, H., Salminen-Vaparanta, N., Henriksson, L., Revonsuo, A., and Koivisto, M. (2012). Unconscious and conscious processing of color rely on activity in early visual cortex: a TMS study. *J. Cogn. Neurosci.* 24, 819–829. doi: 10.1162/jocn_a_00172

Reichel, F. F., Michalakis, S., Wilhelm, B., Zobor, D., Muehlfriedel, R., Kohl, S., et al. (2021). Three-year results of phase I retinal gene therapy trial for CNGA3-mutated achromatopsia: results of a non randomised controlled trial. *Br. J. Ophthalmol.* doi: 10.1136/bjophthalmol-2021-319067 [Epub ahead of print].

Reislev, N. L., Dyrby, T. B., Siebner, H. R., Kupers, R., and Ptito, M. (2016a). Simultaneous assessment of white matter changes in microstructure and connectedness in the blind brain. *Neural Plast.* 2016:6029241. doi: 10.1155/2016/6029241

Reislev, N. L., Kupers, R., Siebner, H. R., Ptito, M., and Dyrby, T. B. (2016b). Blindness alters the microstructure of the ventral but not the dorsal visual stream. *Brain Struct. Funct.* 221, 2891–2903. doi: 10.1007/s00429-015-1078-8

Remmer, M. H., Rastogi, N., Ranka, M. P., and Ceisler, E. J. (2015). Achromatopsia: a review. *Curr. Opin. Ophthalmol.* 26, 333–340. doi: 10.1097/ICU.0000000000000189

Ségonne, F., Dale, A. M., Busa, E., Glessner, M., Salat, D., Hahn, H. K., et al. (2004). A hybrid approach to the skull stripping problem in MRI. *Neuroimage* 22, 1060–1075. doi: 10.1016/j.neuroimage.2004.03.032

Ségonne, F., Pacheco, J., and Fischl, B. (2007). Geometrically accurate topology-correction of cortical surfaces using nonseparating loops. *IEEE Trans. Med. Imaging* 26, 518–529. doi: 10.1109/TMI.2006.887364

Silson, E. H., McKeefry, D. J., Rodgers, J., Gouws, A. D., Hymers, M., and Morland, A. B. (2013). Specialized and independent processing of orientation and shape in visual field maps LO1 and LO2. *Nat. Neurosci.* 16, 267–269. doi: 10.1038/nn.3327

Sled, J. G., Zijdenbos, A. P., and Evans, A. C. (1998). A nonparametric method for automatic correction of intensity nonuniformity in MRI data. *IEEE Trans. Med. Imaging* 17, 87–97. doi: 10.1109/42.668698

Striem-Amit, E., Ovadia-Caro, S., Caramazza, A., Margulies, D. S., Villringer, A., and Amedi, A. (2015). Functional connectivity of visual cortex in the blind follows retinotopic organization principles. *Brain* 138, 1679–1695.

Sun, W., Li, S., Xiao, X., Wang, P., and Zhang, Q. (2020). Genotypes and phenotypes of genes associated with achromatopsia: a reference for clinical genetic testing. *Mol. Vis.* 26, 588–602.

Thiadens, A. A., Slingerland, N. W., Roosing, S., van Schooneveld, M. J., van Lith-Verhoeven, J. J., van Moll-Ramirez, N., et al. (2009). Genetic etiology and clinical consequences of complete and incomplete achromatopsia. *Ophthalmology* 116, 1984–1989.

Tootell, R. B., Mendola, J. D., Hadjikhani, N. K., Ledden, P. J., Liu, A. K., Reppas, J. B., et al. (1997). Functional analysis of V3A and related areas in human visual cortex. *J. Neurosci.* 17, 7060–7078. doi: 10.1523/JNEUROSCI.17-18-07060.1997

Ungerleider, L. G., and Mishkin, M. (1982). "Two cortical visual systems," in *The Analysis of Visual Behaviour*, eds D. J. Ingle, R. J. W. Mansfield, and M. S. Goodale (Cambridge, MA: MIT Press), 549–586.

Varsányi, B., Wissinger, B., Kohl, S., Koeppen, K., and Farkas, Á (2005). Clinical and genetic features of Hungarian achromatopsia patients. *Mol. Vis.* 11, 996–1001.

Wade, A. R., Brewer, A. A., Rieger, J. W., and Wandell, B. A. (2002). Functional measurements of human ventral occipital cortex: retinotopy and colour. *Philos. Trans. R. Soc. Lond. B Biol. Sci.* 357, 963–973. doi: 10.1098/rstb.2002.1108

Wandell, B. A., Dumoulin, S. O., and Brewer, A. A. (2007). Visual field maps in human cortex. *Neuron* 56, 366–383. doi: 10.1016/j.neuron.2007.10.012

Winawer, J., Horiguchi, H., Sayres, R. A., Amano, K., and Wandell, B. A. (2010). Mapping hV4 and ventral occipital cortex: the venous eclipse. *J. Vis.* 10:1.

Winawer, J., and Witthoft, N. (2015). Human V4 and ventral occipital retinotopic maps. *Vis. Neurosci.* 32:E020. doi: 10.1017/S0952523815000176

Winkler, A. M., Greve, D. N., Bjuland, K. J., Nichols, T. E., Sabuncu, M. R., Håberg, A. K., et al. (2018). Joint analysis of cortical area and thickness as a replacement for the analysis of the volume of the cerebral cortex. *Cereb. Cortex* 28, 738–749. doi: 10.1093/cercor/bhx308

Wissinger, B., Gamer, D., Jägle, H., Giorda, R., Marx, T., Mayer, S., et al. (2001). CNGA3 mutations in hereditary cone photoreceptor disorders. *Am. J. Hum. Genet.* 69, 722–737.

Wong, A. M. (2012). New concepts concerning the neural mechanisms of amblyopia and their clinical implications. *Can. J. Ophthalmol.* 47, 399–409.

Yucel, Y. H., and Gupta, N. (2015). A framework to explore the visual brain in glaucoma with lessons from models and man. *Exp. Eye Res.* 141, 171–178. doi: 10.1016/j.exer.2015.07.004 Epub 2015 Jul 11.

Zeki, S. (1990). A century of cerebral achromatopsia. *Brain* 113, 1721–1777. doi: 10.1093/brain/113.6.1721

Zeki, S., Watson, J. D., Lueck, C. J., Friston, K. J., Kennard, C., and Frackowiak, R. S. (1991). A direct demonstration of functional specialization in human visual cortex. *J. Neurosci.* 11, 641–649. doi: 10.1523/JNEUROSCI.11-03-00641.1991

Zelinger, L., Cideciyan, A. V., Kohl, S., Schwartz, S. B., Rosenmann, A., Eli, D., et al. (2015). Genetics and disease expression in the CNGA3 form of achromatopsia: steps on the path to gene therapy. *Ophthalmology* 122, 997–1007. doi: 10.1016/j.ophtha.2014.11.025

Conflict of Interest: The authors declare that the research was conducted in the absence of any commercial or financial relationships that could be construed as a potential conflict of interest.

Publisher's Note: All claims expressed in this article are solely those of the authors and do not necessarily represent those of their affiliated organizations, or those of the publisher, the editors and the reviewers. Any product that may be evaluated in this article, or claim that may be made by its manufacturer, is not guaranteed or endorsed by the publisher.